Master Thesis of GSEP

Laser Cutting of Cathode Electrode($LiFePO_4$) of Li-Ion Battery

리튬이온 전지의 양극전극 레이저 절단

February 2019

Graduate School of Engineering Practice

Seoul National University

박 주 영

Laser Cutting of Cathode Electrode(LiFePO4) of Li-Ion Battery

리튬이온 전지의 양극전극 레이저 절단

지도교수 고승환

이 리포트를 공학석사학위 연구보고서로 제출함.
2019년 01월

서울대학교 공학전문대학원
응용공학과 응용공학전공
박 주 영

박주영의 공학석사학위 연구보고서를 인준함.
2019년 01월

Chair	오 병 수	(Seal)
Examiner	고 승 환	(Seal)
Examiner	이 봉 환	(Seal)

Abstract

Laser Cutting of Cathode Electrode(LiFePO4) of Li-Ion Battery

JOOYOUNG PARK

Department of Engineering Practice

Graduate School of Engineering Practice

Seoul National University

International agreements to limit the use of fossil fuels and global interest in eco-friendly energy have accelerated the development of renewable energy sources. Since the development of the first lithium-ion battery in the 1990s, it has continued to develop and has become an indispensable factor in our daily lives. Increasing productivity is essential to meeting this explosive demand. In order to do so, it is necessary to enhance efficiency in each manufacturing process and improve productivity by reducing the process time by introducing the latest technologies. One such effort is laser cutting of electrodes. The purpose of this study was to find suitable laser sources for the electrode cutting process using laser that had been studied for a long time, and to compare and prove the results after testing with two types of laser.

The positive electrode of a lithium-ion battery coated with $LiFePO_4$ on both sides of the Aluminum foil was tested and analyzed using two lasers. All possible parameters of each laser were tested, the results of each laser's parameters were compared, and the parameters showing good cut quality were found. For all the parameters tested, the cut edge and cross-section pictures were taken using SEM and microscope, and all four defined factors

for the cut quality evaluation were measured. The thickness of the thin samples made it difficult to measure the exact dimensions but tried to obtain the most accurate values. For all the parameters tested, SEM pictures and microscope were qualitatively assessed in order to see how the cut quality changed according to the parameter changes, and the measured values of the cut quality assessment factors were graphed and quantitatively evaluated. The cut samples were analyzed using EDX equipment to find out the changes in components after cutting around cut edge and cross section by selecting one of the samples tested with each laser. And tried to analyze the cause of phenomena theoretically from the perspective of laser-material interaction by selecting some of the results of each laser.

From the results of CW laser experiments, if the heat input is less than 0.2J/mm, Particle and debris are not visible around cut edge in all power intensities. And when power intensities are 1.44×10^8 W/cm^2 and above, the metal of cut edge is also smooth, and solidified melts are not covered in the cross section and look neat. In the same heat input, it can be seen that the higher the power intensity, the better the cut quality. when the heat input was approximately 0.2J/mm, the power intensity about 2×10^8 W/cm^2 showed the best cut quality in CW experiment. The principal causes of the results of the CW experiment assumed that the relatively low peak power and the resulting power intensity caused incomplete evaporation and that boiling became the main mechanism of the material removal, leaving the larger size of droplets around the cut line.

From the results of Pulsed laser experiments, especially noticeable is the metal edges that are uneven and protrude in many places. And the exposed metal color is darker than the CW results. overall the cut section is covered with material of re-solidified molten, the width of the metal is excessively expanded, and its shape is very rough. It shows better quality at 60ns and 90ns

than 30ns, and at 600kHz and 800kHz of 90ns, there are fewer parts around cut edges, and the width of HAZs is narrow. the best result is observed at 90ns, 600kHz, 800 ~1000mm/sec. and the other physical values are pulse energy 0.33mJ, power intensity $1.06x10^9 W/cm^2$ and overlap rate of 93.7%. it is evident that different laser-material interactions occurred at 30ns and 90ns. At 30ns the samples would have been subjected to a violent response due to the high-power intensity, and at 90ns the lower power intensity would have given a relatively benign response. It is assumed that the material removal mechanism at 30ns is 'vaporization' and 'boiling' at 90ns. In other words, theoretically, the different ablation mechanism took place at each pulse duration.

Based on this study, it was found that the results of CW are superior to the results of pulsed, given the lasers used in this experiment. If the goal of this study is to find which ablation mechanism is appropriate for cut quality, then it seems that the ablation mechanism occurred in the CW experiment was more appropriate for cathode electrode of $LiFePO_4$ battery.

Keyword : Laser, Cutting, Lithium ion Battery, Cathode Electrode, $LiFePO_4$
Student Number : 2017-22506

Table of Contents

List of Figures

List of Graph

List of Table

Chapter 1

Introduction

1.1 Background of Study

International agreements on restrictions on the use of fossil fuels and global interest in environmentally friendly energy have accelerated the development of renewable energy sources. As a result of such efforts, Li-Ion Battery first appeared in the early 1990s. It has been developed along with the growth of mobile electronic devices, and it has become an indispensable element in our everyday life. The development of various Li-ion-based battery materials has expanded the range of batteries to suit their applications. Li-ion Batteries are used in low-capacity batteries for mobile devices such as smart phones and notebooks, in high-capacity batteries such as electric vehicles, and energy storage system(ESS) and also the different materials of Li-ion batteries are used in consideration of the characteristics of each application. As the era of smart mobile devices, electric vehicles, and energy storage system is coming, the demand for Li-ion batteries is explosively increasing. In order to meet such demand, productivity improvement is essential. To do so, battery manufacturers are introducing the latest technologies to increase efficiency and shorten process times to improve productivity. One such effort is to apply a laser to electrode cutting of Li-ion batteries.

Until now, the sample has been cut using a mechanical knife, but a physical device such as a knife has to have direct contact with the sample, and the knife blade is dull by cutting the metal contained in the electrode. It is essential to periodically resharpen knife blades or replace them, and can’t not help avoid stopping the production process in order to avoid the problem of cut quality being altered by a dull knife blade. The current disadvantage of this mechanical punching raises the

unit price of the battery, and it is necessary to reduce the production cost and improve the productivity by introducing a new process. In order to overcome the disadvantages of the conventional process, electrode cutting using a laser was attempted. Because of its many advantages, Lasers are used in various processes in various industries and has been becoming a reliable process tool. The application of the laser process would be an alternative for battery manufacturers because it can be a breakthrough in the production of Li-ion batteries.

1.2 Purpose of Research

The electrode cutting of Li ion batteries using laser was first attempted about 10 years ago. At that time, there were not enough suitable lasers to apply for electrode cutting. Only low-power pulsed lasers and single mode lasers could be used. At first, it was difficult to find a cut quality acceptable as a limit to the available laser. It was concluded that it was possible to simply cut and the laser power required for the process was inferred from the experimental results. Since then, the development of laser sources has been taken place rapidly, and high-power pulsed and single mode lasers have become available.

Until now, laser electrode cutting has been mainly conducted using pulsed lasers, and for anode electrode, acceptable results were found with pulsed laser. However, for cathode electrode, there has been many studies using various pulsed lasers for a long period of time, but unlike anode, a good cut quality has not been achieved. Studies using single mode CW lasers were mostly excluded from the time after the initial low power experiments. The slow progression in the cathode electrode may be due to the inadequacy of the laser used in the research so far and the material properties may not be suitable for the laser process. However, materials can not be changed, but Laser has a wide range of options.

Therefore, this study is limited to $LiFePO_4$ which is one of the cathode electrode

material, and this research is to conduct experiments by using CW laser which has been neglected so far and pulsed laser which has been studied for a long time. The purpose of this study was to investigate the causes of physical phenomena by comparing and analyzing the results of experiments using two types of laser, and to find out more suitable cutting mechanism and laser.

Chapter 2

Fundamentals of Laser

2.1 Introduction to LASER

A LASER is a device that emits light through a process of optical amplification based on the stimulated emission of electromagnetic radiation. The term "LASER" originated as an acronym for "Light Amplification by Stimulated Emission of Radiation".[1] Laser not only amplifies or increases the intensity of light but also generates the light. Laser emits light through a process called stimulated emission of radiation which amplifies or increases the intensity of light. Some lasers generate visible light but others generate ultraviolet or infrared rays which are invisible.[2]

Type	Laser	Wavelength
Gas	Helium Neon (HeNe)	632nm
	Helium Cadmium (HeCd)	422nm
	Argon Ion (Ar)	488, 514nm
	Krypton Ion (Kr)	647nm
	Carbon Dioxide (CO_2)	10600nm
	Nitrogen (N)	337nm
	Xenon Chloride (XeCl)	308nm
	Krypton Fluoride (KrF)	248nm
	Xenon Fluoride (XeF)	350nm
	Argon Fluoride (ArF)	193nm
Sold State	Ruby	694nm
	Neodyum:YAG (Nd:YAG)	1064nm 532nm 266nm
	Neodium:Glass (Nd:Glass)	1064nm
Fiber	Ytterbium (Yb) Erbium (Er) Thulium (Tm)	1030~1120nm 1550nm 1940nm
Disk	Yetterbium:YAG (Yb:YAG)	1030nm
Slab	Carbon (Laser Crystal)	10600nm
Semi-Conductor	GaN	400~450nm
	GaAlAs	600~900nm
	InGaAsP	1100~1600nm
Liquid (Dye)	Various Dyes	300~1800nm 1100~1600nm

Table 2-1: Lasers categorization, revised from[57]

Lasers are categorized on the basis of the “active medium” used to generate the laser beam. This medium may be a solid, liquid or a gas. Lasers with a solid medium are divided into crystal-type solids, termed solid state lasers, and semiconductor lasers. The following table lists some typical lasers and the wavelengths emitted by them. [57]

2.2 Operation fundamentals

In the view of quantum physics, The energy levels of atoms are known as quantum states.[4] Electrons within an atom can change their states. Light or energy is emitted as an electron moves from a higher level to a lower level and is absorbed when the reverse transition takes place.[3] Those two specific energy levels of an atom are illustrated in Figure 1-1.[1]

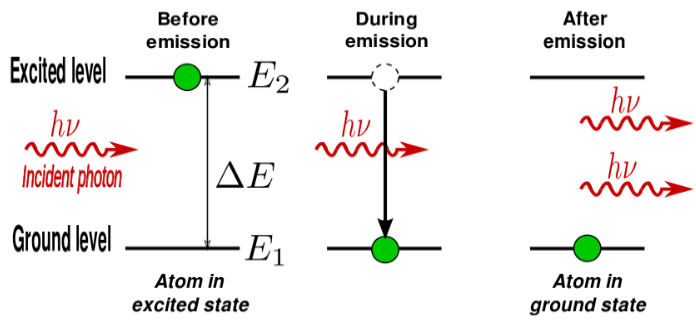

Figure 2-1: Schematic of laser amplification in atomic energy states

$$E_2 - E_1 = \Delta E$$

$$= \frac{hc}{\lambda} = h\nu$$

where c is the velocity of light = 3×10^8 (exactly 299, 792, 458) m/s, λ is the wavelength(m), h is Plank’s constant(4.135667×10^{-15} eV.s), ν is the frequency of transition between the energy levels (Hz), and $\_E$ is the energy difference between the levels of interest.[3]

2.2.1 Absorption of radiation

Absorption of radiation is the process by which electrons in the ground state absorbs energy from photons to jump into the higher energy level. There are two energy levels E1, E2 of electrons depicted in Figure 2. the electrons in the lower energy state need sufficient energy in order jump into the higher energy state. the ground state electrons gains sufficient energy and jumps from ground state (E_1) to the excited state (E_2). The absorption of radiation or light occurs only if the energy of incident photon exactly matches the energy difference of the two energy levels ($E_2 - E_1$). [2]

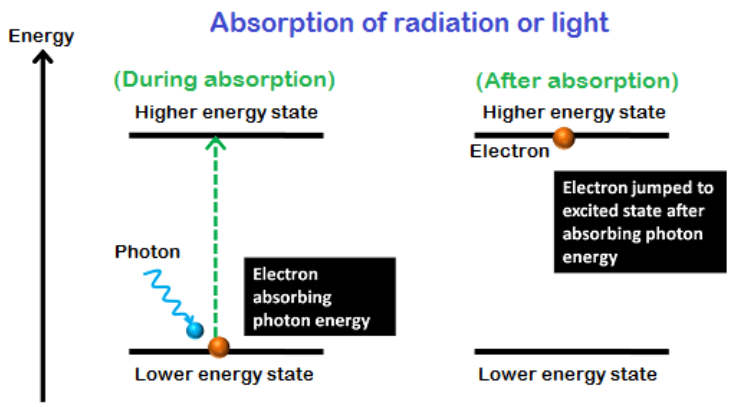

Figure 2-2: Schematics of Absorption of radiation or light [2]

2.2.2 Spontaneous radiation

Spontaneous emission is the process by which excited electrons return to the ground state through emitting light. [2] When an electron is excited from a lower energy level (E1) to higher energy level, it can not be maintained forever. The electrons in the excited state can decay to a lower energy state, which is not occupied by a specific time constant that characterizes the transition. Natural decay take place without external influence, emitting light, is called Spontaneous emission [1]

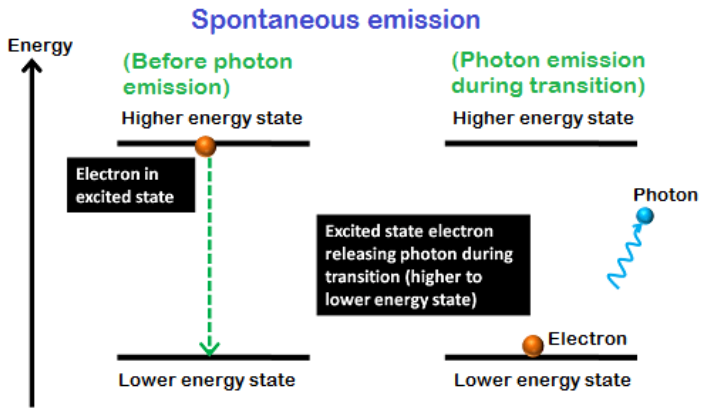

Figure 2-3: Schematics of spontaneous emission [2]

The photons emitted in spontaneous emission process constitute ordinary incoherent light. In other words, the photons emitted in the spontaneous emission process do not flow exactly in the same direction of incident photons.[2]

2.2.3 Stimulated emission

Stimulated emission is the process by which incident photon interacts with the excited electron and forces it to return to the ground state. In stimulated emission, the light energy is supplied directly to the excited electron instead of supplying light energy to the ground state electrons.[2]

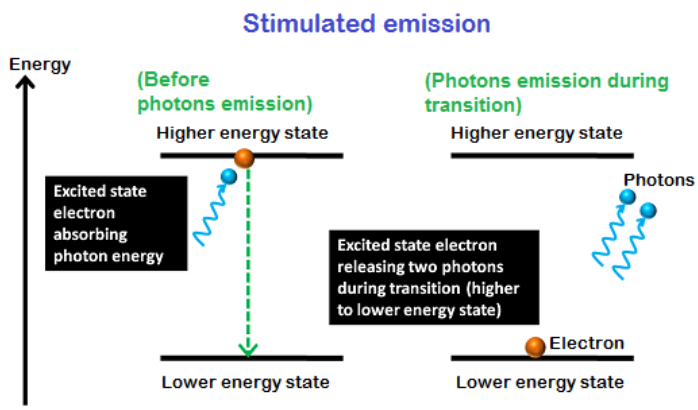

Figure 2-4: Schematics of stimulated emission [2]

Unlike the spontaneous emission, the stimulated emission is not a natural process it is an artificial process. In spontaneous emission, the electrons in the excited state will remain there until its lifetime is over. After completing their lifetime, they return to the ground state by releasing energy in the form of light. [2]

2.2.4 Population inversion

If N1 is the number of atoms at the lower energy state(E1) and N2 at the higher energy state(E2), The condition where N2 >N1 with more atoms existing at the higher energy level than at the lower energy level is referred to as population inversion. Population reversal does not occur under normal thermal equilibrium conditions. In order it to be possible, the atoms in the laser medium must be excited or pumped in the non-equilibrium state. This is done with a significant amount of

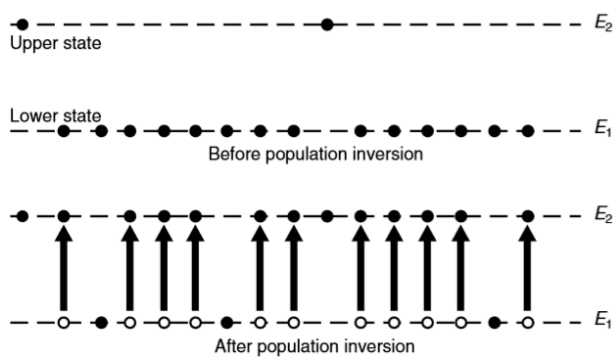

Figure 2-5: Schematics of population inversion[3]

energy fused into the medium using an external source. This process increases the number of atoms at higher levels while reducing the number of atoms at lower energy levels. [3]

2.2.5 Amplification

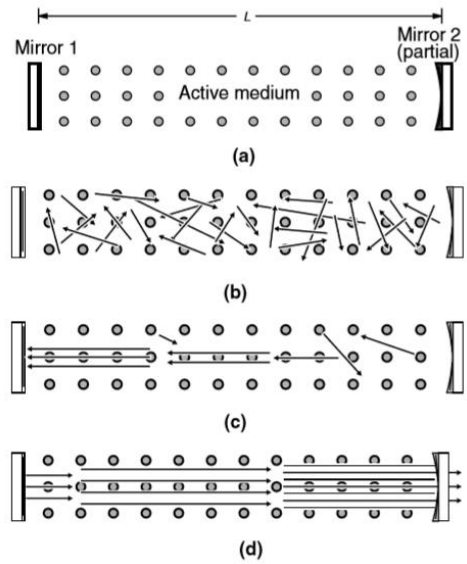

Figure 2-6: Schematics of Amplification [3]

In a real laser, the active medium is typically placed between two mirrors, which together form a resonator (Figure 2-6a). Initially, spontaneous emission causes photons to be generated in all directions (Figure 2-6b). However, when the stimulated emission becomes significant, electromagnetic waves traveling along the resonator axis oscillate between the two mirrors (Figure 2-6c). When a population inversion is present, the radiation is amplified every time it passes through the medium that results in the accumulation of signal intensity (Figure 2-6d). A useful output beam is obtained by making one of the mirrors partially transparent. This output beam is the laser from the system. [3]

2.3 Fiber Laser Fundamentals

Although the first report of the fiber laser was manifested in early 1960s by Snitzer et al., it started its journey into the commercial field in mid-1990s after the invention of cladding pump principle by H. M. Pask et al.[5, 6, 7]

Finally in 2009, IPG Photonics Inc. developed and commercialized a single-mode all-fiber laser system with a record power of 10 kW. In addition to this, development

of a 100 kW multimode fiber laser was reported at ~1 μm wavelength in 2012 which is the highest ever power from a solid state laser to date. [5, 8]

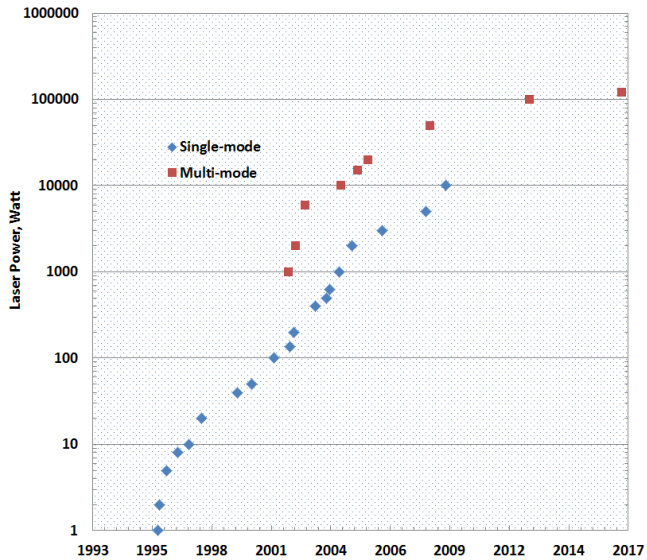

Figure 2-7: Power scaling history of Fiber laser [12]

This remarkable advances in fiber laser technology in past two decades have rapidly blown up its market demand around the world. The advantages of fiber lasers – compactness, high average power, excellent beam quality, longer lifetime, easy handling capability, high efficiency and low maintenance cost. A significant number of fiber laser based technologies have been commercialized in recent past because of their remarkable impacts in wide application ranges. For last several years fiber laser market has exhibited highest growth among all laser technologies and continuing on that path. [5,9,10]

2.3.1 Characteristics of Optical Fiber

Fiber lasers are a variation of standard solid state lasers, with clad fiber as a laser medium rather than rod, slab or disk. Laser light is emitted by the dopant at the center core of the fiber, and the core structure ranges from simple to very complex. A key

feature of fiber lasers is the high surface to volume ratio of the fibers so that heat can be dissipated relatively easily. [11]

A fiber is a cylindrical dielectric waveguide consisting of an inner core and an outer cladding. It is mainly made of optically low loss materials such as quartz or silica glass. Light is guided from a built-in central core inside a cladding made of a material with a slightly lower refractive index than the core. From the point of view of ray optics, all incident rays at the boundary between the core and the cladding at an angle greater than the critical angle experience a total internal reflection. These rays are directed to the cladding through the core without bending. [13]

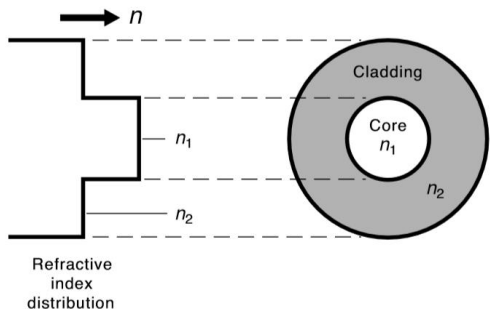

Figure 2-8: Basic structure of a fiber optic cable

1) Core: This is the inner portion through which light is transmitted and is made of transparent glass(or plastic) of relatively higher refractive index. Core diameters typically vary between 4um and 30um for single-mode fiber, and between 50um and 1000um for multimode fibers

2) Cladding: This is a concentric outer layer with a relatively low refractive index. This reduces scattering losses due to discontinuity on the core surface and prevents the core from absorbing surface contaminants. The cladding may also be a glass or plastic material. [3]

let the light incident on the optical fiber end angle θ with the waveguide axis. If θ is less than θa, the refracted light is incident on the core-cladding interface at an angle larger than the critical angle θc, resulting in total internal reflection, which is the

passing angle. Then the light remains in the core. At angles greater than θa, no internal reflection occurs and light propagates into the cladding. The incident light propagating within the core is more commonly defined using numerical aperture NA. This is the measurement value of the condensed or condensed light of the optical fiber and is defined as follows

$$\mathrm{NA} = \mathrm{Sin}\theta_a$$

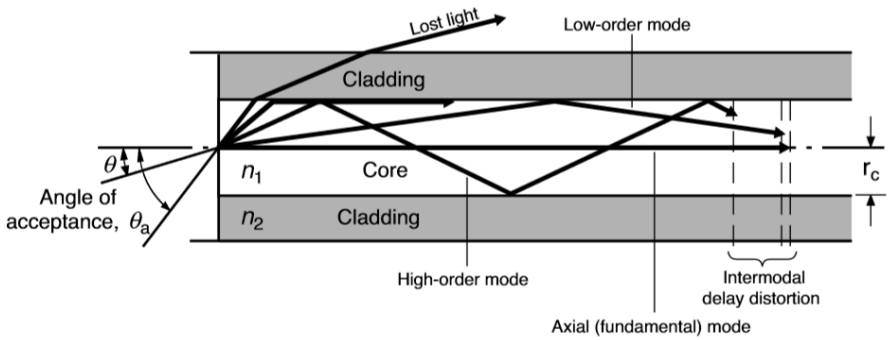

Figure 2-9: Propagation of a light ray in an optical fiber

This is given by

$$\mathrm{NA} = \sqrt{n_1^2 - n_2^2}$$

As the NA increases, the amount of light that can enter and stay inside the fiber increases. However, the bandwidth that can be transmitted decreases.

2.3.2 Fiber Laser Configuration

Diode pump sources can be many individual pump diodes, a single diode or an array. The doped fiber has a unique structure acting as cavity mirror at both ends. Indeed, these are fiber bragg gratings, which can be fabricated inside a fiber. There is no bulk optics at the end unless the output beam is anything other than fiber. Because the

fiber optic can be coiled, the laser cavity can be up to several meters long if desired. [11] The schematic of fiber laser is depicted in Figure 2-10.

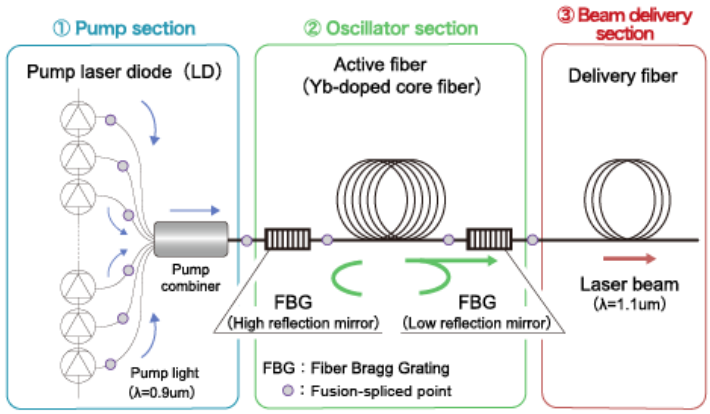

Figure 2-10: Schematic of fiber laser[14]

Fiber laser also has three components, such as traditional lasers. The optical circuit consists of three main sections: (1) a pump section, (2) an oscillator section, and (3) a beam delivery section.

(1) Pump section: The laser light from the pumping laser diode is passed through the optical fiber to the pump combiner. The pump coupler couples pump light from multiple LDs into a single mode fiber.

(2) Oscillator section: Pump light from pump coupler is propagated through double clad fiber (active fiber). The pump light excites Yb ions and is amplified by FBG (Fiber Bragg Gratings). The FBG acts like a mirror with high and low reflectivity. The laser light is emitted from the low reflectivity FBG.

(3) Beam transmission unit: composed of an optical fiber for passing laser light from the oscillator sector to a processing optics or a beam coupler. [14]

2.3.2.1 Pumping source

The pumping source in the fiber laser is laser diodes. Several diodes are coupled into one fiber and enter the active fiber. There are two types of diodes. One is a single emitter type, each of which serves as a source, and the other is bar stack type in the form of monolithic.

2.3.2.2 Active fiber

Fiber lasers are usually based on glass fibers doped with active rare earth ions. Plastic optical fibers are generally not used because they are generally absorbent, but are difficult to drink and are very sensitive to high light levels. Rare earth metal ions absorb pump light at wavelengths shorter than the laser wavelength, except in the case of up conversion fiber lasers. This allows optical amplification with stimulated emission. These doped fibers are called active fibers and are primarily high efficiency gain media due to their strong optical confinement. [13]

2.3.2.3 FBG (Fiber Bragg Grating)

The part that plays the role of mirrors at both ends of a traditional laser resonator is FBG. Laser light caused by stimulated emission, amplifies back and forth between the mirrors on both sides by making special changes to the fiber core. FBG is a longitudinal variation of refractive index in the core of an optical fiber illustrated in figure 2-11.

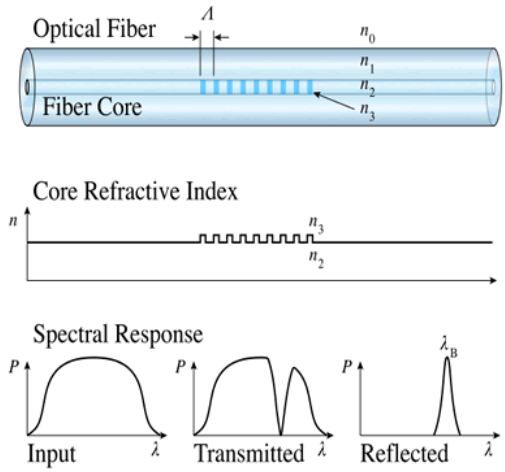

Figure 2-11: Fiber Bragg Grating structure, with refractive index profile and spectral response [16]

The refractive index of the fiber core is modulated at a period of λ. When light having a broad spectrum is emitted to one end of an optical fiber containing a fiber Bragg grating, a part of the light having a wavelength corresponding to the Bragg grating wavelength is reflected to the input end, with the rest of the light through to the other end. Figure 2-12 presents this reflection phenomena. [15]

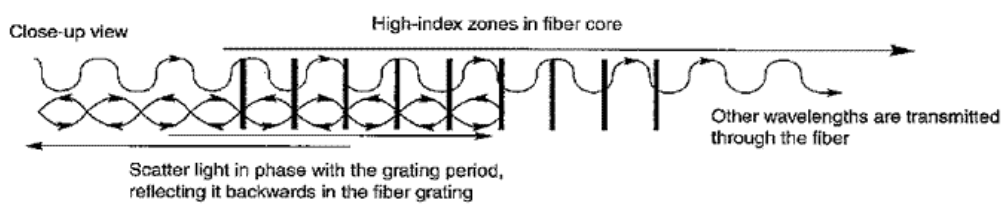

Figure 2-12: The reflection phenomena in FBG[15]

From the momentum conservation requirement of the Bragg grating condition, the following equation can be obtained:

$$2\left(\frac{2\pi n_e}{\lambda_B}\right) = \frac{2\pi}{\lambda}$$

where n_e is the effective refractive index of the fiber core, and λ_B is the wavelength of the light reflected by the Bragg grating. Therefore, the Bragg grating wavelength λ_B can be expressed as

$$\lambda_B = 2n_e\lambda$$

The effective refractive index quantifies the velocity of the propagating light compared to the velocity in the vacuum. n_e depends not only on the wavelength in the case of a multimode waveguide but also on the mode in which the light propagates. This is also known as a modal index. The fundamental principle behind the operation of fiber Bragg grating (FBG) is Fresnel reflection. Where light traveling between media of different refractive indices may both reflect and refract at the interface. [15,16]

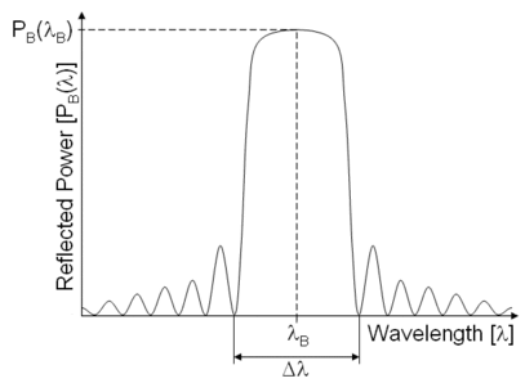

Figure 2-13: The reflection phenomena in FBG [16]

The wavelength spacing between the first minima, (as shown in above figure), or the bandwidth $\Delta\lambda$ is given by,

$$\Delta\lambda = [\frac{2\delta n_0 \eta}{\pi}]\lambda_B$$

Where δn_0 is the variation in the refractive index (n_3-n_2), and η is the fraction of power in the core. [16]

2.3.3 Fiber Laser Characteristics

2.3.3.1 CW Mode

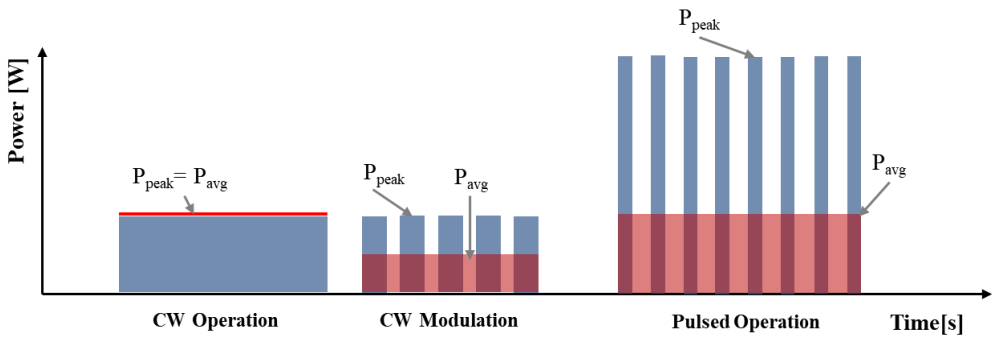

Figure 2-14: Operation mode (a) CW, (b) CW modulation, (c) Pulsed

CW has a constant power output during whole operation time, so the peak power is same with average power as shown in Figure 2-14(a). To obtain continuous emission, an equilibrium state must be obtained inside the laser between the energy transmitted to the gain medium through the pumping system, and the energy emitted by the laser. CW modulation can be obtained by blocking the beam of a CW laser to obtain the desired pulse duration and repetition as shown in Figure 2-14(b). [17]

2.3.3.2 Pulsed Mode

Pulsed emits a light of high peak power with short duration of time periodically. So pulsed laser has several parameters such as Peak power, Pulse duration, Pulse repetition rate.

1) Pulse Duration is the lasting time of one pulse and can also be described as full-width at half of the maximum (FWHM) amplitude of the laser pulse. The schematic of pulse duration is depicted in Figure 2-15.

2) Pulse repetition rate(PRR) or pulse repetition frequency refers to the number of pulses emitted per second and is represented by Hz, The time period T=1/Hz [17]

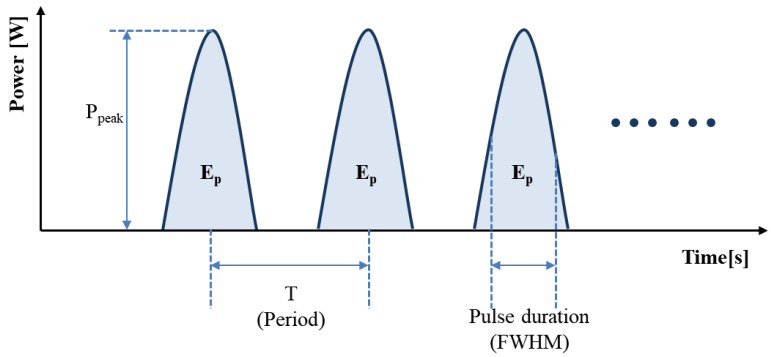

Figure 2-15: Definitions of pulse parameters

3) Peak power is the power of the highest point of pulse, which need to be distinguished from average power. It can be derived from $P_{Peak}=E_{pulse}/T_{width}$

4) Pulse energy is the energy of one pulse, which is same with the area of pulse shape in the Power-Time graph. It can also be calculated from $E_{pulse}=P_{avg}/PRR$

5) The pulse overlap rate is a percentage of the overlap of each pulse by the moving laser beam. It depends on the size of the beam, the moving speed of laser beam, and the pulse repetition rate. For pulsed laser cutting, the samples may be completely separated at or above a certain overlap rate, and the quality of the cut section is also affected by overlap rate.

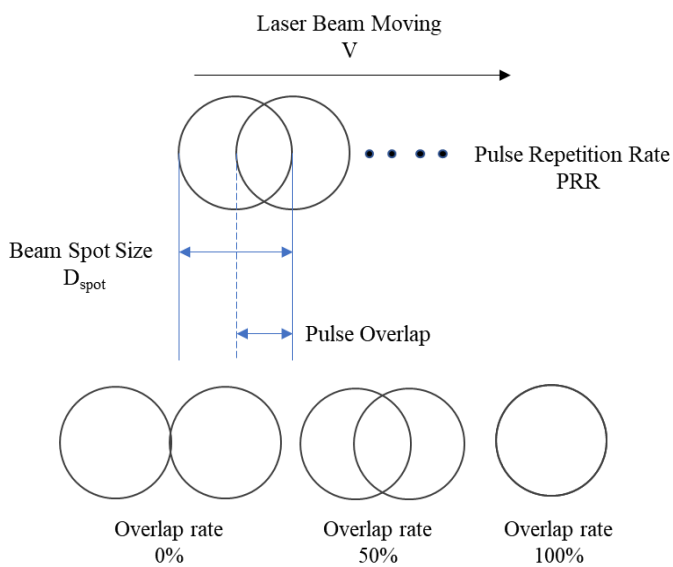

Figure 2-16: Schematics of definition of overlap rate

Pulse overlap rate can be calculated from

$$Pulse\ Overlap\ rate = \left(1 - \frac{v}{PRR \cdot D_{spot}}\right) \cdot 100\%$$

2.3.3.3 Single mode vs Multi mode Fiber

Beams of fiber lasers are divided into single mode and multimode depending on the classification by the core size. The mode means optical paths where light travels along the core. Thus, single mode means one optical path because the narrow core accepts only small portion of incoming light, whereas multimode has many optical paths because the core is wide enough to accept large portion of incoming light. As illustrated in Figure 2-17, Fiber consists of external cladding and internal core. Usually about fiber lasers, A core size less than 25um is referred to as single-mode fiber or beam, and a core size greater than 50um is referred to as multimode fiber or beam.

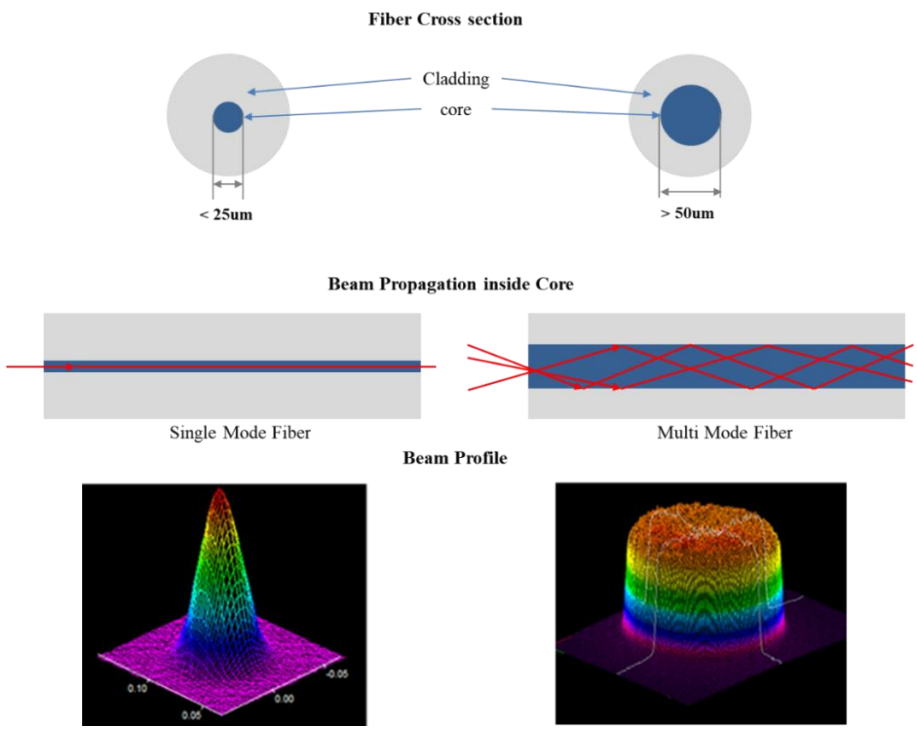

Figure 2-17: Single mode(left) vs Multimode(right) fiber & beam

These two modes differ in spatial intensity of the beam, with the single mode being closer to the Gaussian profile and the multimode showing similar intensity of the entire area, namely flat-top shape. In general, Single mode fiber with 14um core shows 1.05 of M^2, multi-mode with 50um core is approximately M^2=6 and M^2=12 for 100um core. The larger the fiber core, the greater the value of M^2.

2.4 Laser Beam Optics

2.4.1 Beam Propagation

In general, the laser beam propagation can be approximated assuming that it has an ideal Gaussian intensity profile corresponding to the theoretical TEM_{00} mode. However, the actual laser output is not Gaussian. To accommodate this dispersion, M^2 is defined to account for the deflection of the laser beam from the theoretical Gaussian. In the theoretical Gaussian case, M^2=1, but the actual laser beam is always M^2> 1. In all cases, the M^2 factor affects the characteristics of the laser beam and cannot be ignored in optical design.

In TEM_{00} mode, the beam emitted from a laser begins as a perfect plane wave with a Gaussian transverse irradiance profile as shown Figure 2-18(a).

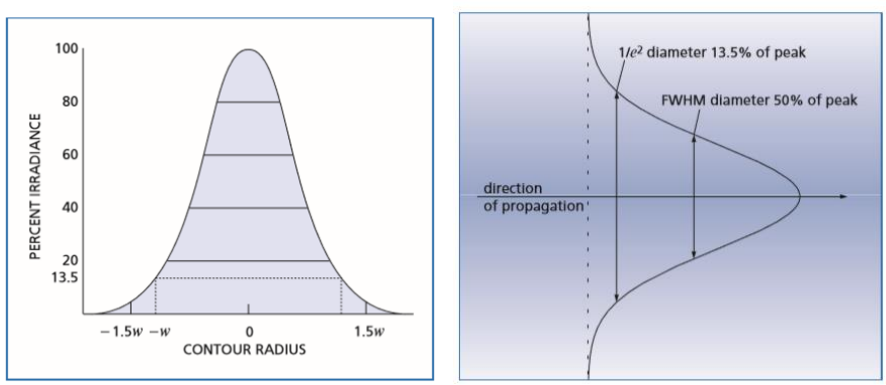

Figure 2-18: (a)Irradiance profile and (b) Diameter of Gaussian beam

The Gaussian shape is cut at some diameter by the internal dimensions of the laser or by the limiting opening of the optical train. It must be defined the diameter in some way to specify and discuss the transmission characteristics of the laser beam. There are generally two acceptable definitions. One is the diameter at which the beam radiation falls to $1/e^2$ (13.5%) of its peak, and the other is the diameter at which the beam radiation falls to 50% of its peak, which is also FWHM (full width half maximum). Generally beam diameter $1/e^2$ definition is widely used.

Diffraction makes it possible to have a perfectly collimated beam, as the wave propagates horizontally when the wave propagates. The diffraction of the laser beam exactly matches the prediction of pure diffraction theory. Even though the Gaussian TEM_{00} beam-wavefront is perfectly flat in some planes, it quickly gains curvature

$$w(z) = w_0 \left[1 + \left(\frac{\lambda z}{\pi {w_0}^2}\right)^2\right]^{1/2}$$

where z is the distance propagated from the plane where the wave-front is flat, λ is the wavelength of laser beam, w_0 is the radius of the $1/e^2$ irradiance contour at the plane where the wave-front is flat, w(z) is the radius of the $1/e^2$ contour after the wave has propagated a distance z. But, real laser beam is differs from ideal Gaussian beam by the factor of M^2, So the equation needs to be modified as follows.

$$w(z) = w_0 \left[1 + \left(\frac{\lambda z \cdot M^2}{\pi {w_0}^2}\right)^2\right]^{1/2}$$

Figure 2-19 illustrates changes in wave front radius with propagation distance.

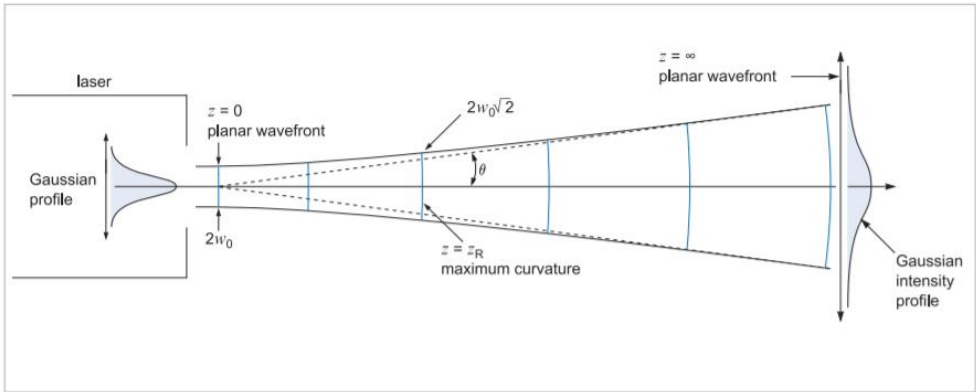

Figure 2-19: Changes in wave-front radius with propagation distance

2.4.2 Divergence

The Gaussian beam does not diverge linearly. Generally, the beam divergence angle near the beam waist is very small. However, when moving away from the waist, the divergence angle approaches the asymptote limit. Generally, the divergence angle refers to the far-field angular radius of half angle divergence of the Gaussian beam. The vertex of the cone is centered on the waist as shown in Figure 2-19.

w(z) asymptotically approaches the value for large z,

$$\mathrm{w(z)} = \frac{\lambda z}{\pi w_0}$$

the divergence angle θ depicted with dotted line in figure 18 approaches the value

$$\theta = \frac{w(z)}{z} = \frac{\lambda}{\pi w_0}$$

2.4.3 Raleigh range or length

(z_R) defined as the distance over which the beam radius spreads by a factor of $\sqrt{2}$, is given by

$$z_R = \frac{\pi {w_0}^2}{\lambda}$$

Also, considering real laser beam, it needs to incorporating M^2 factor.

$$z_R = \frac{\pi {w_0}^2}{\lambda \cdot M^2}$$

The Raleigh range considered to be the dividing line between near field divergence and mid-range divergence, is the distance from the waist at which the wave front curvature is maximum. Also, another special meaning of Raleigh range is the distance of twice the area of the beam spot size. So beam intensity is half the focused point. There are many people who define this as DOF(Depth of Focus)

2.4.4 Beam Spot Size

There are two kind of laser output, that is, collimated and diverging beam. So there are two ways to get a beam spot size.

① Collimated Beam output

In case the collimated beam into focusing lens, the calculation of the beam spot size is as follows.

$$D_{spot} = \frac{4 \cdot f_{foc} \cdot \lambda \cdot M^2}{\pi \cdot D_{Col}}$$

Where D_{spot} is spot size at focus point, D_{col} is the collimated input beam size, f_{foc} is the focal length of the lens. Figure 2-20 illustrated collimated beam input to focusing lens.

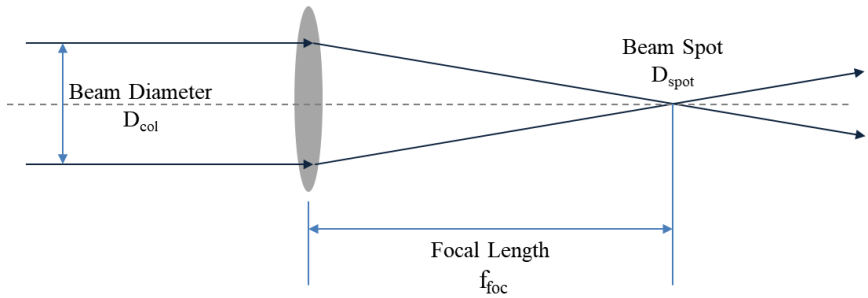

Figure 2-20: Schematic of collimated beam input to focusing lens

② Diverging Beam output

The output of most IR high power lasers is in the form of delivering beam. Therefore, most processing optics consist of a combination of collimating and locating lens. In this case, the beam spot size can be obtained as follows. Figure 2-21 illustrated diverging beam input to collimating and focusing lens.

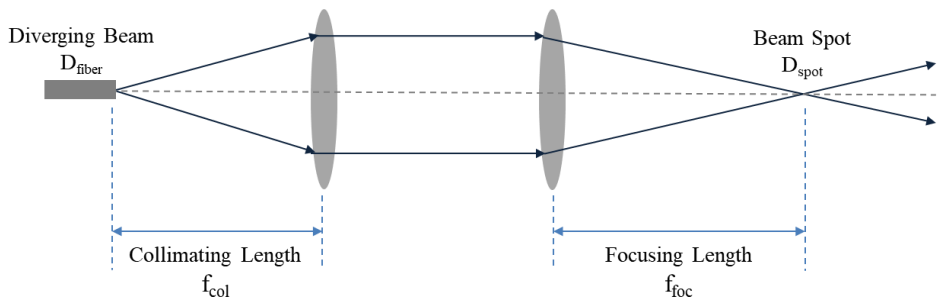

Figure 2-21: Schematic of diverging beam input to collimating and focusing lens

Optics magnitude is

$$\mathrm{M} = \frac{f_{foc}}{f_{col}}$$

Then the beam spot size is

$$D_{spot} = D_{fiber} \cdot M = D_{fiber} \cdot \frac{f_{foc}}{f_{col}}$$

2.4.5 Beam Quality

2.4.5.1 BPP(Beam Parameter Product)

BPP is a quality factor of a laser beam and it represents how small it can make a focused beam spot. It is the product of Divergence angle(half-angle) and Radius of the laser beam at its beam waist. Figure 2-22 illustrates beam propagation around focusing point.

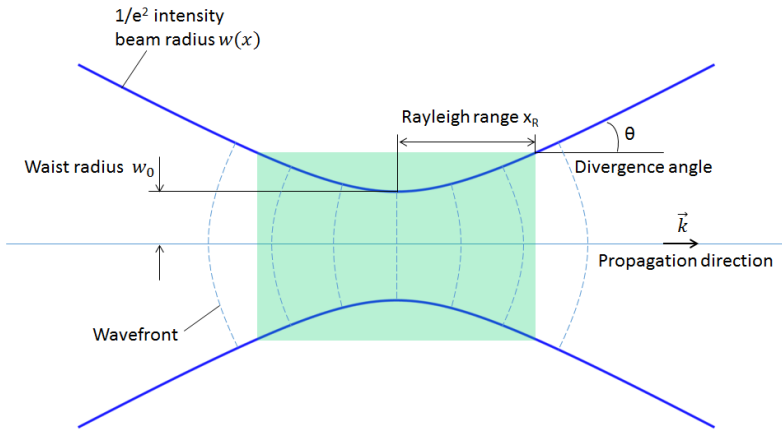

Figure 2-22 : Geometry of laser beam propagation around focusing point [19]

$$BPP = w_0 \cdot \theta \ [mm \cdot mrad]$$

2.4.5.2 M^2

As another factor of measuring beam quality, a dimensionless beam propagation parameter was developed in 1970s, based on the fact that for any given laser beam the product of the beam waist radius(w_0) and the far-field divergence (θ) are constant as the beam propagates through an optical system and the ratio [20]

$$M^2 = \frac{w_{0R}\theta_R}{w_0\theta}$$

Where w_{0R} and θ_R, the beam waist and far-field divergence of the actual beam, respectively is an accurately representation of the propagation characteristics of the beam. For a true gaussian beam $M^2=1$.

The concept of an 'Embedded Gaussian' shown in figure 2-25, is useful to understand real beam. A mixed-mode beam that has a waist M times larger than the embedded Gaussian will propagate with a divergence M times greater than the embedded Gaussian. Consequently the beam diameter of the embedded Gaussian, but it will have the same radius of curvature and the same Rayleigh range(z=R).

$$M^2 = \frac{Mw_{0R} \cdot M\theta_R}{w_0\theta}$$

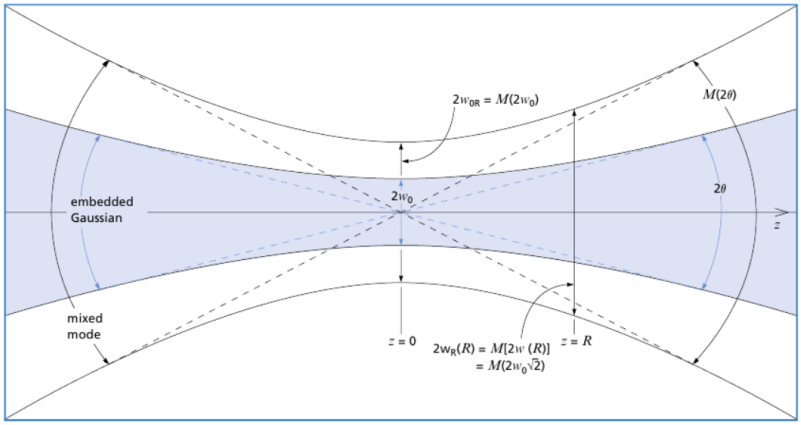

Figure 2-23: The embedded Gaussian beam [20]

We defined M^2 before. For a pure Gaussian beam, M^2=1, and the beam-waist beam-divergence product is given by

$$w_0\theta = \lambda/\pi$$

It follows then that for a real laser beam,

$$w_{0R}\theta_R = \frac{M^2\lambda}{\pi} > \frac{\lambda}{\pi}$$

Then, the relation between BPP and M^2 becomes

$$\text{BPP} = \frac{M^2\lambda}{\pi} \ [mm \cdot mrad]$$

2.4.5.3 The significance of Beam Quality

One of the main characteristics of high-power lasers is excellent beam quality at high power. Figure 2-24 summarizes the benefits of high-quality beams in material processing. For the same collimated beam size, a higher spot quality emission results in a smaller spot size in the workpiece [2-24 (a)]. Or, for the same spot size in the workpiece, the higher the beam quality, the smaller and lighter the focusing beam

optics are required. This leads to lighter processing heads and higher throughput rates. 2-24 (b)]. Finally, remote beam processing is possible because the same beam size and focusing optics and beams with higher beam quality for the same spot size can be focused far away. 2-24 (c)]. [22]

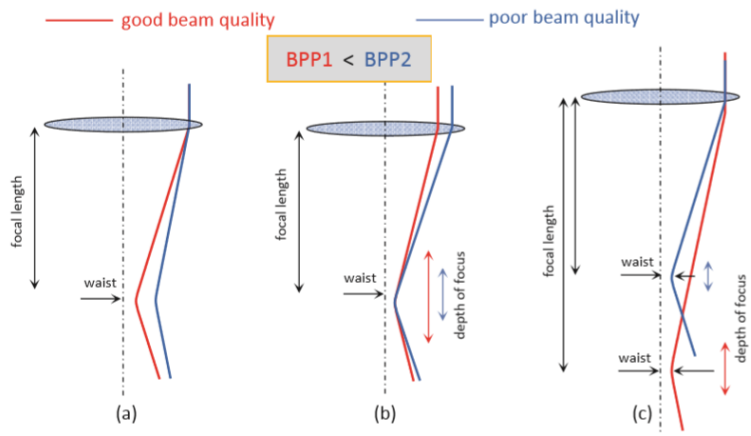

Figure 2-24: Impact of good beam quality on material processing [22]

BPPs of typical lasers are compared in figure 2-25 by O'Neill [23]. This graph shows the extent to which the beam spreads with respect to the distance, when it is made in the same beam size at the focus position. Fiber lasers with the smallest BPP can be found to have no significant change in beam size beyond the focus position. The advantages of this excellent beam quality were reviewed earlier.

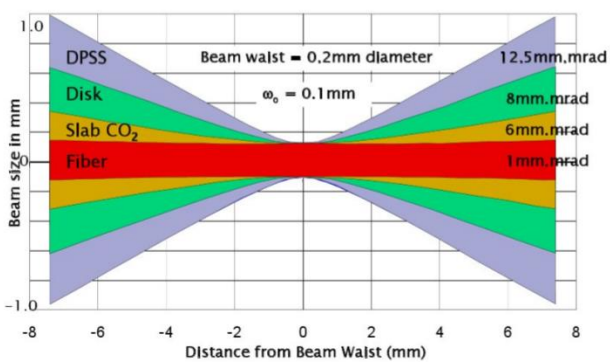

Figure 2-25: Comparison of BPP for typical lasers [23]

2.5.6 Depth of Focus

DOF(Depth Of Focus) is the distance over which the focal spot size changes to some extent. The extent may vary depending on users. Some consider Raleigh range to be a DOF, while others consider ±5% change of the beam spot size to be a DOF.

Raleigh range is

$$z_R = \frac{\pi {w_0}^2}{\lambda \cdot M^2}$$

If the allowable degree of spot size variation is to be ±5%, substituting $w(z)_0=1.05w_0$ into the w(z) equation and solve for z=Δz,

$$\Delta z \approx \pm \frac{0.32\pi {w_0}^2}{\lambda \cdot M^2}$$

Another definition of DOF is the beam size over which 80% of the power intensity at the focal point is maintained. that is [3]

$$\Delta z \approx \pm \frac{\pi {w_0}^2}{4 \cdot \lambda \cdot M^2}$$

2.6 Laser Material Processing

The laser beam is the heat source for laser material processing. Although lasers are generally regarded as light sources, they are a form of energy and can be a useful source of intense heat when focusing. Because lasers have lower monochromatic, coherent, and divergent characteristics than typical light sources, they can produce high energy concentrations. As a result, most materials can be used to heat, melt and evaporate. Processes in which lasers are commonly used include welding, cutting, surface modification (including heat treatment) and forming. The power intensities and exposure times required for various processes are shown in Figure 2-26. For a laser beam, the highest power density is achieved with the beam in the Gaussian (TEM00) mode. [3]

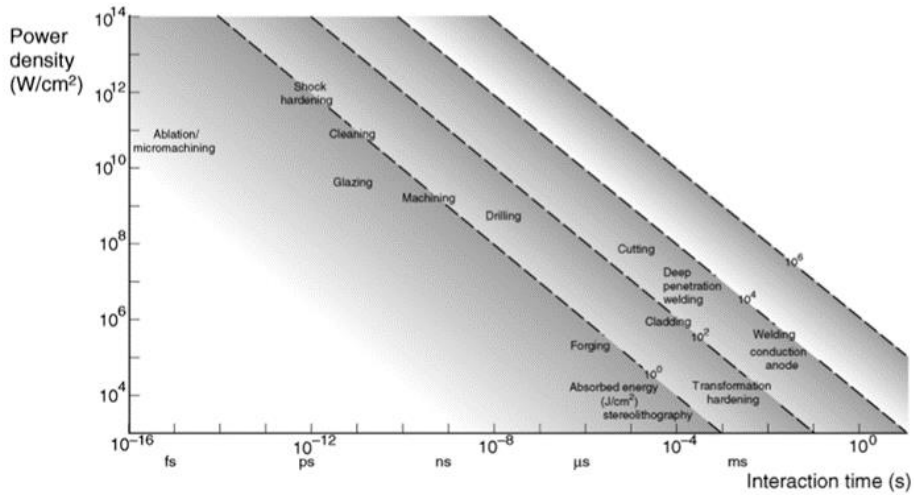

Figure 2-26: Power intensity and interaction times for various laser processes. [3]

2.6.1 Fusion cutting

Fusion cutting is characterized by melting the material and by expelling the melt respectively the with an external processing gas jet, coaxial to the laser beam. A high gas pressure is needed to expel melts and cut quality is affected by both gas pressure and standoff which is the distance between the end of nozzle and the workpiece surface. usually the nozzle is positioned close to the processing zone with a stand off between 0.3 and 1 mm above the workpiece surface. [25]

Usually, laser cutting in steel industries means fusion cutting. Cutting a wide steel plate into desired shape, mainly using CW laser and cutting head, takes up the largest part of the laser industry.

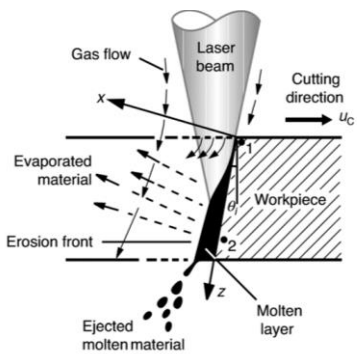

(a)

(b)

Figure 2-27: Schematic of (a) fusion cutting process [3], (b) Industrial cutting machine [Bystronic inc.]

2.6.2 Ablation Cutting (or Sublimation Cutting)

In ablation cutting, the workpiece material can be removed by vaporization or ablation leaving the material separated. Realizing ablation cutting, a special system technology is needed. A high-power laser beam is focused on the workpiece to a very small diameter under 50μm and the beam intensity should be more than 10^8 W/cm^2, which is enough to vaporize steel material. [25]

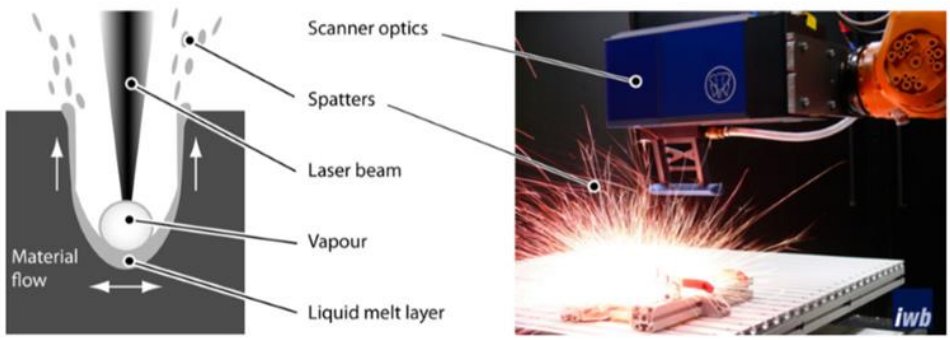

Figure 2-28: Schematic of (a) ablation cutting process, (b) ablation cutting using scanner [25]

Ablation cutting usually uses remote optics such as scanner because processing gas is not required. Scanner can manipulate laser beam very fast, with which moving speed can reach > 5000mm/sec. this cutting process is used to cut thin sheets such as thin steel plates, ceramics, and polymer films. Pulse lasers of under ns are usually used for ablation cutting to minimize the thermal effect and to achieve high processing speed taking advantages of scanner system. However, if the beam size can be made small enough, like SM mode, CW laser can also be used for the process.

Chapter 3

Lithium Ion Battery

3.1 Lithium-Ion Battery(LIB)

Secondary batteries refer to the battery that can be recharged and reused hundreds or more times even after being recharged. There are various types of secondary batteries such as, lead storage battery, nickel-cadmium battery, lithium-Ion battery etc. Lithium-ion batteries are the most capable battery for its excellent performance so that electronics with light weight and limited volume such as notebook, smartphone, camera, portable products and machines etc. have been used Li-ion batteries.

Restrictions on the use of fossil fuels and international interest in eco-friendly cars have accelerated the development of lithium-ion batteries, and PHEV and EV markets have grown since the first commercialization of hybrid vehicle in the 1990s. With the advent of the era of electric vehicles, the market for lithium ion batteries has been growing rapidly. As the energy storage system (ESS) industry, which is essential for maximizing the utilization of new and renewable energy, it is expected that the scope of use of secondary batteries and the market will explode.[25]

Lithium-ion batteries are increasingly being used to reduce prices and stabilize performance through mass production and technology development through standardization of products.

3.1.1 Li-Ion battery principles

The operating principle of Li-ion battery is illustrated in fig.3-1. Lithium ions extract from anode to insert in cathode in the discharge process. The reverse direction

of moving of ions is charging process. $FePO_4$ is the second phase that is present on electrochemical extraction of lithium from $LiFePO_4$. The extraction of lithium from $LiFePO_4$ to charge the cathode can be described by formula (1) and the insertion of lithium into FePO4 on discharge as formula (2). [25]

Charging Process : (1) LiFePO4 — xLi+ — xe- → xFePO4 + (1 — x)LiFePO4

Discharging Process : (2) FePO4 + xLi+ + xe- →xLiFePO4 + (1 — x)FePO4

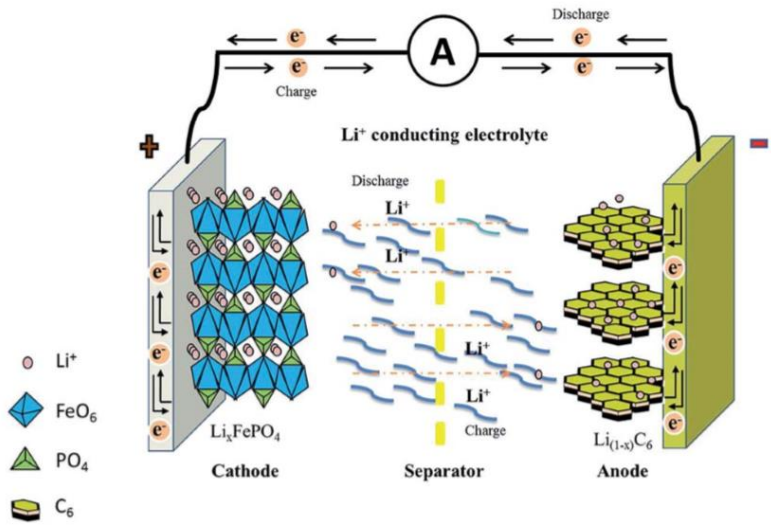

Figure 3-1: Schematic structure of Li-Ion battery [24]

A lithium-ion battery cell contains four main components as shown in Figure 3-1.

1) Cathode

The cathode electrode is a thin aluminum foil coated with the active material contains lithium ions that is added to increase conductivity and the adhesive binder which helps the active material and the conductive additive to settle well on the aluminum substrate. There are several active materials used for cathode materials such as, LiCoO2, LiMnO2, LiFePO4 etc.

Depending on the type of active material used for cathode, the battery's capacity and voltage are determined, so the cathode plays an important role in determining the characteristics of the battery.

The higher the amount of lithium, the greater the capacity. The greater the potential difference between negative and positive, the higher the voltage. The major requirements of a successful cathode material in a Li-ion battery are as follows

- High free energy of reaction with Lithium.
- Should be able to host lithium ions within its structure.
- The material should have less irreversible losses.
- Should have high lithium ion diffusivity.
- Should not react with electrolyte.
- Low cost of synthesis. [26, 27]

2) Anode

Anode electrodes are also a thin copper foil coated with graphite as an active substance. Anode's active material serves to allow the current to flow through an external circuit, allowing a reversible absorption/discharge of Lithium Ions emitted from cathodes. When the battery is charged, the lithium ions are stored in the cathode and not in the cathode. In this case, if the conductor connects the negative to the negative (discharge state), lithium ions are naturally reversed through an electrolyte to the negative, and electrons (e-) separated from the lithium ions move along the wire to generate electricity. The prerequisites for anode material in Li-ion batteries should be as follows.

- High capacity and energy density to handle Li ions.
- Good capacity retention capability.
- Reduced irreversible capacity loss in first few cycles.
- Low price and environmental friendly. [26, 27]

3) Electrolyte

Electrolyte is an important component. This serves as the medium for moving only lithium ions between the cathode and anode. A high ionic conductive substance is

mainly used as an electrolyte, which moves lithium ions back and forth easily.

The electrolyte consists of salt, solvents and additives. The salt is the passage through which lithium ions pass, and the solvent is the organic liquid used to dissolve the salt, and the additive is added in small quantities for a specific purpose. The electrolyte produced in this way allows the ion to move into the electrode and does not pass through the electron. The rate of movement of lithium ions also depends on the type of electrolyte. Therefore, only electrolytes that meet strict conditions can be used.

Based on the physical state of the electrolyte there are 3 types.

- Liquid Electrolyte (mixture of Li based salt with organic solvents).
- Gel Polymer Electrolyte (Polyethylene oxide, Polyacrylonitrile).
- Solid Electrolyte. [26, 27]

4) Separator

The separator acts as a physical barrier between the positive and negative. It prevents direct flow of electrons and carefully passes the micro-hole inside the ions only. Therefore, all physical and electrochemical conditions must be met. The separator that is currently commercially available is a synthetic resin such as polyethylene and polypropylene. The separator has to be chosen based on numerous criteria which are as follows

- It should be an electronic insulator.
- It should have minimal interactive resistance with the electrolyte.
- Physically and chemically stable, uniform thickness with high puncture strength. [26, 27]

3.1.2Types of Li-ion Battery

Lithium-ion batteries are usually called by the name of cathode material. There are several cathode materials that have been developed and commercialized so far. Briefly reviewing some cathode materials,

1)Lithium Cobalt Oxide($LiCoO_2$)

Lithium cobalt is widely used in applications such as cell phones, notebooks and digital cameras. The cell consists of a cobalt oxide for cathode and a graphite carbon for anode. The cathode electrode has a layered structure, and lithium ions move from the negative electrode to the positive electrode during discharging. The flow reverses during charging. Disadvantages of lithium cobalt are relatively short life span, low thermal stability and limited load performance. [28]

2)Lithium Manganese Oxide ($LiMn_2O_4$)

This structure forms a three-dimensional spinel structure that improves the ion flow of the electrode, thereby lowering internal resistance and improving current handling. Another advantage of spinel is its high thermal stability and improved safety, but cycle and calendar life are limited.

Lithium manganese is used in power tools, medical devices, hybrid and electric vehicles. [28]

3)Lithium Nickel Manganese Cobalt Oxide ($LiNiMnCoO_2$ or NMC)

Nickel-manganese-cobalt (NMC) is one of the most successful Li-ion batteries. Similar to Li-manganese, these systems can be tailored to serve as energy cells or power cells. Silicon-based anodes can reach over 4,000mAh, but have low loading capacity and low life cycle. Silicon added to graphite has its disadvantages of developing and contracting anode during charging and discharging, creating a cell that is mechanically unstable. NMC is the battery of choice for power tools, e-bikes and other electric powertrains. [28]

4)Lithium Iron Phosphate($LiFePO_4$)

Lithium Phosphate offers excellent electrochemical performance with low resistance. This is possible with nanoscale phosphate cathode materials. The main advantages are high current stability, long cycle life, high thermal stability, high safety and improved durability during abuse. Lithium Phosphate is more resistant to full charge conditions, and maintaining a high voltage over a long period of time is less stressful than other lithium ion batteries. As a compromise, the lower nominal voltage of 3.2 V / cell reduces the specific energy below the specific energy of cobalt mixed lithium ions. [28]

5)Lithium Titanate ($Li_4Ti_5O_{12}$)

Lithium titanate replaces graphite in the anode of a typical lithium-ion battery, and the material is formed into a spinel structure. The cathode can be lithium manganese oxide or NMC.

LTO has advantages over conventional cobalt-mixed Li- ions with graphite anodes by achieving zero strain characteristics, There is no SEI film formation and lithium plating during rapid charging and discharging at low temperatures. Thermal stability at high temperatures is superior to other lithium ion batteries. However, the battery is expensive. [28]

6)Lithium Nickel Cobalt Aluminum Oxide ($LiNiCoAlO_2$)

Lithium nickel cobalt aluminum oxide (NCA) batteries have been available for special use since 1999. It shares similarities with NMC by providing high specific energy, reasonably good specific power and long life. Safety and cost are moderate. NCA further improves chemical stability by the addition of aluminum as a further development of lithium nickel oxide. [28]

3.1.3 Comparison of characteristics of several Li-ion batteries

Figure 3-2 shows the six characteristics of various lithium-ion batteries compared to specific energy, specific power, safety, performance, life span, and cost. Because each battery has its advantages and disadvantages, its use may vary depending on its purpose.

The meanings of the six assessment items are as follows:

▪Safety for battery is a status of safe operation without thermal runaway which can be caused by an overcharged battery, too high discharge rates, or a short circuit.
▪Specific energy is a capacity for storing energy per kilogram of weight.
▪Specific power that batteries can deliver per kilogram of mass.
▪Life span has two measurement, cycle stability & overall age. Cycle stability is the number of times a battery can be fully charged and discharged before being degraded to 80% of its original capacity at full charge. Overall age is the number of years a battery can be expected to remain useful.
▪Performance means that batteries can be optimized for either high or low temperatures without any functional degradation. [28]

Figure 3-3 shows a table of all the measurable items of the current commercialized battery. Unlike Figure 3-2, which was evaluated qualitatively, it contains quantitative figures and more detailed evidence. It helps to understand an overview of Li-ion batteries.

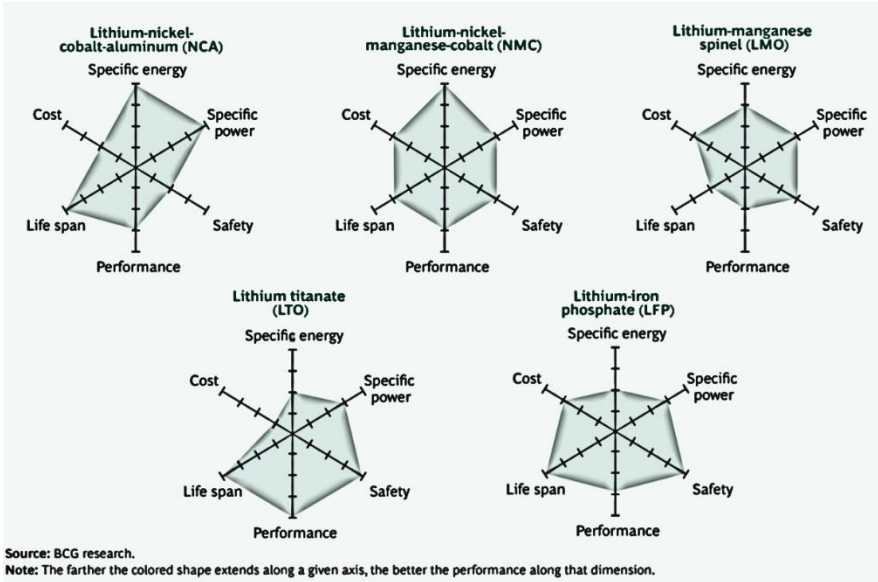

Figure 3-2: A comparison of cathode materials in Li-ion battery[28]

	Lithium Cobalt Oxide	Lithium Manganese Oxide	Lithium Nickel Manganese	Lithium Iron Phosphate	Lithium Nickel Cobalt Aluminum Oxide	Lithium Titanate
Chemistry	$LiCoO_2$	$LiMn_2O_4$	$LiNiMnCoO_2$	$LiFePo_4$	$LiNiCoAlO_2$	Li_2TiO_3
Abbreviation	LCO	LMO	NMC	LFP	NCA	LTO
Nominal voltage	3.60V	3.70V (3.80V)	3.60V (3.70V)	3.20, 3.30V	3.60V	2.40V
Full charge	4.20V	4.20V	4.20V (or higher)	3.65V	4.20V	2.85V
Full discharge	3.00V	3.00V	3.00V	2.50V	3.00V	1.80V
Minimal voltage	2.50V	2.50V	2.50V	2.00V	2.50V	1.50V (est.)
Specific Energy	150–200Wh/kg	100–150Wh/kg	150–220Wh/kg	90–120Wh/kg	200–260Wh/kg	70–80Wh/kg
Charge rate	0.7–1C (3h)	0.7–1C (3h)	0.7–1C (3h)	1C (3h)	1C	1C (5C max)
Discharge rate	1C (1h)	1C, 10C possible	1–2C	1C (25C pule)	1C	10C possible
Cycle life (ideal)	500–1000	300–700	1000–2000	1000–2000	500	3,000–7,000
Thermal runaway	150°C (higher when empty)	250°C (higher when empty)	210°C(higher when empty)	270°C (safe at full charge)	150°C (higher when empty)	One of safest Li-ion batteries
Safety	Low	Medium	Medium	High	Medium	High
Production Cost	Low	Low	Low	Medium	Low	Medium
Maintenance	Keep cool; store partially charged; prevent full charge cycles, use moderate charge and discharge currents					
Packaging (typical)	18650, Prismatic, Pouch cell	Prismatic	18650, Prismatic, Pouch cell	26650, Prismatic	18650	Prismatic
History	1991 (Sony)	1996	2008	1996	1999	2008
Applications	Mobile Phones, Tablets, Laptops, Cameras	Power tools, Medical devices, Powertrains	E-bikes, Medical devices, EVs, Industrial	Power tools, EVs Medical devices	Medical devices, Industrial, EV(Tesla)	UPS, EVs, Solar street lighting
Comments	High energy, limited power. Market share has stabilized.	High power, less capacity; safer than Li-cobalt; often mixed with NMC to improve performance.	High capacity and high power. Market share is increasing. Also NCM, CMN, MNC, MCN	Flat discharge voltage, high power low capacity, very safe; elevated self-discharge.	Highest capacity with moderate power. Similar to Li-cobalt.	Long life, fast charge, wide temperature range and safe. Low capacity, expensive.

Figure 3-3: Summary of Characteristics of Li-ion batteries, revised from [30]

3.2 Li-Ion Battery Cell Manufacturing Process

A lithium-ion battery consists of three types of foils: anode, cathode and separator. This semi-finished product is manufactured in the first phase of the value chain. The electrodes are manufactured from a coating process in which the active layer is applied to the copper for anode or aluminum for cathode foil. The separator consists of porous or perforated polymeric film typically extruded from polymeric particles. The next step is the cutting of the electrodes and the separator. For z-folding and single sheet stepping, pre-cut electrode sheets are required. For the subsequent stepping process, the separator foil shall be cut in advance. The cells are stacked during the next process step. Routine procedures commonly used are single-stacking, flat-winding or z-folding. The layered cells are then completed by combining conductors of copper and aluminum foil, packaging stacks, filling cells with electrolytes, and sealing packages under vacuum. Finally, the cell is formatted and sent to the (first charge) test and grading process station. Figure 3-4 shows a complete value chain for the production of lithium-ion batteries.[31]

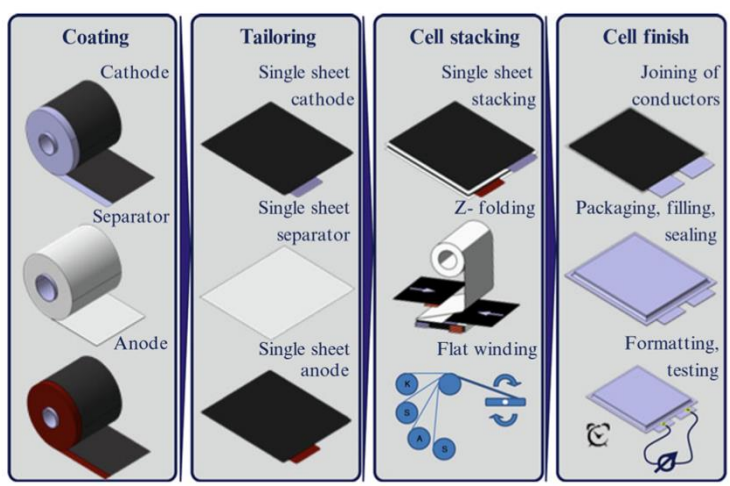

Figure 3-4: Process chain of manufacturing of Li ion battery cells [32]

3.3 Electrodes Cutting Process

Li ion batteries can be made in various types such as cylindrical (e.g. 18650, 26650), prismatic, button, and pouch type etc. as shown figure 3-5. This process is known as electrode cutting or tailoring or sizing. In the previous process, the electrodes are prepared with active materials coated on both sides of the aluminum and copper foils wrapped in a roll. Electrodes of anode and cathode wrapped in roll should be cut to match various battery sizes with a partially protrusion of each uncoated metal foil so that power can be connected out of the cell. Because three materials have to be cut in the same number to make a cell, this process takes long time and can be a bottle-neck process in battery manufacturing. This process is also very important as it is directly linked to safety such as battery failure and explosion and life span of battery, by the cut quality of electrodes. Therefore, this process should satisfy both cutting speed and cut quality.

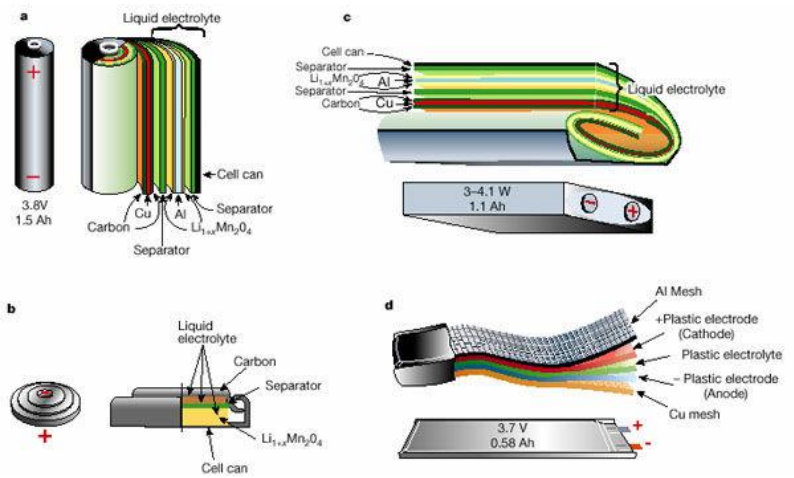

Figure 3-5: Various types of Li ion batteries

3.3.1 Mechanical Notching vs Laser Cutting

The shearing is a process of cold plastic deformation that consists in cutting metal foils through the action of shear forces between two form tools: the punch and the matrix, which may take various forms on the basis of' application. The sheet of

electrode comes from a roll and is placed on the sharp edge of the matrix, while the punch, moving from high downwards, notches the material with its sharp edge. Between punch and matrix is a well-defined gap, which gap will have to be constant along all the entire contour of the cutting edge to ensure good processing conditions, and to provide uniformity in the distribution of pressures resulting in uniform wear of the molds. [33]

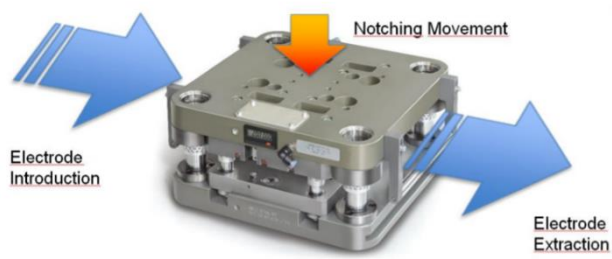

Figure 3-6: Mechanical notching tools [33]

It is was verified that after approximately one million cycles of the machine it is necessary to re-sharpen the blade. The initial investment cost on the notching machine will therefore depend on its daily production of electrodes. Assuming a high rate production, in 3 days presumably reaches the maximum limit of cycles beyond which it is necessary regrinding the tools. [33] In addition, it is inevitable that production will be discontinued during the equipment's maintenance and the design of the knife should be changed if the shape of the cut is changed. In this way, Green Lion[33] has reviewed that the maintenance costs of mechanical notching are significant. In addition, wear of the machine tools causes unstable process and poor cutting quality. These poor cutting qualities, characterized by edge bending, buzzing and flaking, can lead to fatal failure of the entire module as the main cause of short circuiting and high heat generation within the battery cell.[35] On the other hand, laser processing is recognized in the industry as a highly efficient and reliable manufacturing method, which is an alternative method of the mechanical notching process. Laser cutting is about three times of the initial investment cost according to

the article [33] because of the high price of the Laser and optics. However, Fiber lasers can be used almost indefinitely without the cost of maintenance, if there is no laser failure. Figure 3-7 shows the cumulative operation cost comparison between mechanical notching and Laser cutting.

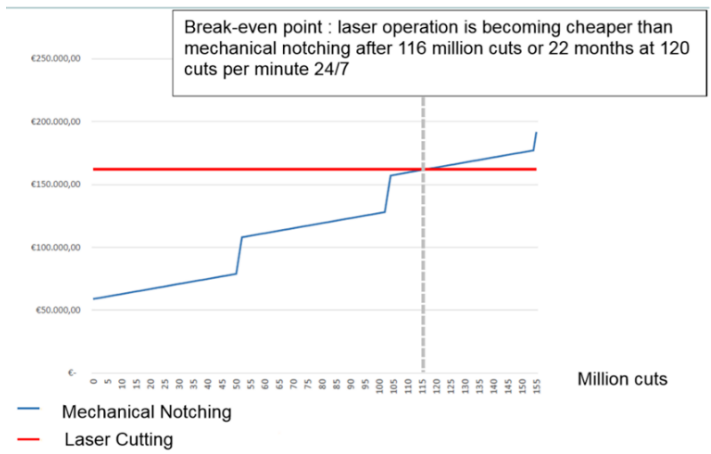

Figure 3-7: Cost comparison between mechanical notching and laser cutting [33]

The initial investment of the mechanical cutting machine is approximately 56,000 euros in the sum of the machine interface and the two notching tools. On the other hand, the initial investment in laser cutting is approximately 160,000 euros, including Laser and optics, the machine interface and fume collector. Assuming that the machine operates 24 hours a day, 7 days a week at a rate of 120 sheets per minute, the cumulative maintenance costs of the notching machine will exceed that of the laser machine from 22 months on. If production continues, laser cutting will be advantageous. [33]

The characteristics of mechanical notching and laser cutting reviewed earlier are summarized in Figure 3-8.

Mechanical Notching	Laser Cutting
	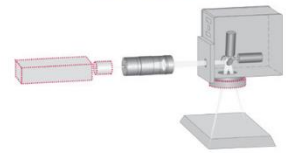
-Complex mechanical system -Contact process leads slight bending of cut edge -Need periodic maintenance for high tool wear and tool replacement -Need redesigning cutting tools when electrode shape changed -Can't be applied to Roll-to-Roll process	-Very simple system -Contactless process -No need periodic maintenance -Easy and fast change of cutting geometry And can cut complex geometries -Can be applied to Roll-to-Roll Process

Figure 3-8: Comparison characteristics of mechanical notching and laser cutting.

In order to cope with the rapid increase in battery demand, the development of the production process is essential and laser cutting is considered as an alternative to conventional mechanical cutting process. As laser cutting has many advantages, it is expected to be a breakthrough if process conditions are met the requirements.

Chapter 4

Literature Review

4.1 Literature review on laser electrode cutting

Some research has been reported on the electrode cutting of lithium-ion batteries using laser. The anode electrode with graphite coated on both sides of copper foil has been used so far without significant changes. In the case of anode, the application of the laser cutting process is visible. But the cathode electrode with lithium metal oxide coated on both sides of the aluminum foil has been developed and are changing constantly as previously reviewed. Differences in chemical components will obviously affect the quality of laser cutting, and several studies have been conducted on laser cutting of such cathode material.

Reviewing several studies on laser electrode cutting,

1) In the study of M. Luetke et al. [35] They defined the minimum cutting speed of 1 m/sec, which is comparable to mechanical punching and tried to find an appropriate laser power. They used two kinds of laser in experiments; CW 5000W with spot size 25um and Pulse 50W with 100ns, 50kHz & 100kHz with spot size 25um. Materials to be cut were coated on aluminum foils (cathode material) with a total thickness of 130μm with LMO active material and coated copper foils (anode material) with a thickness of 120μm. They found that CW 250W is sufficient to top the requested speed 1m/sec, and 3m/sec for the anode and 2m/sec for the cathode were achieved with 500W.

Based on the results of the pulsed 50W, They calculated the pulsed laser power capable of 1m/sec and concluded that a lase power in the range from 100W to 150W is need to cut cathode and anode at 1m/sec.

They also examined cutting quality within the entire irradiation area for CW lasers as well as pulsed lasers for which no significant defects were found. Some small, isolated bubbles in the micron range are observed. Consequently the appearance of the cutting edge itself can be stated as uncritically. Even at higher laser powers up to 5000 W cutting qualities in terms of clearance and frazzling width are acceptable.

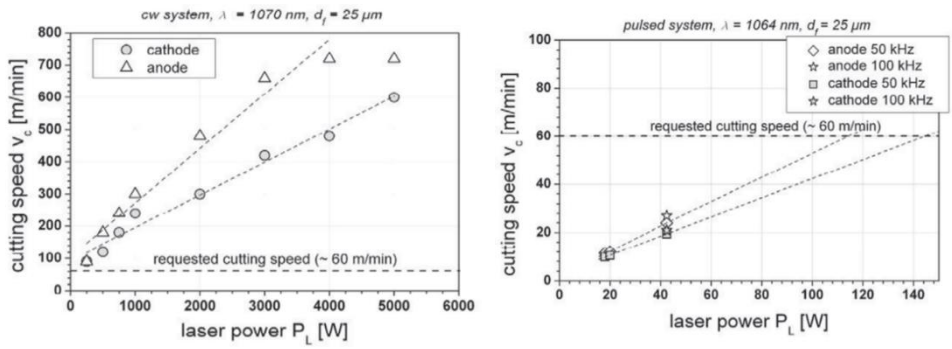

Figure 4-1: Cutting speed with CW(a), Pulsed(b) power variation [35]

For moderate laser powers typical values of the clearance width are around 20µm. The amounts of the frazzling width are close to 10µm. Summarizing about the cut quality, higher repetition rates and thus lower pulse energy and peak power are leading to slightly improved cutting speeds as well as a reduction in the overhang.

2) D. Lee et al.[36] investigated the numerical studies of the mathematical model for cutting of copper and aluminum foils used as current collector of the lithium-ion battery with a SM laser. They reviewed physical phenomena taking place on laser-material interaction including fluid flow, heat transfer, evaporation, multiple internal reflections, free surface evolution, and surface forces with proper material phase changes. With the modeling they concluded that the cutting copper is a laser intensity and interaction time dependent process and the cutting aluminum depends more on lase intensity than interaction time, represented in Figure 4-2. [36]

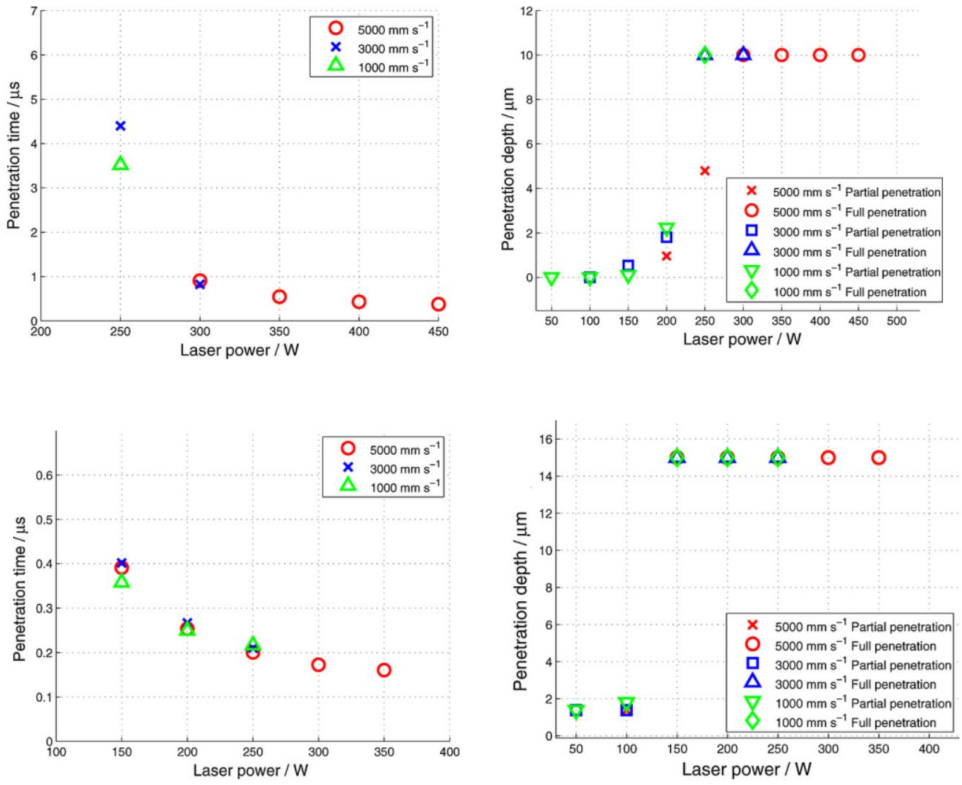

Figure 4-2: Cutting penetration time & depth of Copper(a, b) and Aluminum(c, d) [36]

Also they conducted experiments on pure copper and aluminum and one side-coated active material using SM laser and compared the results of simulation and experimental.

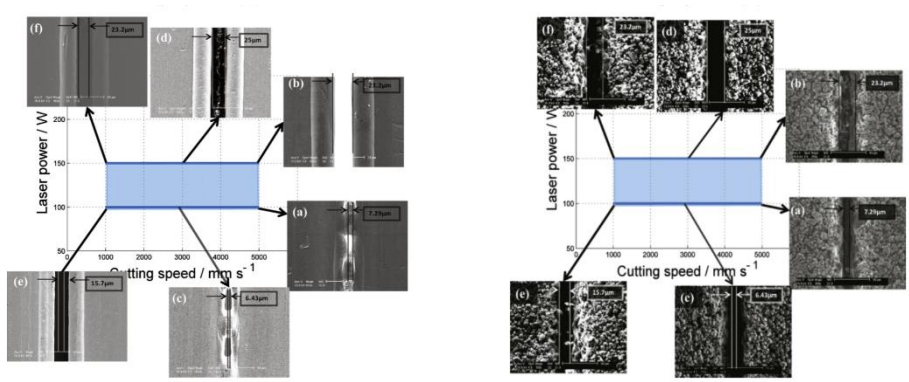

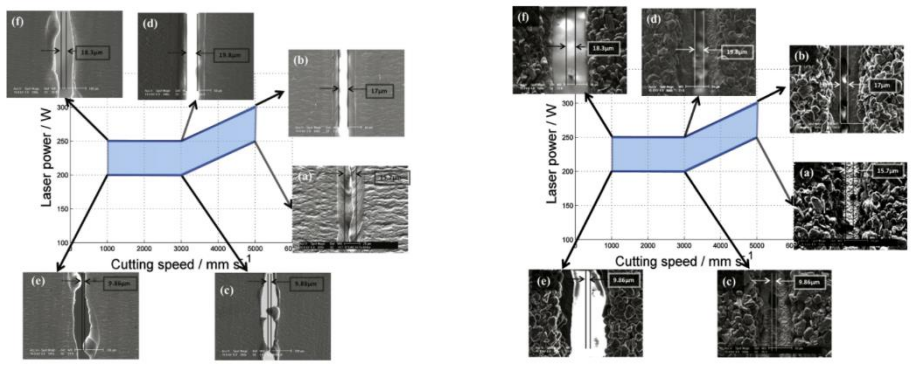

Figure 4-3: Comparison of cutting results of pure metal and one-side active material coated electrodes [36]

The authors concluded that the simulation results for pure copper agree well with the experimental results for pure copper with single side coated graphite at a laser scanning speed of 3000 mm/s. Simulation results of pure aluminum at a laser scanning speed of 5000 mm/s are well matched to pure aluminum results of a single side coated $LiCoO_2$.

3) A. Lutey. et al.[37] implemented laser cutting of graphite coated anode(copper 10um, graphite 47um on both side) and LiFePO4 coated cathode(aluminum 20um, LiFePO4 45um on both side) electrodes using 5 different laser sources; 2 IR(1064nm) pulsed lasers, 1 SM CW laser, 2 green(532nm) lasers, with power and speed variations as parameters shown in Figure 4-4.

Table 2
Laser parameter groups under test conditions.

Parameter group	1	2	3	4	5	6	7	8	9	10	11	12
Wavelength (nm)	1064	1064	1064	1064	1064	1064	1064	1064	532	532	532	532
Operating mode[a]	P	P	P	P	P	P	P	CW	P	P	P	P
Pulse duration (ns)	4	30	30	200	200	200	120	–	4.5	4.2	1.4	1.4
Repetition rate (kHz)	500	500	100	500	100	20	100	–	20	10	500	100
Beam quality (M^2)	1.5	1.5	1.5	1.5	1.5	1.5	2	1.05	2	2	1.2	1.2
Spot diameter (μm)	25	25	25	25	25	25	54	46	27	27	16	16
Rayleigh range (μm)	320	320	320	320	320	320	1080	1460	540	540	325	325
Max. average power[b] (W)	19	19.2	18.8	19.1	18.8	18.7	84.8	315	4.3	2.8	8.2	1.6
Max. pulse energy[b] (μJ)	38	38	188	38	188	935	848	–	215	280	16	16
Max. fluence[b] (J cm^{-2})	15	15	74	15	74	369	74	–	75	97	16	16

[a] P, pulsed; CW, continuous wave.
[b] Values at sample surface.

Figure 4-4: Test parameters of A. Letey et al [37]

They tried to find the relationship between ablation depth and laser power by analyzing 3D profile of the specimen, and between per-pulse ablation depths and pulse fluence by calculating a numerical function. They concluded that

- Pulsed exposures with shorter pulse durations and higher exposure velocities lead to higher cutting efficiency than either CW exposure, longer pulse durations or lower exposure velocities.

-Exposure at 532 nm leads to penetration at 25–40% less average power than at 1064 nm

- Highest coating layer ablation efficiency at 1064 nm is achieved with pulse fluences <15 J/cm^2, while highest overall cutting efficiency is achieved with pulse fluences in the range 35–40 J/cm^2 for the cathode and 100–110 J/cm^2 for the anode.

-Defect size and coating layer delamination width are both linked to cutting efficiency, with highest quality achieved for a given wavelength when overall cutting efficiency is optimized.

4) A. Lutey et al.[38] performed laser cutting on another cathode material-LiNiMnCoO2(LNMC) with nanosecond pulsed fiber laser; 20W, 4~200ns, 20~500kHz, 8~935uJ, while varying the pulse duration, PRR, laser pulse fluence but constant cutting speed of 100mm/sec. The materials to be cut were 110um thickness for anode and 150um thickness for cathode with LNMC active material. From the experiments, they tried to find the minimum average power and assess the cut quality via SEM analysis. and then they compared two results of LiFePO4(A. Lutey et al [37]) and LNMC.

Parameter group	1	2	3
Pulse duration (ns)	4	30	200
Repetition rate (kHz)	500	100	20
Max. average power (W)	19	18.8	18.7
Max. pulse energy (μJ)	38	188	935
Max. laser pulse fluence (J/cm^2)	15	74	369
Pulse overlap* @ 100 mm/s (%)	98.7	93.6	68.9

(a)

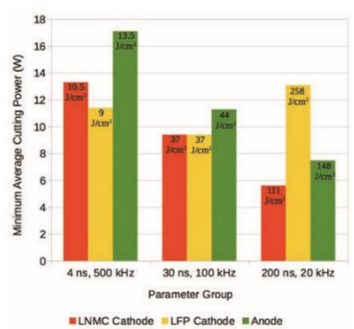

(b)

Figure 4-5: (a)Test parameters, (b) minimum cutting power and pulse fluence at 100mm/sec [38]

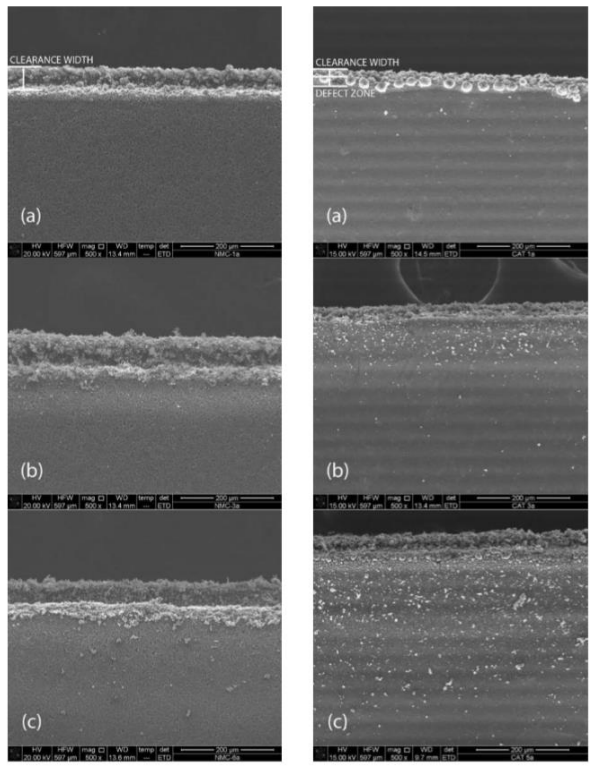

Figure 4-6: SEM image of (a) LNMC cut edge (b) LFP cut edge

They concluded that minimum average cutting power and cut edge quality have been found to be strongly dependent on laser pulse fluence and repetition rate over the tested parameter range and LNMC cathodes and polycrystalline graphite anodes require lowest average cutting power with a repetition rate of 20 kHz and laser pulse fluence in the range 110-150 J/cm2, while LFP cathodes require lowest power with a repetition rate of 100 kHz and fluence of 35-40 J/cm2. Cut quality for LFP cathodes is more strongly dependent on process parameters than the other tested electrodes, with highest quality coinciding with highest cutting efficiency. [38]

5) A. Dimir et al[39] also implemented experiments with two pulsed fiber lasers differing in wavelength and pulse duration. One is 1064nm with 50W, 20-80kHz, 250ns, the other is 532nm with 5W 20-300kHz, 1ns as shown in Figure 3-7. They

tried to find maximum cutting speed of the two lasers.

Table 1. General specifications of the used laser systems.

	IR laser	Green laser
Brand and model	IPG YLP-1/100/50/50	IPG YLPG-5
Architecture	Fibre, Q-switched	Fibre, MOPA
λ	1064 nm	532 nm
Max P_{avg}	50 W	6 W
PRR	20-80 kHz	20-300 kHz
Max. E	1020 µJ	20 µJ
τ	250 ns	1 ns
d_0	39 µm	22 µm

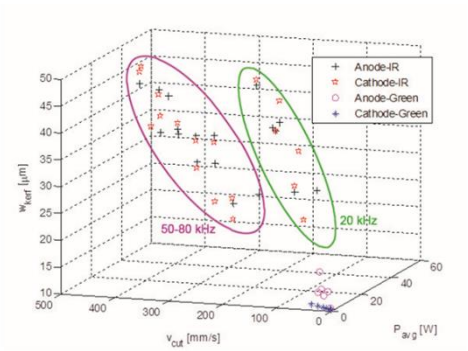

Figure 4-7: Specification of lasers and kerf width of experiments. [39]

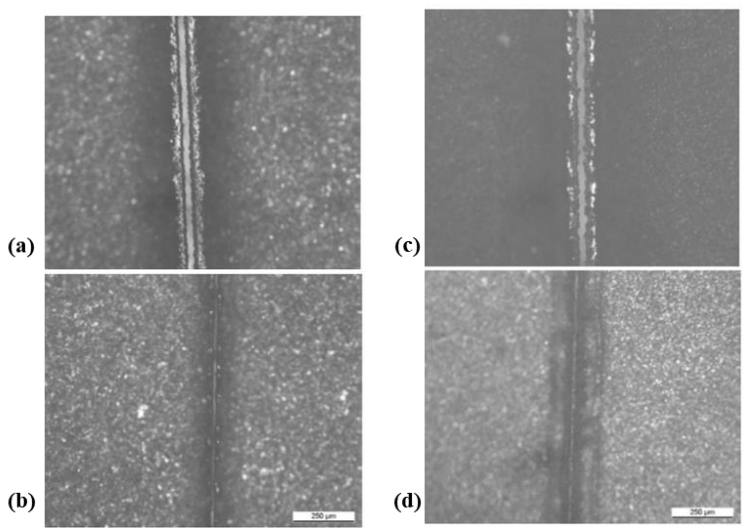

Figure 4-8: SEM images (a) IR, (b) Green for Anode, (c) IR, (d) Green for Cathode [39]

The authors reported that with IR 50W pulsed laser, the max. cutting speed was 500mm/sec for both electrode materials and kerf and clearance width are above 40um for both. And with Green 5W pulsed laser, the max. cutting speed was 40mm/sec for anode and 75mm/sec for cathode. kerf and clearance width 12um and 38um for anode and <10um kerf and no clearance width observed.

They also concluded that the green laser shows greater promise for improved quality on cathode, and the clearance was effectively eliminated on cathode with the green laser, whereas the anode clearance remained similar to the one realized with IR laser.

Researches on laser cutting of Li ion battery electrodes have been reported so far since 2011. Most of the previous studies focused on finding out how much laser power is needed to cut the electrode material, and suggested the possible laser power to apply for the manufacturing process. Some studies have compared the results of the experiment using different operation modes(CW and Pulsed) or using different wavelengths(IR vs Green). But there was not much analysis on cut quality. The reason may be that they do not know the cut quality acceptable in real batteries. Also, the lasers used in their experiments seem difficult to apply to the actual process due to the low power level. However, the pioneering studies seem to be sufficient to provide direction for laser cutting.

Chapter 5

Laser Ablation Principles

5.1 Laser Ablation Principles

When a high intensity of laser beam is incident on a substrate, a part of beam is absorbed by surface of the material, which increase temperature of the material partially. If sufficient energy is applied, the material undergoes melting and vaporization, which eventually leads to materials removal. This is the mechanisms by which ablation takes place. There are 2 kinds of ablation, Photochemical ablation and Photothermal ablation depend on the energy source and the material. Photochemical ablation is that

If the photon energy level of laser is sufficient enough, this photon energy can break molecular bonds, causing ablative decomposition of the irradiated area, especially taken place in organic materials. On the other hand, Photothermal ablation takes place in normal materials like metals, ceramics. In this mechanism there are 3 kinds of phenomena. [3]

1) Normal Boiling

It requires a relatively long pulse duration and involves nucleation of heterogeneous vapor bubbles which may form at the outer surface of the liquid or at the interface between the liquid and the surrounding solids. The normal boiling process occurs within the absorption depth ($1 / \alpha$, where α is the absorption coefficient). The surface temperature is constant and equal to the vaporization temperature corresponding to the pressure of the surface. The surface and the temperature gradient directly beneath it are zero (ie, $\partial T / \partial z = 0$).

2) Normal Vaporization

Refers to the conversion of a condensed phase (solid or liquid) into a vapor phase as atoms or molecules are released from the outer surface. It can occur with any influence and pulse duration, and there is no temperature threshold. This process is not related to nucleation and the surface temperature is not constant because the vapor pressure is not zero. The contribution of normal vaporization to the ablation can be ignored on a time scale of less than 1 ns and at very low temperatures.

3) Explosive Boiling (or Phase Explosion)

The laser power intensity should be high enough and the pulse duration should be short enough so that the temperature of the surface and its immediate area reaches about 90% of the thermo-dynamic threshold temperature (ie, 0.90 Tct). As a result, homogeneous bubble nucleation occurs, and the material quickly transitions from the superheated liquid to the vapor / liquid droplet mixture. Uniform nucleation is possible because the rate at which it occurs is significantly increased near the critical temperature. Again, the surface temperature gradient and the temperature gradient directly below it are zero. [3]

5.2 Material Removal Mechanism

Material removal occurs in most laser applications. It is the main process in cutting and drilling and it acts as an incidental phenomenon in welding. However, this principle of physics is so complex that it has been not yet fully understood. There are two main types of material removal. One is melt ejection by vaporization-induced recoil force in cutting, drilling, and the other is melt evaporation in high power or short pulse ablation.

5.2.1 Laser-Material Interaction Time

A criterion to determine the key removal mechanism is proposed by Semak and Matsunawa [49]. It is suggested that the laser beam-material interaction time, The interaction time t_{int} can be employed to define the key process:

(i) if $t_{int} << t_{th} = r_b/V_m$, vaporization removal dominates the process, and

(ii) if $t_{int} >> t_{th} = r_b/V_m$, melt ejection dominates the process,

where t_{th} is the threshold time, which is the minimum time required to initiate the melt ejection-dominated process, r_b is the beam radius and V_m is the melt ejection velocity.

5.2.2. Melt ejection by vaporization-induced recoil force

The vaporization recoil pressure becomes the primary factor removing melt from the interaction zone under the regime of hydrodynamic flow. The absorption of the laser beam at the material's surface results in an increase in the surface temperature. The vaporization-induced recoil pressure increases with increasing surface temperature and this induces the ejection of the melt from the interaction zone. Both melt ejection and evaporation provide the propagation of solid-liquid and liquid-vapour boundaries into the material similarly to drilling. [59]

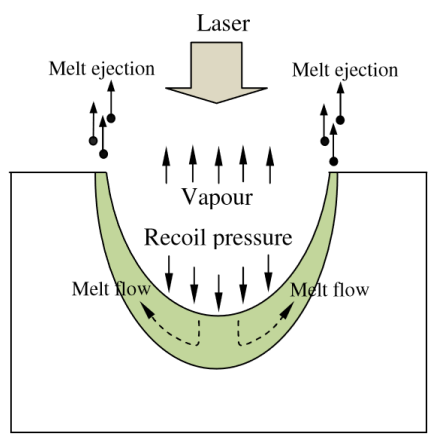

Figure 5-1: Schematic of material removal by laser beam [45]

Material removal can occur in liquid and vapor form. In normal vaporization, the substrate material is first heated to the vaporization temperature through the melting

point. In this case, part of the beam energy is used to melt the substrate, and the formed molten material (liquid layer) directly contacts the substrate. A portion of this molten material is further vaporized by the beam. The resulting steam generates steam or recoil pressure to push the steam out of the target and to force the molten material to the sides. Chen and Wang [46] found that the repulsive pressure in the laser processing of titanium was 0.25 ~ 0.5 MPa, corresponding to the laser intensity of 1 ~ 3.3MW / cm^2. [45]

5.2.3 Melt vaporization

Some of the process happening during ns laser-material interaction are depicted in Figure 5-2, which include laser absorption in the surface and material excitation, temperature rise and surface melting, ablation and plasma formation, laser-plasma interaction, shock wave formation, and finally, in case with sufficiently high ambient pressure, plume collapse. There are three regimes separated by different time zone (shown in dotted lines in figure 5-2)

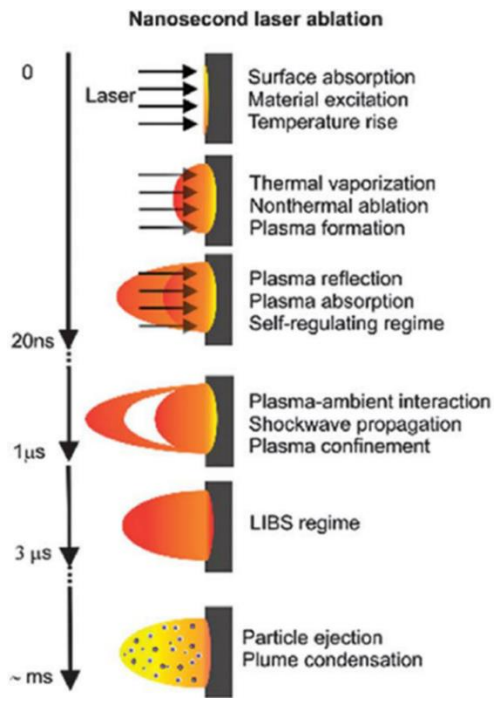

Figure 5-2: Schematic of process involved in ns laser ablation in atmosphere air, with an approximate timeline of their occurrence [58]

(i) laser-target and laser-plasma interaction occurring during the laser pulse,

(ii) plasma expansion and confinement,

(iii) plume condensation

The characteristics of laser produced plasmas depends on numerous parameters, such as target material, laser wavelength, pulse duration, and irradiance, as well as ambient gas pressure and composition. [58]

In general, liquid removal is the main form of material removal at low beam power, and evaporation is the dominant form at high power. For beams of much greater intensity and shorter pulse durations, the repulsive pressure may be high enough to induce shock waves transmitted through the material. The shock wave can also be generated as a result of the interaction of the laser and the plasma. [3, 45]

5.2.4 Explosive Boiling

A number of studies have been reported to try to understand the material removal mechanism during laser ablation, and an understanding of the explosive boiling was introduced by Kelly and Miotello. They found that explosive boiling is the most efficient mechanism for thermal ablation in a short time. [40, 43]

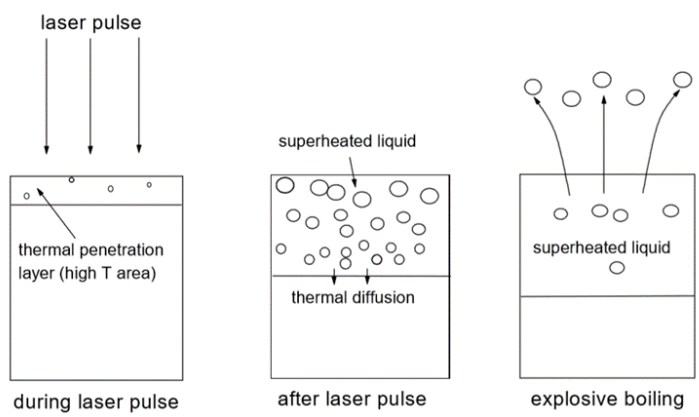

Figure 5-3: The kinetic process of explosive boiling [42]

According to the thermodynamic theory of explosive boiling, the liquid begins to overheat and becomes metastable if it exceeds the temperature limit of about 0.8 Ttc. Above this temperature, homogeneous bubble nucleation occurs, resulting in the

target material being radically deformed into a mixture of liquid droplets and vapor in a superheated liquid, which is radically released from the target. The reaction mechanism of explosive boiling is depicted in Figure 5-3. [41. 42]

5.3 Threshold Irradiance

N. M. Bulgakova et al.[40] reported that the evidence for transition form normal vaporization to phase explosion was obtained for a number of materials based on the measurements of ablation rate as a function of laser fluence. According to their reports, there is a threshold value of laser fluence at which a sudden increase of mass removal occurs. This jump in ablation rate is accompanied by the appearance of considerable amounts of droplets in the plume, which indicates a transition to a different vaporization regime. Figure 5-4 shows that there is a threshold point of fluence on ablating graphite, at which abrupt increase in ablation rate takes place. In their researches, the values of threshold fluence varies with material.

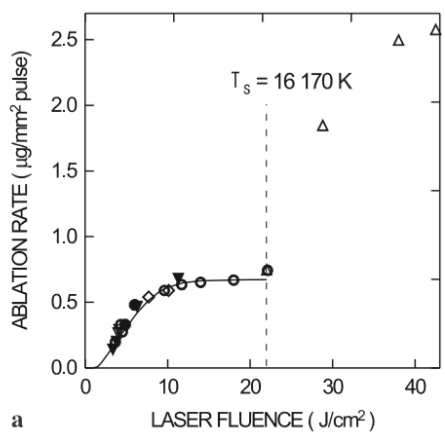

Figure 5-4: Mass removal per pulse as a function of laser fluence for the graphite. Rev. from [40]

In addition, J.H. Yoo et al [44] demonstrated the evidence of threshold irradiance by their experiments that mass removed by high power laser irradiation (10^9 ~10^{11} W/cm^2) on silicon was investigated by measuring the crater morphology and then the craters show a strong nonlinear change in both and volume and depth when the laser irradiance is less than or greater than 2.2×10^{10} W/cm^2. They proposed that

explosive boiling may be a dominant mechanism for mass removal for laser irradiances greater this threshold.

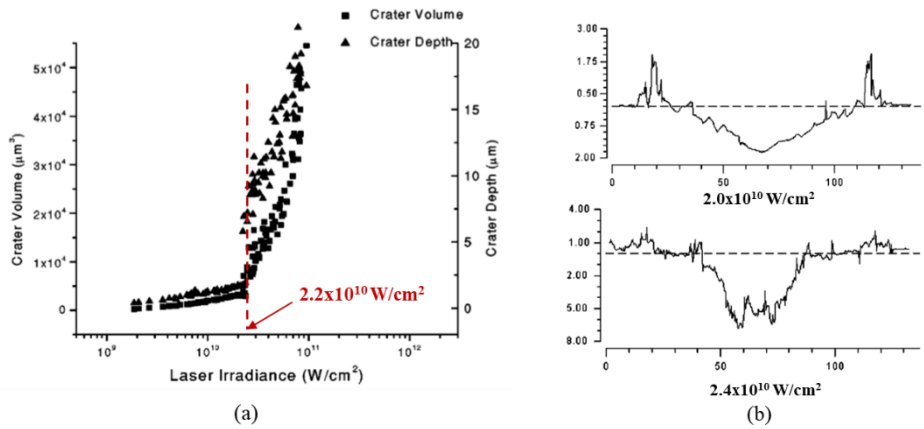

Figure 5-5: (a) Crater volume and depth as a function of laser irradiance, (b) Cross-sectional view of the craters at certain irradiance. Reused from [44]

Figure 5-5 (a) shows a dramatic increase at threshold irradiance in the measured crater depth and volume. Figure 5-5 (b) represents the change of cross-sectional shape at below and above the threshold irradiance.

Below the threshold and above the threshold, the shock waves that lasted for several tens of nanoseconds after the laser pulse were formed due to the pressure difference between the high-density plasma column and the atmosphere. If the laser dose exceeds the threshold value, large particles are emitted in the size of about 300-400 ns after shock wave. [48]

It can be summarized that ablation with below threshold irradiance is governed by normal evaporation and with above threshold is dominated by explosive boiling.

5.4 Plasma Effects

Another parameter to consider is plasma shielding, which plays an important role in determining the laser irradiation limit for explosive boiling. The plasma shielding effect can be explained by plotting the laser time profile transmitted through the plasma in Figure 5-6. If the laser irradiance is relatively low, the laser pulse will remain almost unaffected by the plasma and retain its original profile.

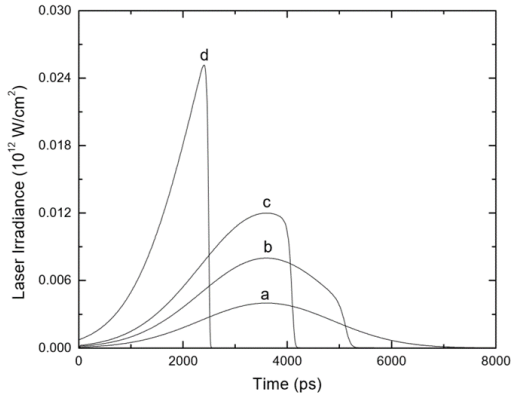

Figure 4-6: Temporal profiles of laser intensities a: 10^{10}, b: $2x10^{10}$, c: $3x10^{10}$, d $1x10^{11}$ W/cm^2

However, when the laser irradiance is larger than 2 x 10^{10} W/cm^2, the trailing part of the laser pulse is truncated, as clearly seen in figure 5-5 (c and d). [48] This phenomenon can be explained by plasma absorption of laser irradiance. As a result, the ablation rate can be saturated.

Chapter 6

Experiments and Analysis

6.1 Experimental Setup

6.1.1 Laser systems

Two kind of fiber Lasers operating different modes were used in this experiment. Single mode CW(Continuous Wave) Laser(YLR-1000-SM, IPG Photonics inc.) and high power nanosecond pulsed laser(YLP-HP-1.5-30x90-133-200, IPG Photonics inc.) One, single mode CW Laser with maximum output average power of 1kW is a single mode beam having beam quality factor of M^2=1.05. The other, Pulsed Laser could generate up to 200W average power, and operated with 133kHz-1000kHz in pulse repetition rate and 30ns, 60ns, 90ns in pulse duration and beam quality factor of M^2=1.3. Other specifications of laser parameters are listed up in the Table 6-1.

Parameters	CW	Pulsed
Laser Model	YLR-1000-SM	YLP-HP-1.5-30x90-133-200
Average Power [W]	1kW	200W
Wavelength [nm]	1070nm	1065nm
Beam Quality(M2)	1.05	1.3
Polarization	Random	Random
Max. Pulse Energy [J]	-	1.5mJ
PRR [Hz] (Pulse Repetition Rate)	-	400k~1000kHz(30ns) 200k~1000kHz(60ns) 133k~1000kHz(90ns)
Pulse Duration [ns]	-	30~90ns
Spot Diameter [um] (F-theta 100mm)	23um	21um

Table 6-1: Specifications of two Lasers used in the experiment

(a) (b)

Figure 6-1: SM CW Laser(a), Pulsed Laser(b) (IPG Photonics Inc. USA)

6.1.2 Scanning systems

The experiment was prepared to implement a remote cutting method using a scanner, which has 20mm aperture and maximum moving speed about 6m/sec and 2D galvanometer type from Scanlab inc.. F-theta 100mm for the focusing lens having 70mm x 70mm scan field was selected to implement the smallest beam size. The calculated beam spot size on the focal plane is 23um for CW, 21um for Pulsed through the 100mm focusing lens.

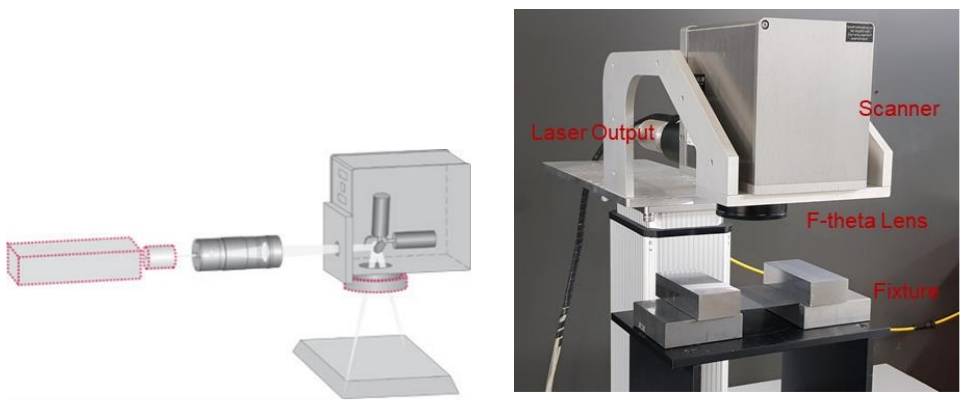

(a) (b)

Figure 6-2: Schematic of Scanner[Scanlab inc.](a), Experimental set-up(b)

6.2 Test Specimen

6.2.1 Cathode Electrode of Li-Ion Battery – $LiFePO_4$

The cathode material to be tested comprised an aluminum foil with a thickness of 15um as a current collector coated with 110um $LiFePO_4$ as a active material on both

sides. So the total thickness of the electrode material to be tested is about 240um. Cross-section of the cathode electrode is presented in Fig. 6-3.

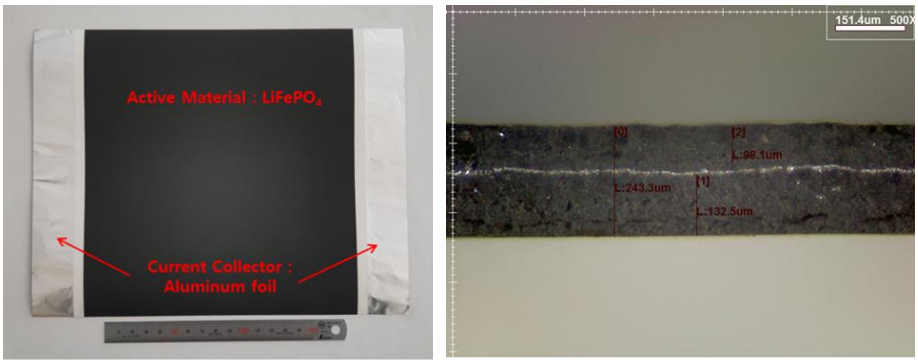

(a) (b)

Figure 6-3: Test sample(a), Cross section of the sample(b)

The coated active material(LiFePO4) was analyzed with EDS(Energy Dispersive Spectrometry). According to the results of EDS analysis, the material is consist of about 38% of Oxygen and 35% of Iron and 18% of Phosphorus and 9% of Carbon. It is noted that Li element is not shown on the results because the low atomic number(Li=3) element could not be detected. Additionally the analysis of components of anode material is attached and it consist of 98% of carbon and 2% of oxygen.

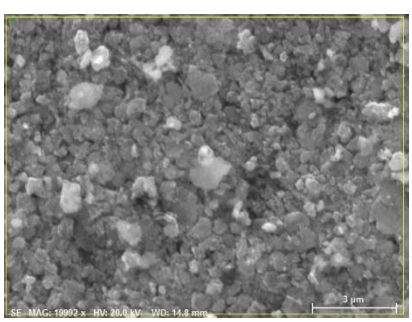

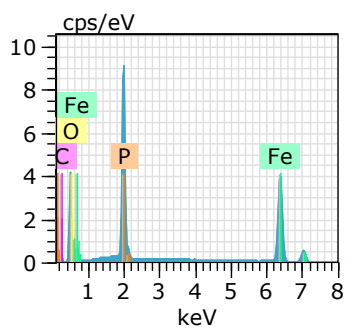

Spectrum: 1

Element	Series	norm. C [wt.%]	Atom. C [at.%]	Error (3 Sigma) [wt.%]
Carbon	K-series	8.70	16.81	4.92
Oxygen	K-series	37.85	54.93	13.75
Phosphorus	K-series	18.10	13.57	2.06
Iron	K-series	35.35	14.70	2.75
Total:		100.00	100.00	

(a)

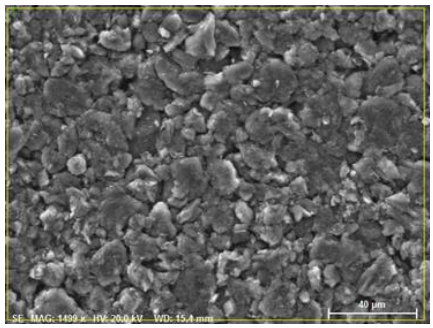

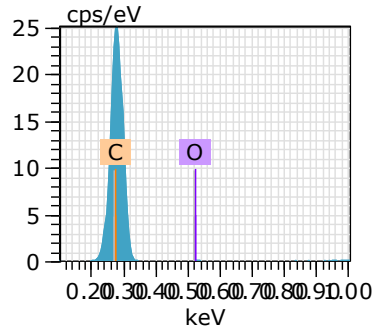

Spectrum: 1

Element	Series	norm. C [wt.%]	Atom. C [at.%]	Error (3 Sigma) [wt.%]
Carbon	K-series	97.92	98.43	32.37
Oxygen	K-series	2.08	1.57	1.76
	Total:	100.00	100.00	

(b)

Figure 6-4: Results of element analysis of Cathode(a), Anode(b)

6.2.2 Optical Properties of the Material

The incidence of a laser beam on a material is accompanied by absorption and scattering phenomena producing attenuation and spatial redistribution of the beam energy. When a laser beam is incident on a material, a part of the laser beam is reflected and/or scattered at the surface, the remaining part penetrates in the material, of which apart is absorbed and the rest is transmitted out as shown in figure 6-5. The absorbed laser energy usually heats the material raising its temperature. Depending upon the absorbed laser power density and the interaction time the laser beam can heat, melt, vaporize, and ablate material, and can also form plasma.

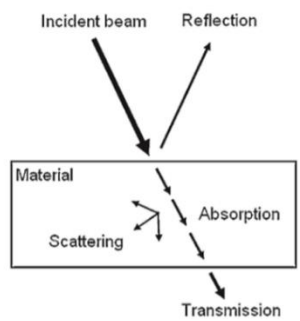

Figure 6-5: Possible interaction of laser light with material [54]

it is useful distinguishing among back scattered, absorbed, and forward-scattered radiation and to introduce the reflectivity ($R=Er/E$), absorption ($A=Ea/E$), and transmittance ($T=Et/E$) parameters of the material

$$A+ R + T= 1$$

but, for opaque materials, the absorptivity can be neglected. [55]

Absorption rate of the material at specific wavelength of laser light was measured with spectro-photometer. Absorption rate is about 28% and reflectivity is about 72% for the aluminum foil at 1070nm wavelength of laser. Absorption rate and reflectivity are about 93% and 7% for the active material of cathode at 1070nm. But those materials are not transparent so that transmittance can be neglected. In general, Aluminum and copper in itself are highly reflective material to 1070nm so that absorption efficiency to 1070nm is very low causing back reflection beam to the laser cavity. But the material to be tested is sandwiched with the material having relatively high absorption rate to 1070nm. For reference, the optical properties of anode electrode were added. The copper foil shows about 15% absorptivity, 85% reflectivity and the active material-Graphite- shows about 90% absorptivity, 10% reflectivity respectively at 1070nm, as presented in figure 6-6.

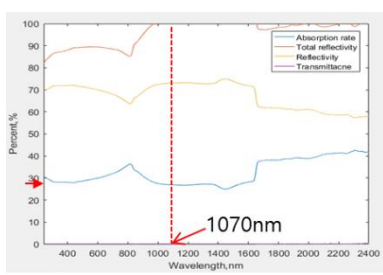

(a)

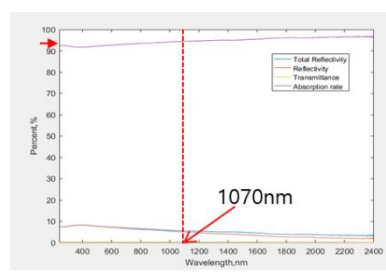

(b)

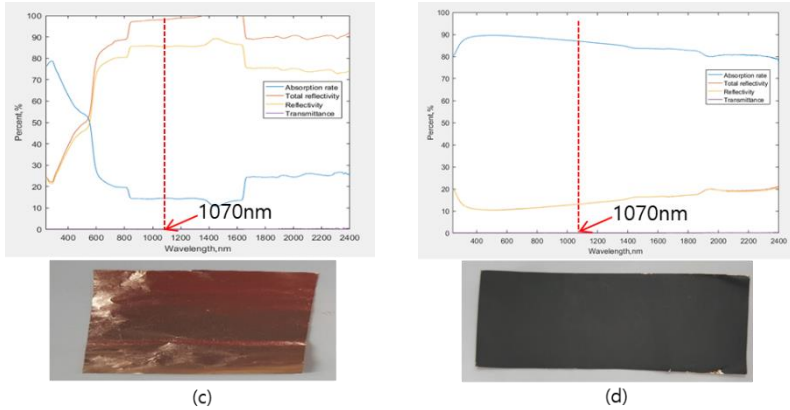

Figure 6-6: Optical properties of materials at specific wavelengths of light Aluminum foil(a), Cathode active material ($LiFePO_4$) (b), Copper foil(c), Anode active material (Graphite) (d)

6.2.3 Thermal Properties of the Materials

No data were available on the physical properties of material $LiFePO_4$. Therefore, only the physical property values of Aluminum, Lithium, Copper, and Graphite, the major substances used for electrode of Li-ion batteries in Table 6-2 were compiled. Due to the unique structure and materials of lithium-ion battery electrodes and differences in the thermal & physical properties of each material, complex reactions are expected.

Property	value
Melting temperature	933.47 (K)
Normal boiling temperature	2792 (K)
Critical point temperature	7963 (K)
Liquid density	2333 (Kg/m^3)
Solid density	2700 (Kg/m^3)
Kinematic viscosity	4.43635E-07 (m^2/s)[93]
Surface tension	0.860-0.000115*(T-933.47) (N/m) [94]
Latent heat of vaporization	1.09E+07 (J/kg)
Latent heat of fusion	3.97E+05 (J/kg)
Solid thermal conductivity	237 (W/mK)
Liquid thermal conductivity	93.752 (W/mK)
Liquid constant-pressure specific heat	1255.2 (J/kgK)
Solid constant-pressure specific heat	896.9607116 (J/kgK)
Liquid thermal diffusivity	3.20E-05 (m^2/s)
Solid thermal diffusivity	9.79E-05 (m^2/s)
Laser absorptivity for flat surface	0.07

(a)

Property	value
Melting temperature	453.85 (K)
Normal boiling temperature	1609.15 (K)
Critical point temperature	3223 (K)
Liquid density	512.5 (Kg/m^3)
Solid density	533.4 (Kg/m^3)
Kinematic viscosity	1.002E+02 (m^2/s) [102]
Surface tension	0.306 (N/m)
Latent heat of vaporization	2.273E+07 (J/kg)
Latent heat of fusion	4.339E+05 (J/kg)
Liquid thermal conductivity	42.332 (W/mK)
Solid thermal conductivity	44.000 (W/mK)
Liquid constant-pressure specific heat	4225.8 (J/kgK)
Solid constant-pressure specific heat	3514.6 (J/kgK)
Liquid thermal diffusivity	1.954E-05 (m^2/s)
Solid thermal diffusivity	2.347E-05 (m^2/s)
Laser absorptivity for flat surface	0.015
Atomic weight	6.941 (g/mol)

(b)

Property	Value
Melting temperature	1357.77 (K)
Normal boiling temperature	2835.15 (K)
Critical point temperature	8280 (K)
Liquid density	7920 (Kg/m^3)
Solid density	8960 (Kg/m^3)
Kinematic viscosity	3.50E-07 (m^2/s) [89]
Surface tension	1.257-0.0002*(T-1356) (N/m) [90]
Latent heat of vaporization	5.23E+06 (J/kg)
Latent heat of fusion	2.05E+05 (J/kg)
Solid thermal conductivity	317 (W/mK) [91]
Liquid thermal conductivity	157 (W/mK) [91]
Liquid constant-pressure specific heat	571.6218 (J/kgK)
Solid constant-pressure specific heat	385 (J/kgK)[92]
Liquid thermal diffusivity	3.62E-05 (m^2/s)
Solid thermal diffusivity	7.63E-05 (m^2/s)
Laser absorptivity for flat surface	0.05

(c)

Property	value
Sublimation temperature (T_b)	4800 (K)[99]
Critical point temperature (T_{cr})	7811 (K) [100]
Solid density (ρ_s)	1730 (Kg/m^3)[101]
Latent heat of sublimation (L_v)	5.98E+07 (J/kg) [101]
Solid thermal conductivity (k_s)	18.1 (W/mK) [101]
Solid constant-pressure specific heat (C_{ps})	2092.48 (J/kgK) [101]
Solid thermal diffusivity (α_s)	5.00E-06 (m^2/s) [101]
Laser absorptivity for flat surface (A_o)	0.81

(d)

Table 6-2: Physical properties of Aluminum(a), Lithium(b), Copper(c), Graphite(d) [56]

6.3 Experiments

Remote cutting is implemented using scanner system without assist gas for the experiments. Samples were prepared 100mm x 100mm size and copper block was used to make sample flat. 50mm length and 8 lines cutting were implemented with spacing 5mm for each parameter at one time.

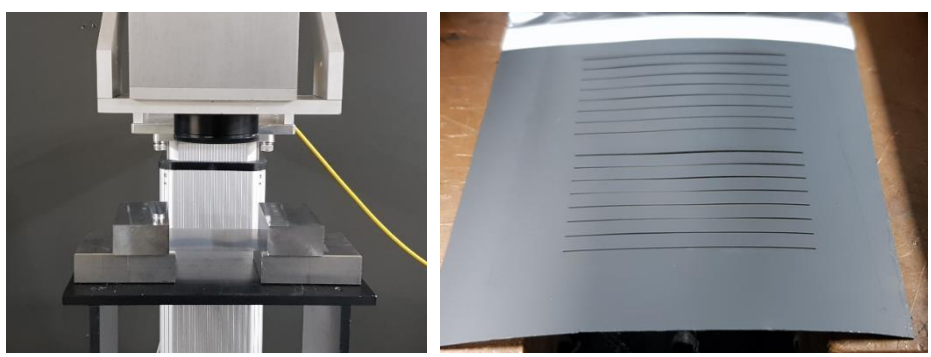

Figure 6-7: Picture of (a)Test set-up, (b) Tested sample

6.3.1 Parameters of CW Laser

With CW laser, 5 parameters group was tested with power and speed variations. Power was varied from 200W to 1kW at intervals of 200W, Speed was varied from 500mm/sec to 5000mm/sec at intervals of 500mm/sec. One parameter group has 10 cuts of speed variations with a fixed power, and 5 power variations make 50

parameters. These tests were conducted 3 times for more accurate analysis. With CW laser peak power is same with average power so that power intensity on the calculated beam spot size 23um is $4.75x10^8 \sim 2.38x10^9$ [W/cm^2]. Heat input varies from 0.33 to 0.02[J/mm]. CW test parameters were listed in Table 6-3.

Power [W]	Cutting Speed [mm/s]	Beam Spot Size [um]	Power intensity [W/cm^2]	Heat Input [J/mm]
200	500 ~5000	23	$4.75x10^8$	0.33~0.02
400			$9.05x10^8$	
600			$1.43x10^9$	
800			$1.90x10^9$	
1000			$2.38x10^9$	

Table 6-3: DOE Parameters of CW Laser

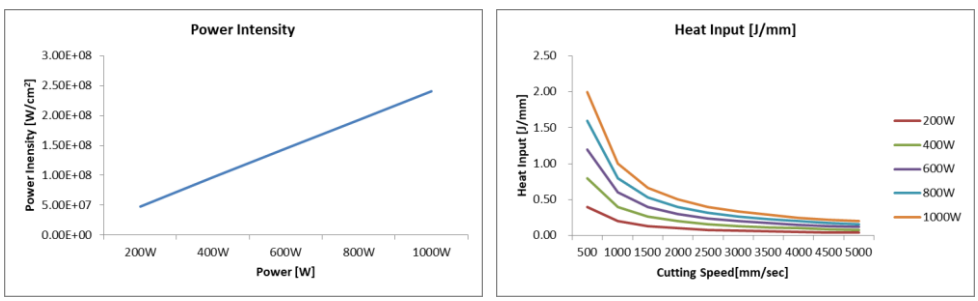

Graph 6-1: Power intensity and heat input of CW laser tests

6.3.2 Parameters of Pulsed Laser

With pulsed laser, there are more parameters than CW laser by the advent of new parameters, that is, pulse duration and PRR(pulse repetition rate). The Pulsed laser used in the experiments operates on 3 range of pulse duration 30ns, 60ns, 90ns with minimum 400kHz, 200kHz, 133kHz for each pulse duration and maximum 1000kHz for all. At each pulse duration, the change of PRR lead to the change of pulse energy, which results in the change of peak power and power intensity. With the pulse duration and PRR variations, 15 parameter groups were tested as shown in Tabl 6-4.

Graph 6-2 shows the change in pulse energy and peak power according to PRR at each pulse Duration. the maximum pulse energy of 1.5mJ comes out at 90ns and 133kHz, 0.2mJ at 1000kHz for all durations. And as PRR increases, the pulse energy

and peak power are reduced.

Power [W]	Pulse Duration [ns]	PRR [Hz]	Pulse Energy [mJ]	Cutting Speed [mm/s]	Beam Spot Size [um]	Peak Power [W]	Power intensity [W/cm^2]	Heat Input [J/mm]
200	30	400	0.5	300 ~1000	21	16,670	$4.81x10^9$	0.2~0.67
		600	0.33			11,000	$3.18x10^9$	
		800	0.25			8,330	$2.41x10^9$	
		1000	0.2			6,670	$1.93x10^9$	
	60	200	1			16,500	$4.76x10^9$	
		400	0.5			8,330	$2.41x10^9$	
		600	0.33			5,500	$1.59x10^9$	
		800	0.25			4,170	$1.20x10^9$	
		1000	0.2			3,330	$9.61x10^8$	
	90	133	1.5			16,670	$4.81x10^9$	
		200	1			11,000	$3.18x10^9$	
		400	0.5			5,550	$1.60x10^9$	
		600	0.33			3,670	$1.06x10^9$	
		800	0.25			2,780	$8.03x10^8$	
		1000	0.2			2,220	$6.41x10^8$	

Table 6-4: DOE parameters of pulsed laser experiments

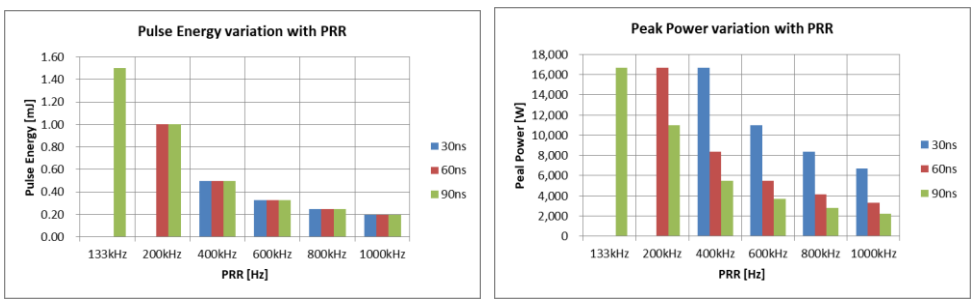

Graph 6-2: Pulse energy and peak power with PRR variation of pulsed Laser

5.4 Analysis of Results

5.4.1 Measurement definition to evaluate cut quality

Kerf width is the opened width where the material is fully separated, Exposed metal width is the width of metal shown as the upper layer of active material is removed more widely viewed at top side. HAZ width is the heat affected zone with deformation or discoloration of active material[50] and is the width where some metal particles or debris of active material spread out on upper side of cut around.

Kerf width was measured with the width of cut formed after processing as both

sides of the separated sample were required, and HAZ and the exposed metal width were measured only one separated side because the other side would not be used. Figure 6-8(a) shows the measuring criteria observed in top side.

The extended metal width shown in figure 6-8(b) is the width of metal viewed at cross-section, which width is inevitably wider than the thickness of the original material because the material is widened through melting and solidification. This value was only measured when the three layers were clearly separated and the value was missing if the boundaries of the measurement were unclear.

Other criteria for cut quality evaluation are metal particles and debris and cracks around cut. But the values of these criteria are difficult to quantify, so evaluated qualitatively by images of microscope and SEM. Fig. 6-8(c) presents the three evaluation criteria.

(a)

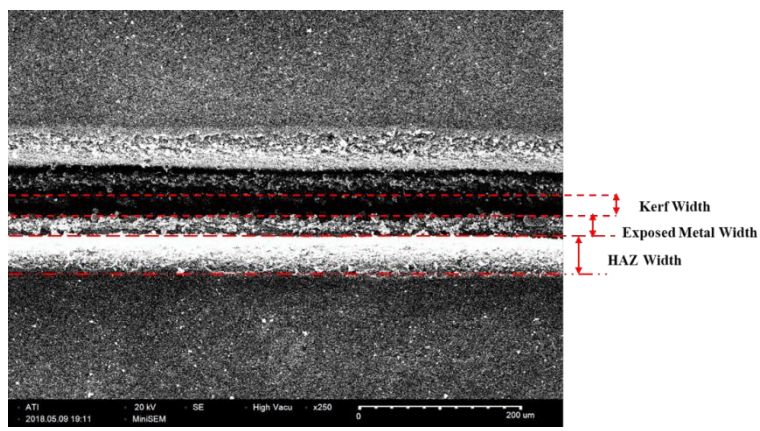

(b)

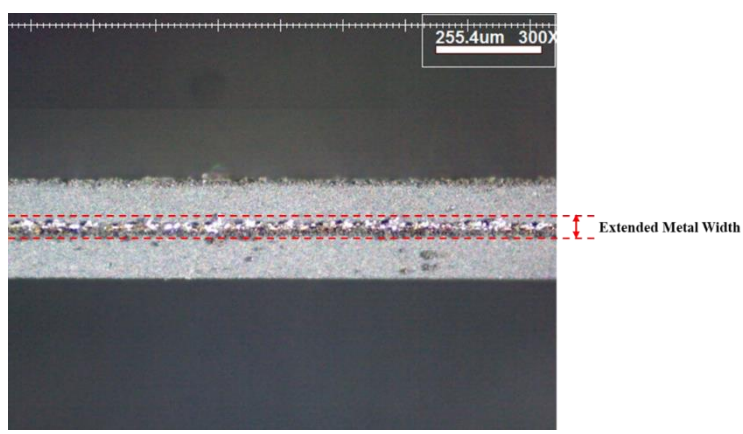

(c) 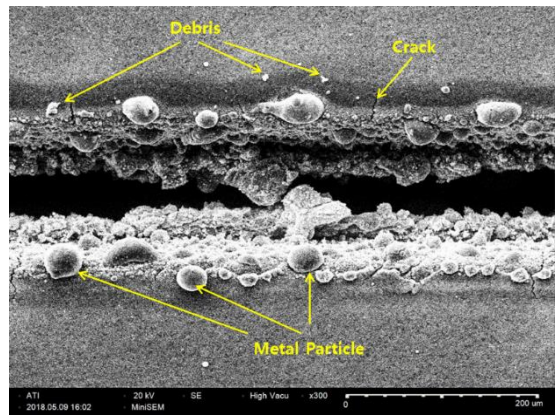

Figure 6-8: Measurement definitions at top side (a), Measurement definitions at cross-section (b), Definition of metal particle and debris and cracks(c)

6.4.2 Prerequisites of cut quality evaluation

In the cutting electrodes of Li-Ion battery process, there are some prerequisites for qualitative or quantitative evaluations

① HAZ should be as narrow as possible.

② The exposed metal should be as narrow as possible.

③ The extended metal thickness on cross section should be as same as possible with the original metal thickness.

④ There should be no particles, debris and cracks around the cut edge.

Cut quality assessment in this thesis will be evaluated based on the above prerequisites.

6.4.2 Results of CW Laser Experiments

6.4.2.1 Maximum cutting speed with CW Laser

Firstly, maximum cutting speed with CW mode is investigated. The cut was determined by whether the samples had been completely separated. It is clear that the higher the power, the faster the cutting speed is as shown in graph 6-3. And minimum heat input being cut at each power is added also to the graph. Except 200W, the minimum heat input with the material being cut increases linearly as the power

increases.

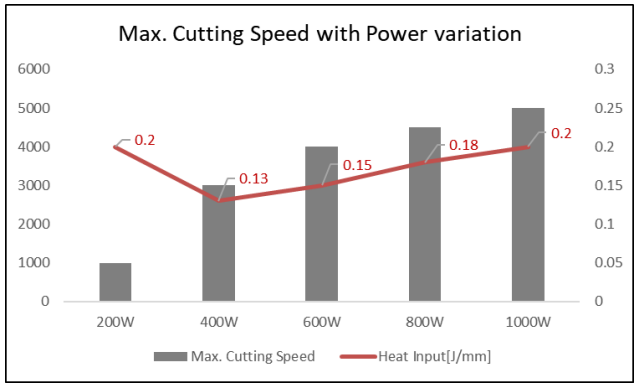

Graph 6-3: Max. cutting speed with CW power variation

5.4.2.2 Cut quality – Qualitative analysis

All cut samples were observed using SEM(Scanning Electron Microscope) and Microscope to measure the defined width for cut quality evaluation. A full set of pictures taken from microscope is attached to make it easy to see the change of cut quality at a glance as the parameters change, presented in figure 6-9. Also a set of SEM images is attached too but all measured data in this experiments taken from microscope. it was difficult to get an exact measured data from SEM, because the sample could not be kept flat in the vacuum chamber of SEM since it was slightly deformed by heat. Figure 6-9 shows all the pictures tested with the parameter variations. Those sets of pictures help checking the results of the cut samples qualitatively as the parameters change at a glance.

Firstly, all the pictures of cut edge presented in figure 6-9(a). At low-speed areas, metal particles and debris, which look quite large, are scattered around cut edge, and the end of the metal also looks quite rough. However, at the fast-speed areas, both metal particles and debris are not seen, and the end of metal look smooth. At the speed of 2000mm/sec or above, particles and debris and cracks around cut edge are not seen in the microscope pictures.

Secondly, all the pictures of cross-section in figure 6-9(b), the aspect of the change becomes more clearly. At low-speed areas, solidified materials are spread dirty on

the cross-section surface and it is difficult to identify the width of metal in the center, while in fast-speed areas, the three layers of raw material are clearly visible. At the speed of 3000mm/sec or above, the cross section shows a clean section without solidified mixture.

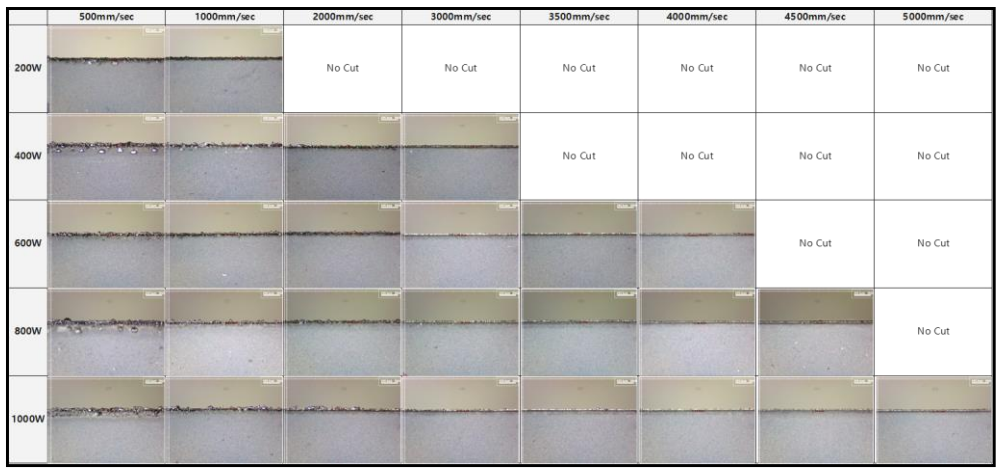

(a)

(b)

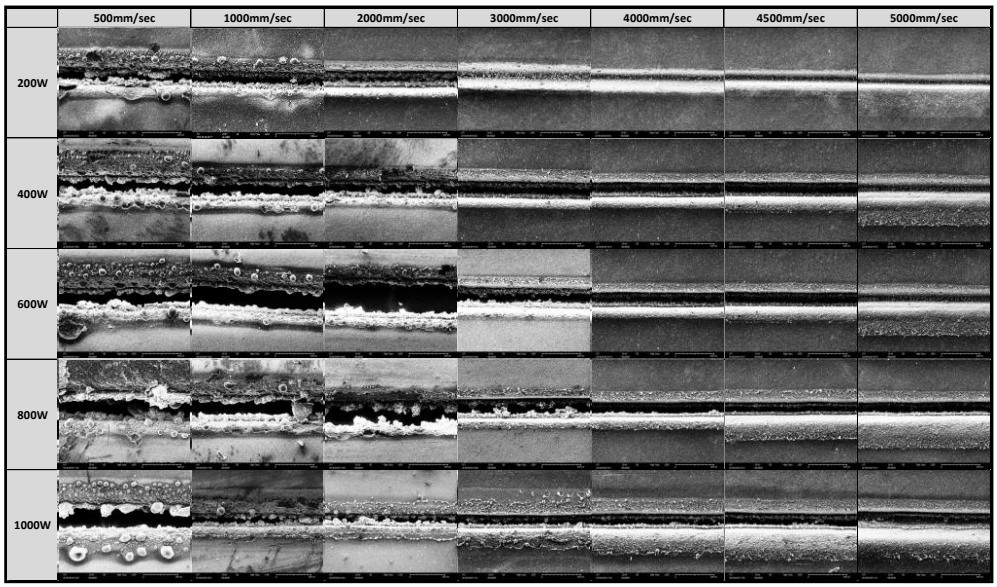

(c)

Figure 6-9: Full set of pictures of one side cut edge (a), Cross-section (b), SEM images of the originally processed samples (c)

From Fig 6-9(c), the enlarged SEM images provide a clearer view of the quality of the cut samples. In the SEM images, contours of cut edge and deformation and discoloration and particles caused by thermal effects are clearly identified around the cut line that was difficult to identify in the microscope images.

The results of the experiment using CW laser were presented with microscope and SEM images. An enlarged picture of the entire parameter showed at a glance how cut quality changed with the parameter variations. In summary, At low cutting speed areas in all power level, metal particles, debris, discoloration, deformation, and delamination are severe, and the ends of metal are quite rough. However, at fast cutting speed areas, the heat affected zone around the cut edge only appears narrow, but the quality of the cut edge is significantly improved compared to the slow cutting speed areas.

6.4.2.3 Cut Quality – Quantitative analysis

The measured values are plotted in graphs against the four previous definitions of width using microscope. All figures were measured as accurately as possible and the

three measurements were averaged. Measurement values are missing if the measurement boundaries are ambiguous.

First, as shown in the graph, kerf width tends to be narrower as speed increases overall. In fast cutting speed areas, the higher the power, the narrower the kerf width is. When power is 1 kW and between 3000mm/sec and 5000mm/sec, the kerf width is the narrowest, and the value is approximately 70um. In fact, Kerf width is not important because only one side of the cut is used for the battery. As the heat input [J/mm] increases due to its low cutting speed, the higher the probability of melting the material and the spatter increases, it is thought that it is necessary to reduce the heat input by as much as possible.

HAZ width also tends to decrease as speed increases. At the same speed, the lower the power, the narrower it tends to be. When power is 600W, it was narrowest at 3000~ 4000mm/sec and the HAZ width value is approximately 20um.

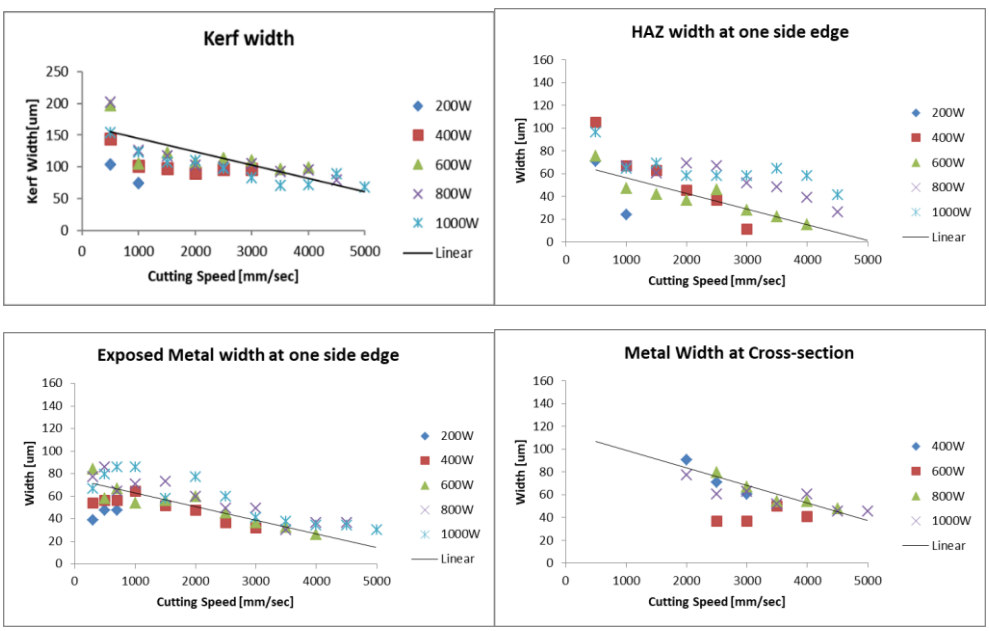

Graph 6-4: Kerf, HAZ, the exposed metal width at top side, The extended metal width at cross section

Exposed metal width is one of the most important evaluation factors of the electrode being used for batteries. The smaller the value, the better the quality. Exposed metal width also tends to decrease as speed increases. When power was 600W to 1000W

in 3500~4000mm/sec speed, 40um of width was observed and the best width was about 30um at Power 600W and 4000mm/sec.

Extended metal width at cross section is another important quality factor. But It was not easy to determine the measurement boundary because the mixture of metal(Aluminum) and active material($LiFePO_4$) was spread across all areas in low speed parameters. The reason for the small number of data is that the measurement values were obtained only in the parameters where the distinction between the metal layer and the active material layer is clearly revealed. The extended metal width is about 40um in areas with power between 600W and 1,000W and speed between 4000mm and 5000mm/sec. Given the original aluminum thickness of 15-20um, this means that the metal was melted and spread widely during the cutting process.

Based on the above results, the best results were found in the areas of parameters of 600W to 1,000W and 4000 to 5000mm/sec. The heat input value is 0.15 to 0.25 [J/mm] and Power intensity $1.44x10^8$ to $2.41x10^8$ [W/cm^2].

6.4.2.4 Effect of Heat input and Power intensity on cut quality

The parameters of the CW experiment are heat input and power intensity. It is evident that cut quality changes with the effects of these two parameters. Heat input is a function of power and speed, and power intensity is a function of power and beam spot size. Cut quality is clearly not a function of one parameter but both heat input and power intensity. If power is the same, the power intensity does not change even if speed changes, but cut quality was changed with speed or power intensity. It was also verified that cut quality is changed in the same case of heat input. Figure 6-10 shows the cut quality changes in heat input and power intensity. The horizontal axis is heat input and the vertical axis is power intensity. Even with the same heat input along the horizontal axis, It can be seen that the cut quality changes when the power intensity changes. In other words, the results of CW show that it is not a function of one parameter but a result of both the heat input and the power intensity.

Pictures are organized for heat inputs of 0.6, 0.4, 0.2, and 0.15J/mm. If there is no

test parameter, values are omitted or replaced by a similar value. Obviously, the lower the heat input, the better the quality of the cut edge and cross section. Especially, if the heat input is less than 0.2J/mm, Particle and debris are not visible around cut edge in all power intensities. And when power intensities are $1.44x10^8$ W/cm^2 and above, the metal of cut edge is also smooth, and solidified melts are not covered in the cross section and look neat. In the same heat input, it can be seen that the higher the power intensity, the better the cut quality. In summary, when the heat input was approximately 0.2J/mm, the power intensity about $2x10^8$ W/cm^2 showed the best cut quality in CW experiment.

	$4.81x10^7$ [W/cm2]	$9.63x10^7$ [W/cm2]	$1.44x10^8$ [W/cm2]	$1.93x10^8$ [W/cm2]	$2.41x10^8$ [W/cm2]
0.53~ 0.67 J/mm	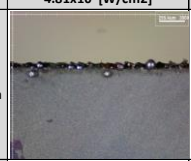		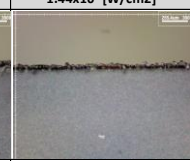		
0.4 J/mm					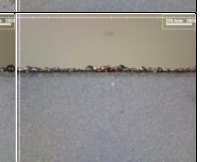
0.2 J/mm	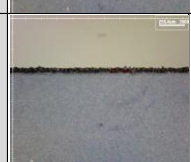	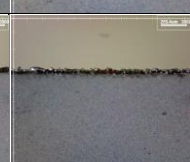			
0.13~ 0.15 J/mm	NA		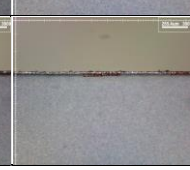	NA	NA

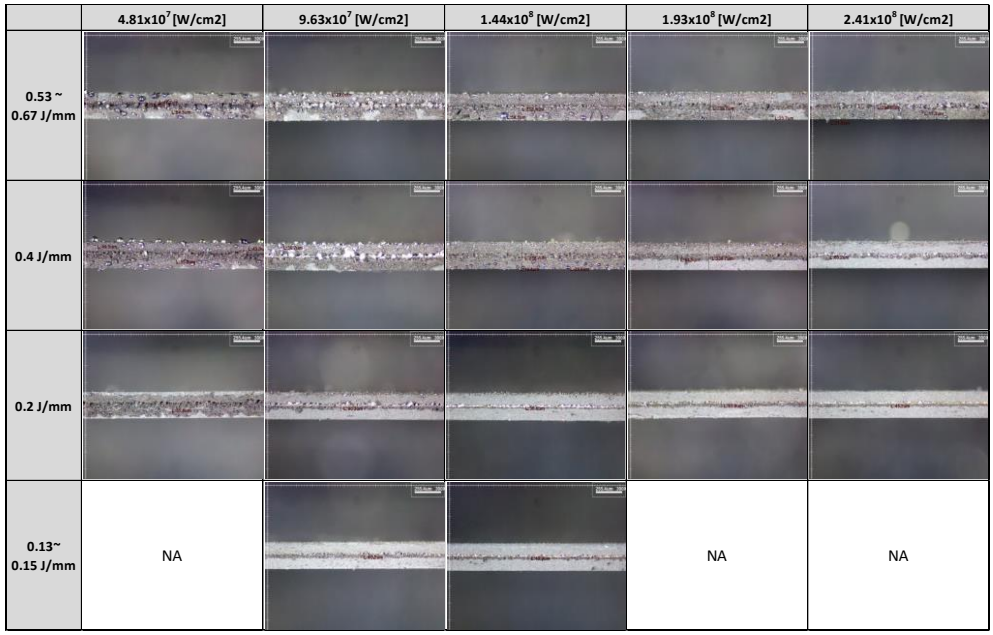

Figure 6-10: Heat input and power intensity effects on cut quality, cut edge(a), cross-section(b)

The area of elliptical shape on the graph 6-5 represents process window where cut quality was the best among the CW test results. Also the picture below is attached with a enlarged size of cut edge and cross section pictures observed in the parameters of the process window. Particle or debris, which has been clearly identified in the low cutting speed area, can be found to be few in this process window area.

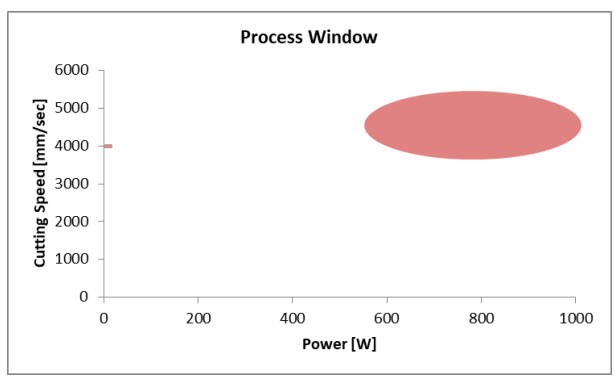

Graph 6-5: Process window of CW Laser tests

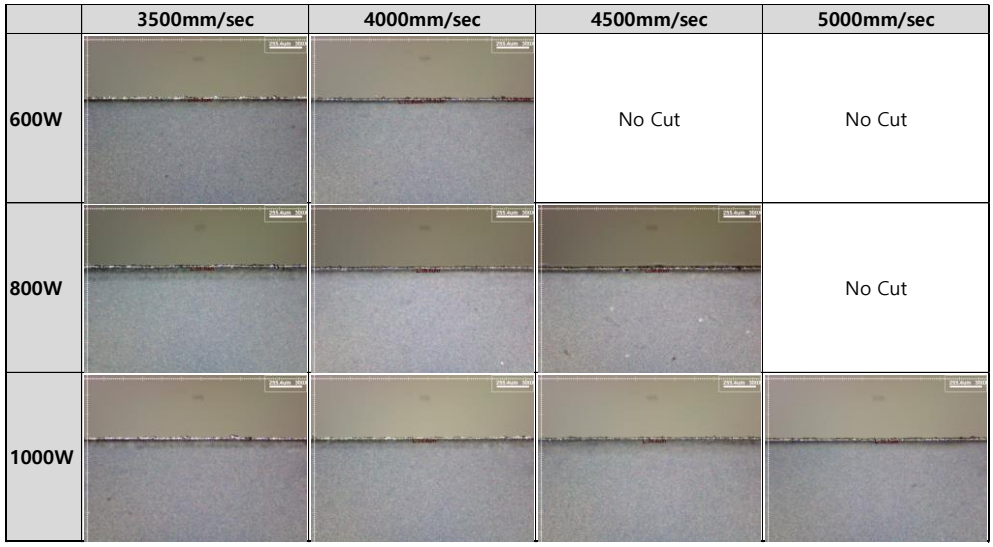

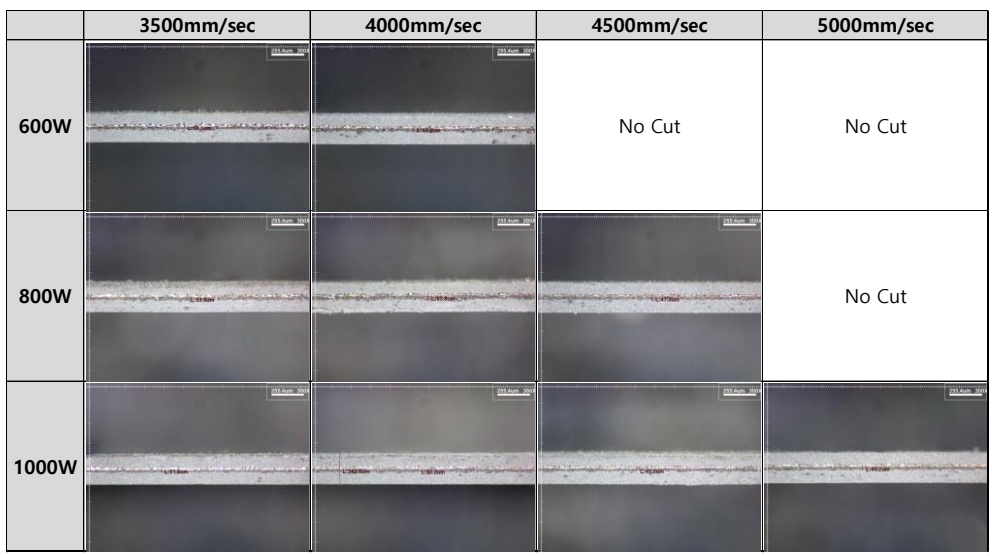

Figure 6-11: Microscope image of Cut edge (a), Cross section (b) in the process window

6.4.2.5 Elements Analysis

EDX (Energy Dispersive X-ray Spectrometer) was used to measure the changes in the material composition of HAZ and the cross section of the cut edge after cutting. One parameter of each CW and Pulse at the same heat input was selected to measure.
-Energy Dispersive X-ray Spectrometer : The electron microscope is a main source and a detector can be mounted within the electron microscope to analyze the composition of the specimen to be observed. All of the elements that make up a

specimen have their own characteristic energy, and each element that is physically examined by the electron gun of the transmissive electron microscope is generated by the interaction of the element of the primary electron and the specimen. [52]

Around cut edge

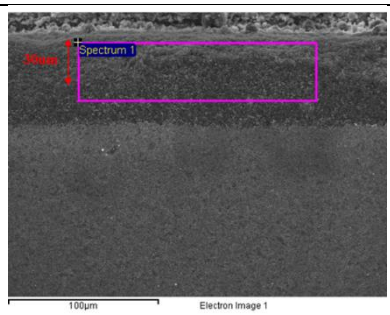

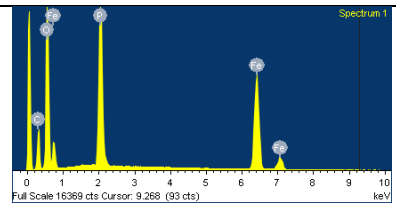

Element	Weight%	Atomic%
C K	23.21	35.71
O K	42.78	49.42
P K	13.63	8.13
Fe K	20.38	6.74
Totals	100.00	

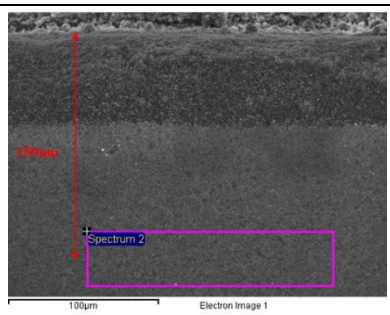

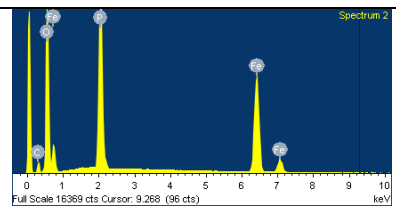

Element	Weight%	Atomic%
C K	10.19	18.07
O K	44.03	58.62
P K	19.07	13.12
Fe K	26.71	10.19
Totals	100.00	

Cross-section

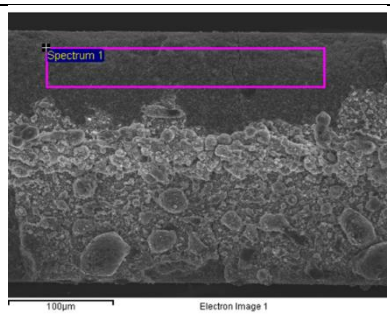

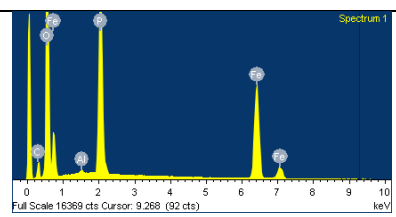

Element	Weight%	Atomic%
C K	11.04	18.16
O K	51.72	63.90
Al K	0.20	0.15
P K	16.45	10.50
Fe K	20.60	7.29
Totals	100.00	

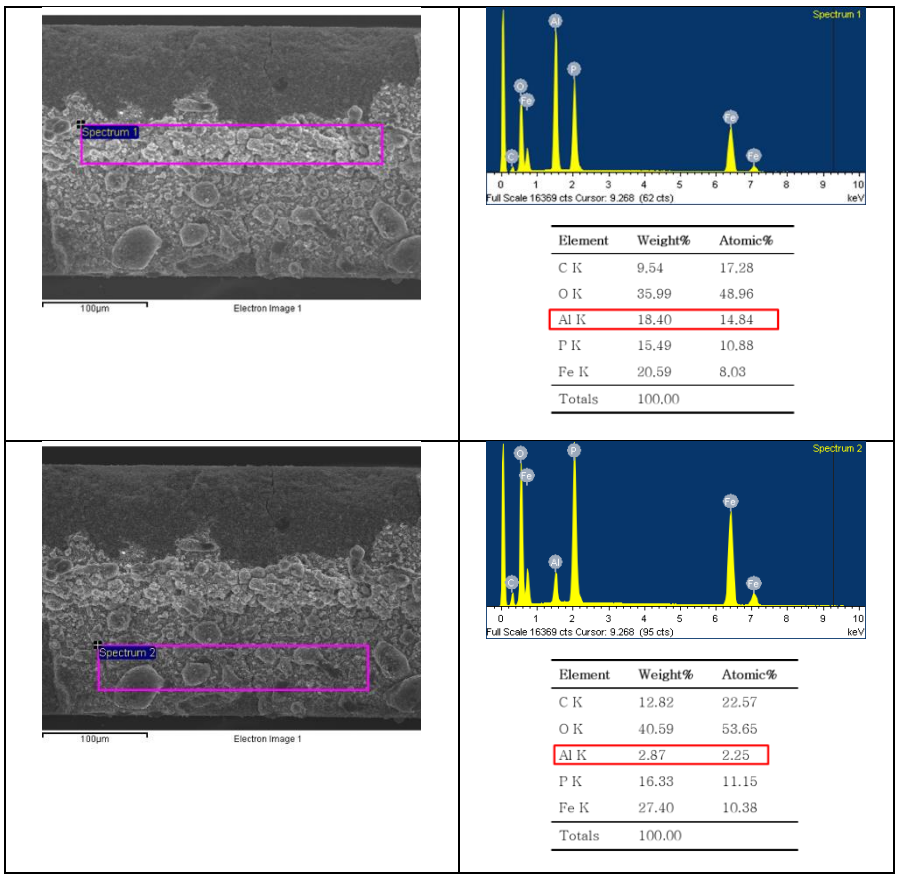

Element	Weight%	Atomic%
C K	9.54	17.28
O K	35.99	48.96
Al K	18.40	14.84
P K	15.49	10.88
Fe K	20.59	8.03
Totals	100.00	

Element	Weight%	Atomic%
C K	12.82	22.57
O K	40.59	53.65
Al K	2.87	2.25
P K	16.33	11.15
Fe K	27.40	10.38
Totals	100.00	

Figure 6-12: Images and data of EDX analysis of CW laser experiments

The upper part of the specimen is an active material layer, and it can be seen that all elements of $LiFePO_4$ were detected except Li element which is because low atomic number elements such as H, Li etc. are not detected by EDX equipment. Three elements detected at a point 30um away from cut edge and at a distance of 150um away are the components of active materials except C (carbon) element. Note that the C element detected at 30um from cut edge is more than twice the amount of C detected at 150um apart. There are several reasons to speculate. First, it can be that the fine particles generated during the reaction of the laser and the material are spread. Second, the black fume generated by the combustion is spread near the cut line. Third, It can be as a results of oxidation of raw materials by the hot plasma. The detection of a significant amount of C at a point 150m away indicates that the combustion particles have dispersed to more than 150um.

In cross section, three sections were measured: the upper active material layer, the

metal layer, and the lower active material layer. As in the first picture, the upper part of the active material layer is visible without any mixture of fusion. Besides O, Fe and P, the elements of active materials, C and a small amount of Al were detected. The second picture is the metal layer, and element O, Fe, and P were all detected at high proportions besides Al. It can be understood that the active material of the upper part reacts with the laser and the resulting weld pool is flowing downward by gravity. The third picture is the lower part of the active material layer, but the lower part of the SEM picture shows a large difference from the upper layer. Material that looks to be a mixture of metal and active material completely covers the active material layer. Al detection appears to have affected the upper layer of metal below, and it is noticeable that compared with the upper active material layer, O component decreased and Fe component increased.

For better understanding, the value of the element weight % detected above is shown in Graph 6-6.

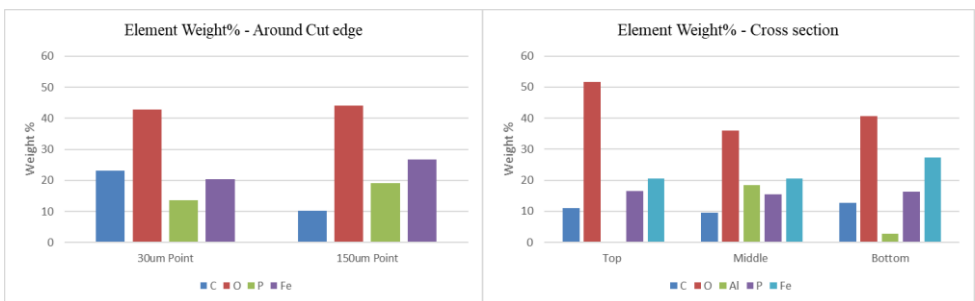

Graph 6-6: Summary of components detected in around cut edge (a), cross section (b)

6.4.2.6 Discussions

When a laser is irradiated on a material, various physical and chemical reactions are involved. Ablation cutting is fundamentally based on thermodynamic or heat transfer mechanisms, and the material undergoes heating, melting, and vaporization processes, leading to loss of material. The electrode material of the Li ion battery necessarily has a sandwich structure of the current collector metal and the active material. For this reason, it can be assumed that the cut quality will vary depending

on the reactivity of each material and laser, unlike the case of a single material. The physical properties of aluminum as a current collector shows very low absorption rate at IR wavelength, high thermal conductivity, melting point and boiling point. On the other hand, the absorption rate of the active material is relatively higher than that of aluminum, and the thermal conductivity, melting point, and boiling point are low respectively. The difference in the physical properties of these two materials seems to be different from the cutting of other materials.

The SEM images of figure 6-12 are the result of high and low cutting speed in CW laser experiments. In both cases, the upper active material layer was removed more widely than the underlying metal layer. It means that the ablation threshold of the metal is higher than the active material, and that laser energy should be set higher than the ablation threshold of the metal layer in order to completely separate the sample. Due to the relatively high ablation threshold value of metal, the upper active material is wider than the beam spot size and is wider than the kerf width of the metal layer. M. Lutey et al [38] assumed this phenomenon as follows. One is that direct ablation of the upper active material layer over a larger width than the underlying metallic layer due to differences in ablation threshold, the other is that heat accumulation and conduction effects from the metallic layer leading to subsequent heating and removal of the active layer beyond the exposed area.

At low cutting speeds, there are many metal particles around cut edge and debris that looks like parts of the active material are spread out far beyond the HAZ. The spherical solids may be re-solidified matters of independent or mixed with Li, Fe and P, which are components of the active material of the upper part or of the current collector Aluminum. Although it is unclear what material is in the SEM image, it is evident in the microscope image that it is metal particles as in figure 6-13(a) (b). The shining spherical solids around cut edge are clearly metals and are smaller than 40um in size. In figure 6-13 (a), it can be assumed that cracks were caused by shrinkage of the material at the time of solidification and the end of active material looks crispy and dry because the binding material is removed by heat effect and then lost bonding

property.

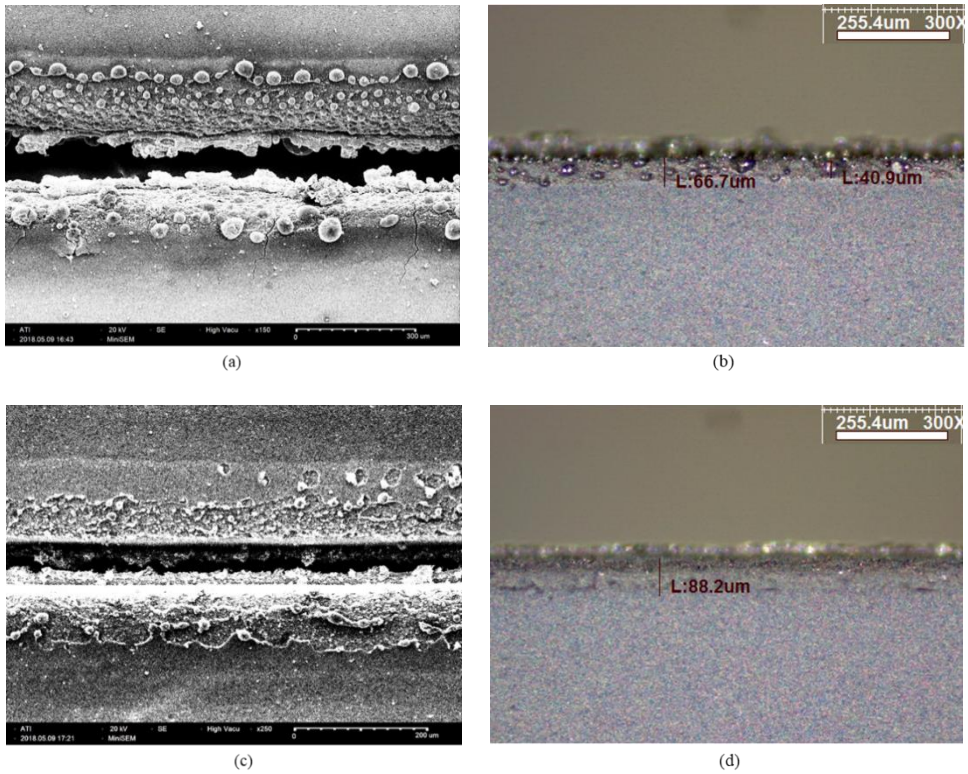

(a) (b) (c) (d)

Figure 6-13: SEM and microscope pictues of 1000mm/sec (a)(b), 4000mm/sec (c)(d) at 800W CW

At high cutting speeds, there are no noticeable spherical shape solids seen a lot at low cutting speeds. An unknown thin layer of material seems to have been peeled off by heat affection. It is assumed to be one of the following. One can be a binder(or unknown coated layer) that bonds the powers of raw materials of active materials, and the other is that one of the material with low melting point of active materials can be re-solidified on the surface thinly due to heat effects as in figure 6-13(c).

It is assumed that the relatively low peak power and the resulting power intensity caused incomplete evaporation and that boiling became the main mechanism of the material removal, leaving the larger voltage droplets around the cut line.

The above reviews clearly show that cut quality can be significantly improved by increasing the speed and reducing the heat input.

6.4.3 Results of Pulsed Laser Experiments

6.4.3.1 Maximum cutting speed with Pulsed Laser

Firstly, the maximum cutting speed was investigated for each parameter of the pulsed laser. The pulsed parameters such as pulse duration and PRR can be changed and the change of these two parameters leads to change of pulse energy and peak power. Changes in these four parameters are expected to affect the cutting speed and quality.

The graph 6-7 shows that the maximum cut rate is different at each parameter. The cutting speed of all parameters with is slower than CW since average power is 200W comparing to CW 1000W. Concerning the maximum cutting speed of CW 200W was 1000mm/sec, the results are comparable. Overall, the longer the pulse duration and the higher the PRR, the higher the maximum cutting speed was obtained.

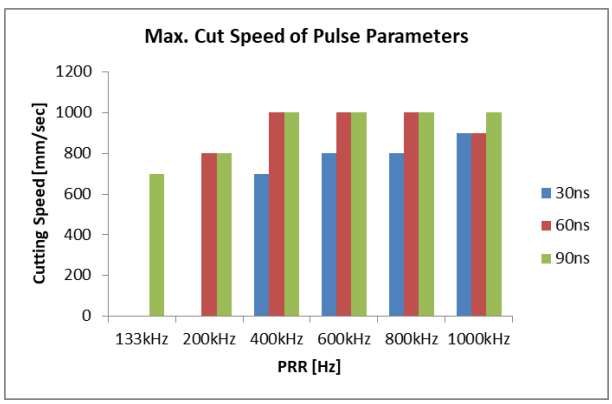

Graph 6-7: Max. cut speed of pulsed laser parameters

6.4.3.2 Cut quality – Qualitative analysis

Pictures of the results of 15 laser parameters and 8 scanning speed parameters are represented in figure 6-13 and 14. It helps to visually determine how each parameter change affects the results of the experiments. Also the maximum cut speed can be seen at each parameter by checking the empty space marked with 'No Cut' without pictures.

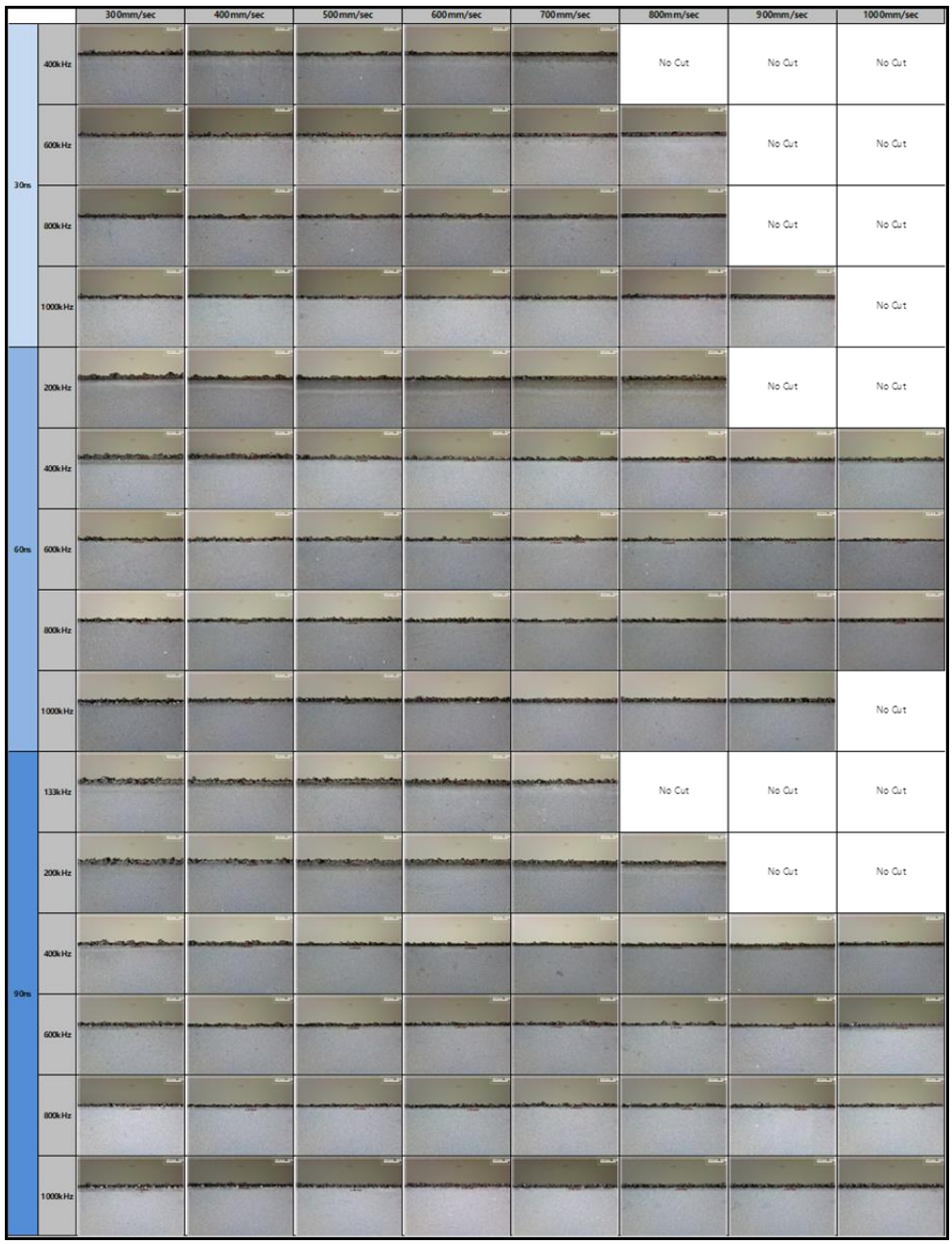

Figure 6-14: Full sets of cut-edge pictures for whole parameters

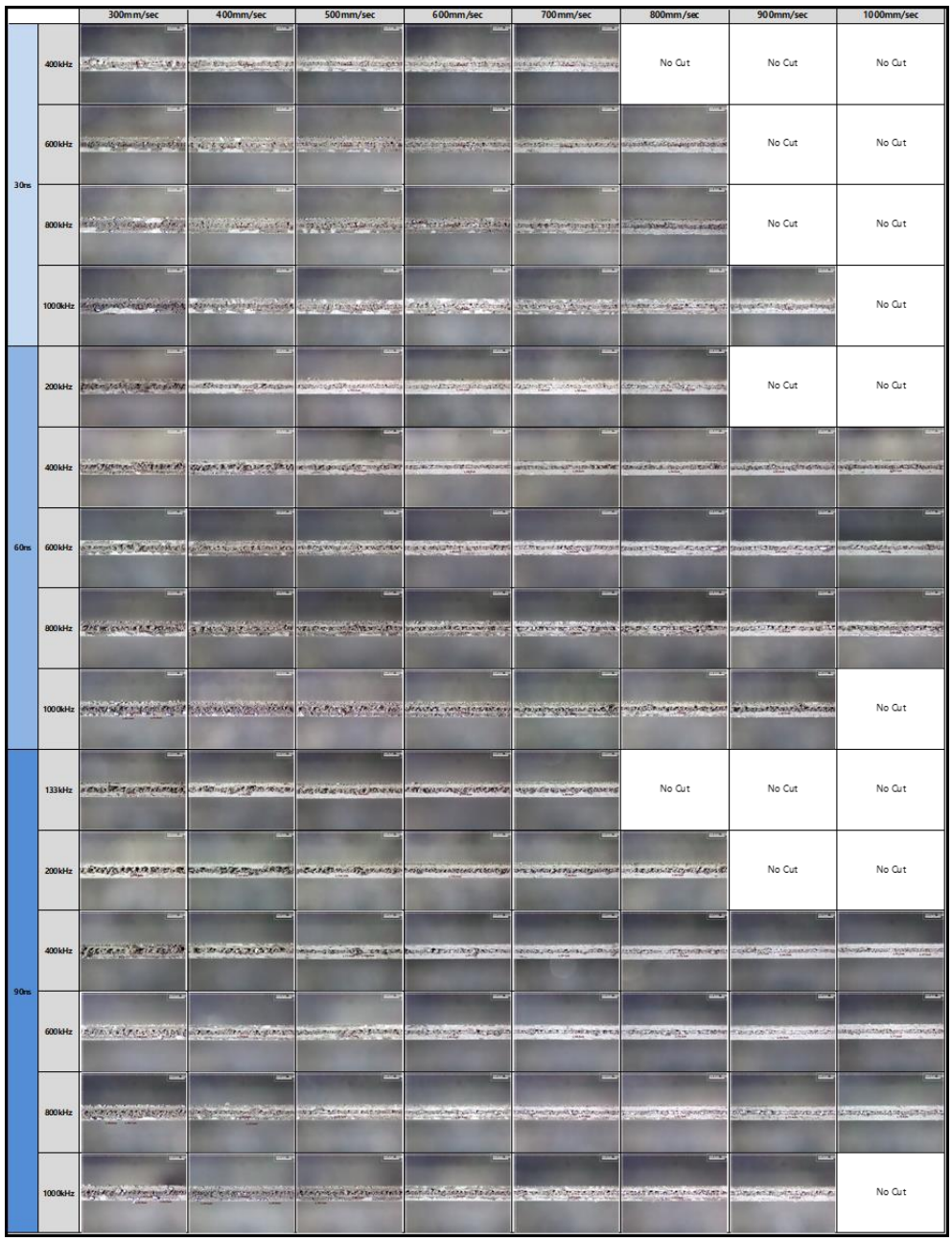

Figure 6-15: Full sets of cross-section pictures for whole parameters

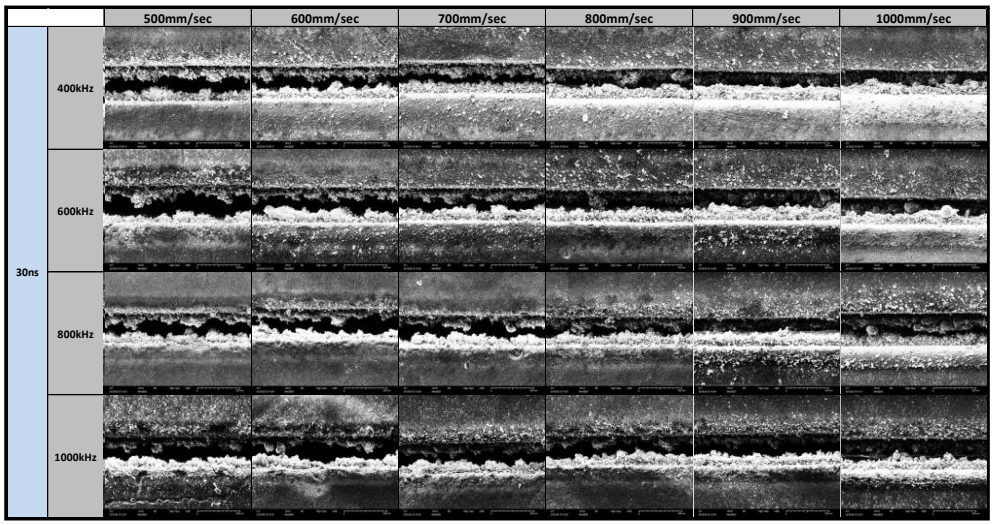
500mm/sec
600mm/sec
700mm/sec
800mm/sec
900mm/sec
1000mm/sec
30ns
400kHz
600kHz
800kHz
1000kHz

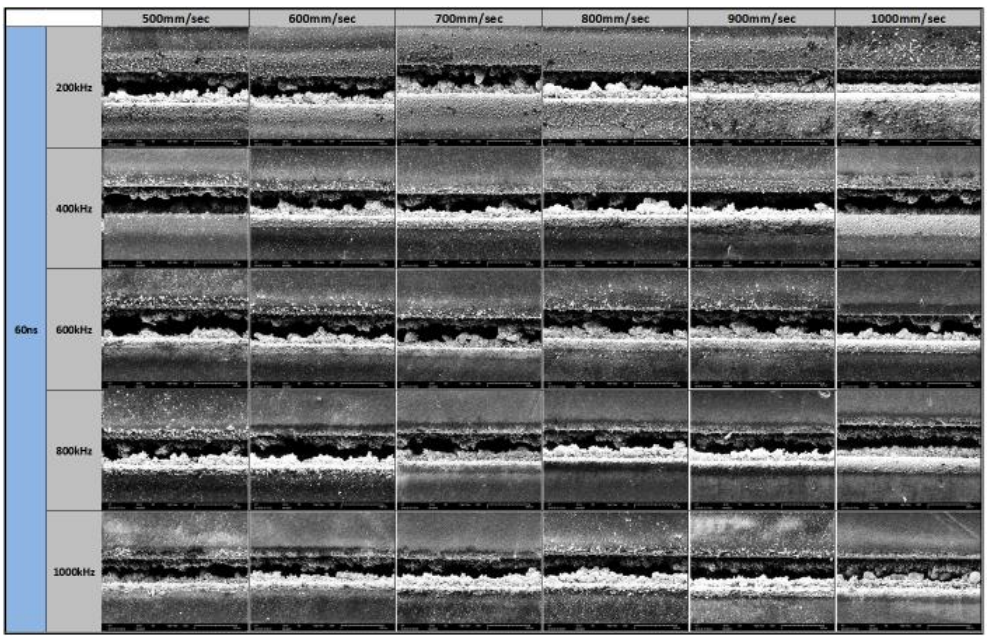
500mm/sec
600mm/sec
700mm/sec
800mm/sec
900mm/sec
1000mm/sec
60ns
200kHz
400kHz
600kHz
800kHz
1000kHz

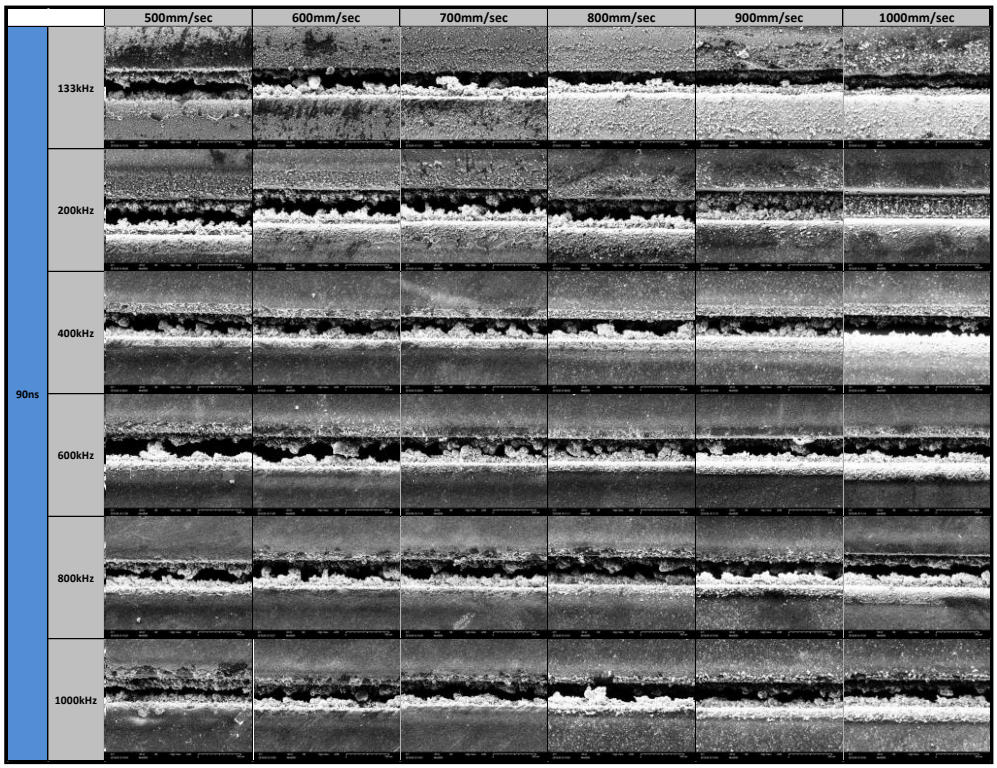

Figure 6-16: SEM pictures for whole pulsed parameters

About cut edge pictures from the top, the quality of the metal edge and HAZ are different according to the changes in PRR in each pulse rotation. In general, the lower the PRR, the wider the exposed metal and the greater the width of the HAZ. However, there is no linear trend according to the parameters. Especially noticeable is the metal edges that are uneven and protrude in many places. And the exposed metal color is darker than the CW results.

About cross-section pictures, it shows a big difference of quality depending on the pulse duration and PRR. Depending on the parameters, the quality is different from good to poor, but overall the cut section is covered with material of re-solidified molten, the width of the metal is excessively expanded, and its shape is very rough. SEM pictures are organized and attached for all parameters. SEM pictures provide more clarity on HAZ and fine particles around cut lines that were difficult to identify with microscope pictures. It shows better quality at 60ns and 90ns than 30ns, and at

600kHz and 800kHz of 90ns, there are fewer parts around cut edges, and the width of HAZ is narrow.

6.4.3.2.1 The effect of Pulse energy

First, the effect of the pulse energies that can be set in laser when a same overlap rates (about 93%, but for better understand, added 1.5mJ & 0.25mJ even though overlap rates are little bit different) was investigated. The pictures are omitted if the parameter is out of range or no-cut. Pictures of cut edge and cross section were arranged for pulse duration on horizontal axis and pulse energy on vertical axis in figure 6-17.

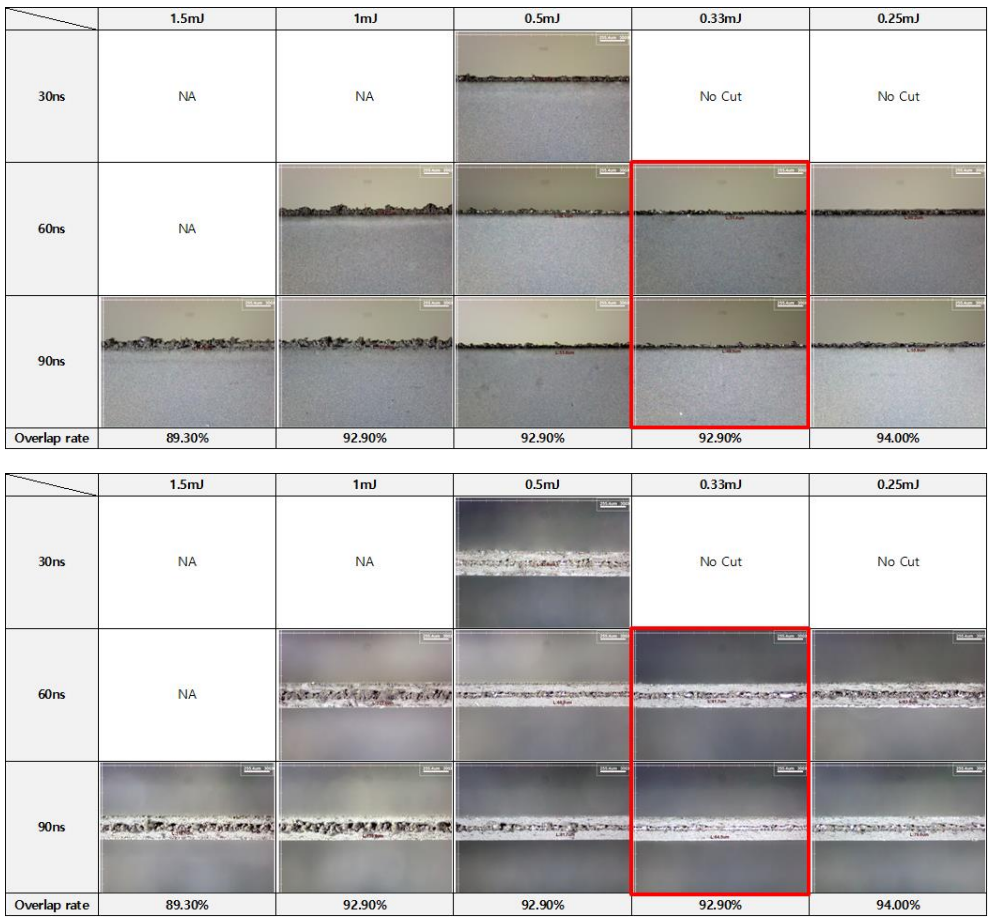

Figure 6-17: Pictures for the effect of pulse energy changes on cut quality

From the cut edge picture of figure 6-17 (a), overall it was found that the extended metal and HAZ width were wide in high-pulse energy areas and narrow in low-pulse

energy areas. Similarly, in cross-section pictues of figure 6-17 (b), the middle metal is spread up and down widely in high-pulse energy areas and narrow in low-pulse energy areas. In the same pulse energy, it looks that the longer the pulse duration, the better the quality of cut edge and cross section.

Cut quality was better in areas marked with red rectangles, and then the pulse energy was 0.33mJ.

6.4.3.2.2 The effects of Heat input

Heat input[J/mm] is the energy radiated per unit length and is a parameter in the laser cutting. As checked earlier, cut quality was better when pulse energy was 0.33 mJ. This time, when the pulse energy is equal to 0.33 mJ, the effects of changes in heat input were investigated.

Heat input is a function of power and speed. However, because of the constant process parameter of 200W power, Heat input is a function of speed only in this experiment. Changes in heat input result in changes in speed and overlap rate. In addition, the pulse energy is the same, which results in changes in the peak power and power intensity.

Pulse Energy 0.33mJ		400mm/sec	600mm/sec	800mm/sec	1000mm/sec	Intensity[W/cm^2]
600kHz	30ns		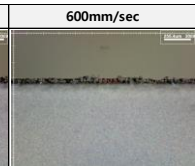	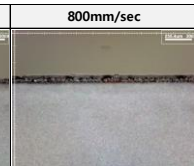	No Cut	3.18x10^9
	60ns					1.59x10^9
	90ns					1.06x10^9
Overlap rate[%]		96.80	95.20	93.70	92.10	
Heat Input[J/mm]		0.50	0.33	0.25	0.20	

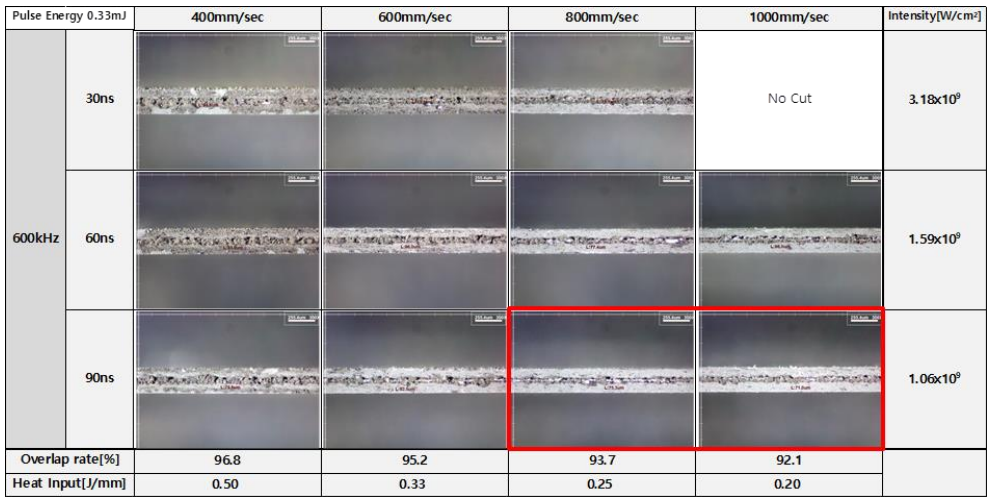

Figure 6-18 : Pictures for the effect of heat input change on cut quality

From pictures of cut edge in figure 6-18, It can't be said something for sure because there is no big difference, but it looks that quality is better in areas with high cutting speed and long pulse duration. From pictures of cross-section, it's a little bit clearer than cut edge. When the heat input is small and the pulse duration is long, the three layers are exposed and the metal layer in the middle is clearly visible.

In summary, at the same pulse energy, cut quality showed better in the parameters of heat input of 0.2 to 0.25 [J/mm], and an overlap rate of 92% to 94%, and power intensity of $1.06x10^9 W/cm^2$.

6.4.3.2.3 The effects of Overlap rate

Figure 6-19 shows the effect of changes in the overlap rate. Overlap rate changes as PRR changes at a fixed scanning speed. Heat input 0.25J/mm and scanning speed 800mm/sec are constant parameters in this investigation.

The cut edge viewed from the top is not so good overall, but A changes of the roughness of cut edge can be seen slightly. The width of the HAZ appears to be the narrowest in the 600 kHz to 800 kHz or the overlap rate 92 to 96%.

As in the previous cases, the cross-section pictures make it clearer. Clear metal lines can be seen in parameters near 93.7%. and the other parameter at that point are the pulse energy of 0.33mJ as that found in the previous case.

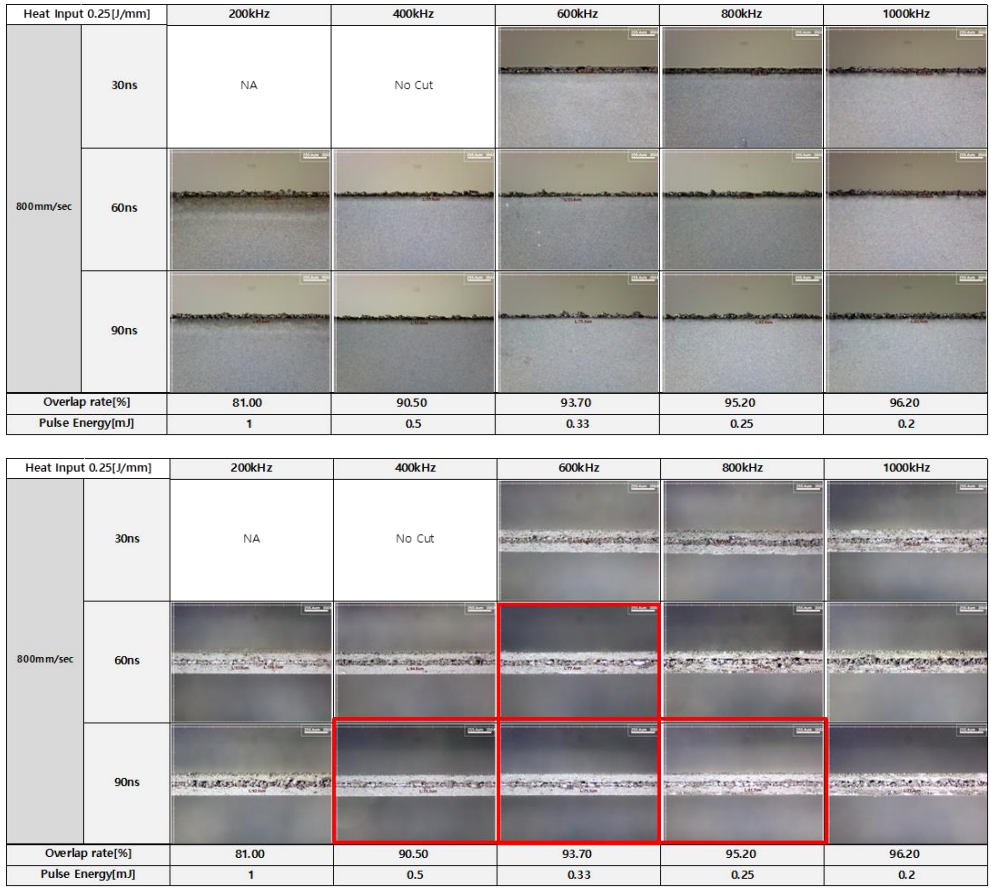

Figure 5-19 : Pictures for the effect of overlap rate change on cut quality

5.4.3.3 Cut quality – Quantitative analysis

5.4.3.3.1 Kerf width

First, for all parameters, the kerf width of the all the cut samples was measured. For the three pulse durations, It was observed how the kerf width changed with changes in PRR and speed. The slope of the trend line is smaller than that of CW, which is because the range of speed changes is small. Overall, as the scanning speed increases, the kerf width tends to decrease in the three pulse durations. The narrowest range we are interested in is about 100um similar in all durations. But at 90ns and 600 to 800 kHz, less than 100um was measured.

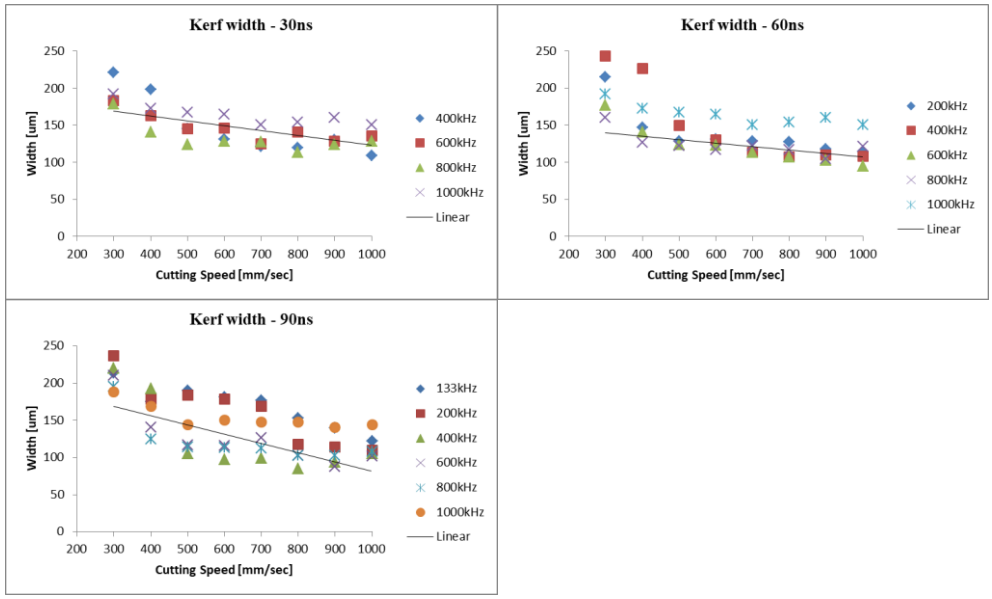

Graph 6-8: Measured values of kerf width variation at 30ns, 60ns, 90ns

6.4.3.3.2 HAZ width

Graph 6-9 represents HAZ width at three pulse durations. HAZ has been measured to the extent of discoloration of the active material or the boundary over which the debris is spread, and if it is unclear to measure, the values are missing. As can be seen in graphs, the measured values are spread widely and when the width is narrowest, the measured value was about 10~20um at 60ns, 800~1000kHz.

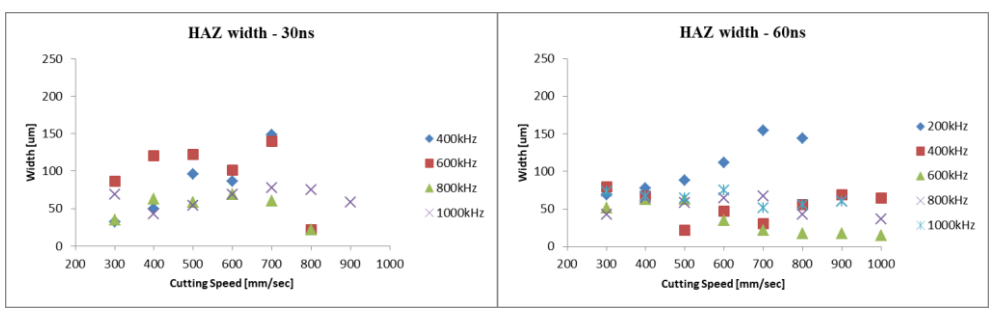

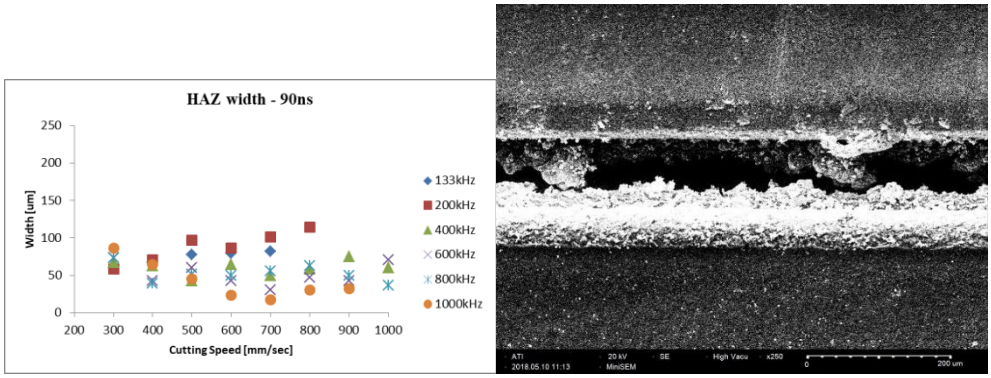

Graph 6-9: Measured values of HAZ width at 30ns, 60ns, 90ns
Figure 6-20 : SEM picture of cut edge at 90ns, 600kHz, 800mm/sec

6.4.3.3.3 Exposed Metal width

Graph 6-10 shows the measurement of the exposed metal width of one side cut edge. Overall, It also shows that the higher the scanning speed, the lower the metal width. However, for all three pulse durations, the minimum value is about 50um and all three are similar. A cut edge picture of the best parameters is attached to aid understanding in Figure 6-21. As shown in the picture, the metal edge looks uneven and rough.

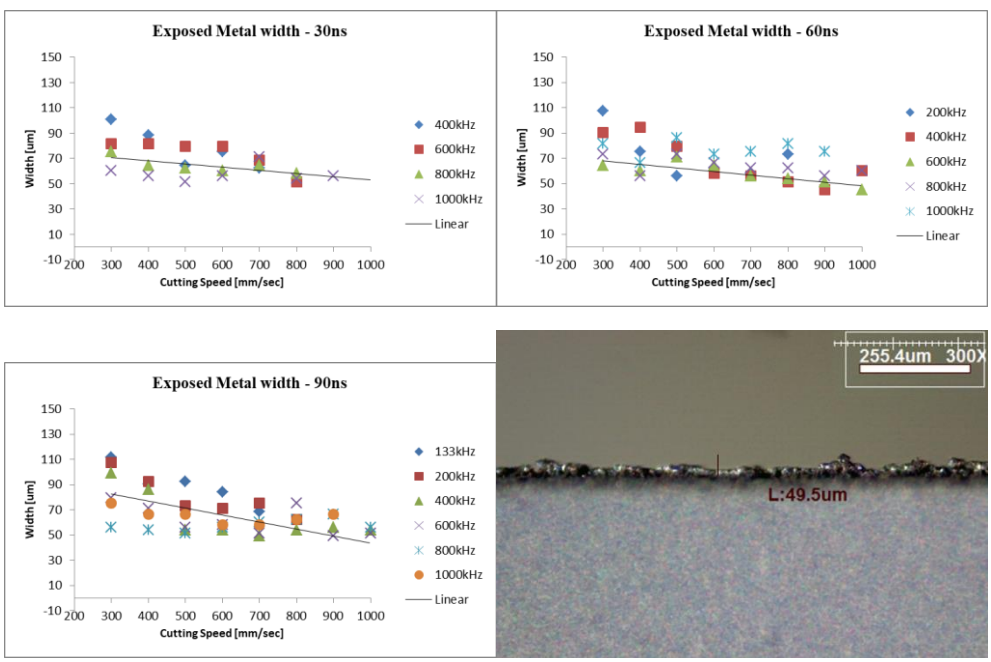

Graph 6-10: Measured values of exposed metal width at 30ns, 60ns, 90ns
Figure 6-21 : Microscope picture of cut edge at 90ns, 600kHz, 800mm/sec

6.4.3.3.4 Extended Metal Width at Cross-Section

The metal width at cross-section was measured as shown in Graph 6-11. The reason for the low number of measured data is that the boundary of three layers were ambiguous and could not be measured. Although there is a general tendency to decrease with increasing scanning speed, it is difficult to specify the parameter with the lowest value. The parameter showing the best result is at 90ns, 600kHz, 900mm/sec and the width is approximately 65um. The microscope image of the parameter is attached in Figure 6-22. The thickness of the metal is uneven, and the section is attached to the particles, so it looks messy.

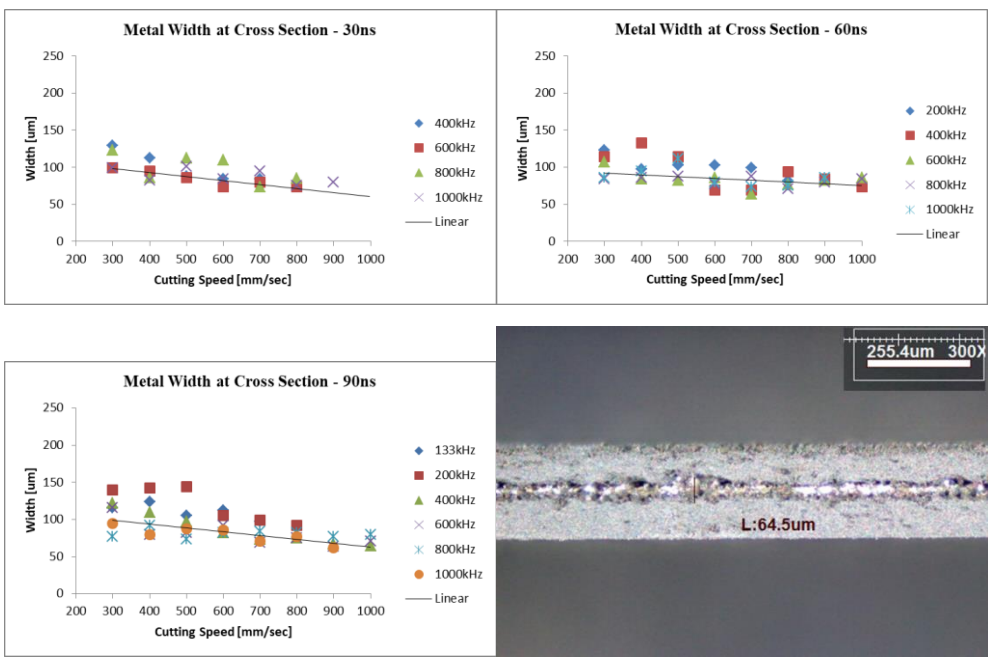

Graph 6-11: Graphs of measured metal width at cross-section at 30ns, 60ns, 90ns
Figure 6-22: Picture of cross-section at 90ns, 600kHz, 900mm/sec

6.4.3.4 Process Window of Pulsed Laser Experiments

Based on the above results, the best result is observed at 90ns, 600kHz, 800 ~1000mm/sec. and the other physical values are pulse energy 0.33mJ, power intensity $1.06 \times 10^9 W/cm^2$ and overlap rate of 93.7%.

The process window of pulsed laser results is depicted on the graph 6-12. Also the pictures are attached with a enlarged size of cut edge and cross section observed in

the parameters near the process window area. Particle or debris, which has been clearly identified in the low speed area, can be found to be few in this process window area.

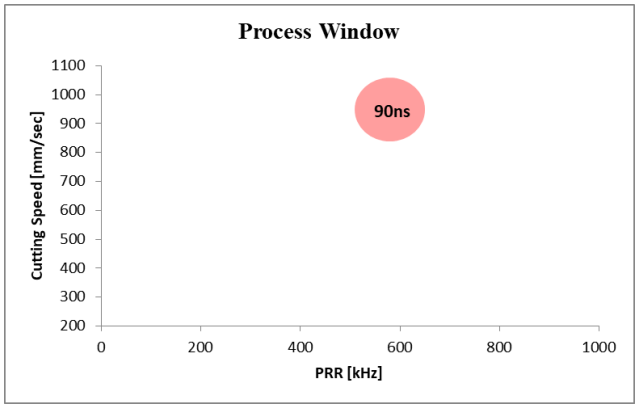

Graph 6-12: Process window of CW laser expriments

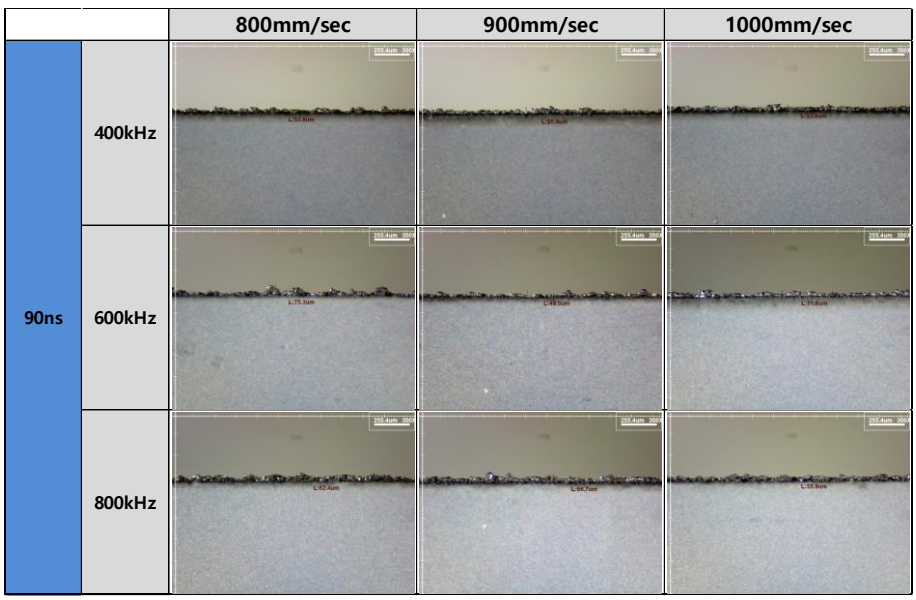

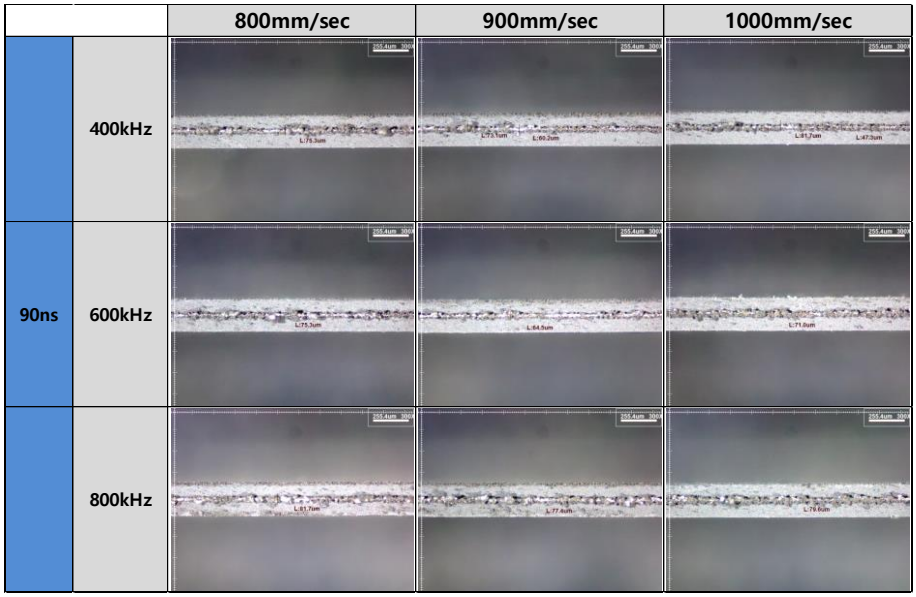

Figure 6-23: Microscope pictures of cut edge(a), cross section(b) in the process window

6.4.3.5 Components Analysis

The components at 30um and 150um away from the upper cut edge were analyzed as in CW. Compared to the results of the CW we looked at earlier, it can be seen that some of the white-colored parts or debris in the SEM pictures spread much more widely around cut edge.

Around Cut edge

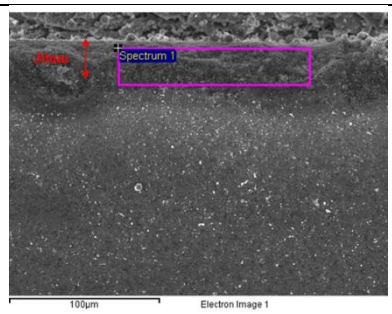

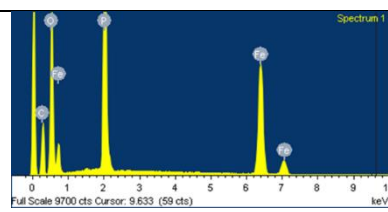

Element	Weight%	Atomic%
C K	24.40	37.15
O K	42.49	48.58
P K	13.05	7.70
Fe K	20.07	6.57
Totals	100.00	

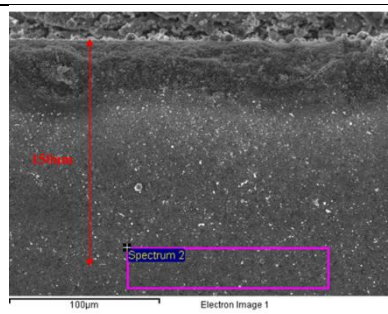

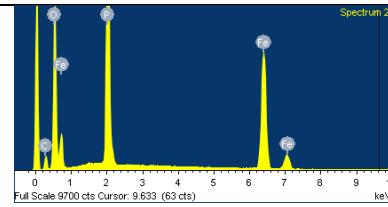

Element	Weight%	Atomic%
C K	11.07	19.41
O K	44.08	58.03
P K	18.66	12.69
Fe K	26.19	9.88
Totals	100.00	

Cross-section

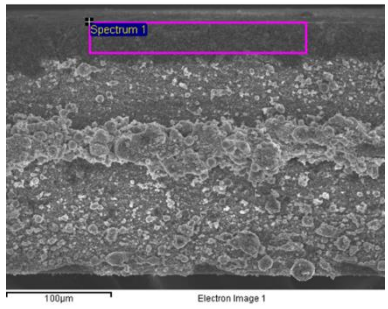

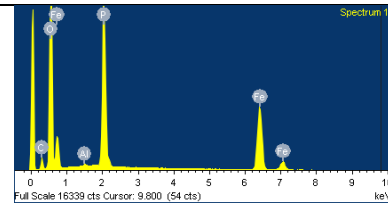

Element	Weight%	Atomic%
C K	11.12	18.16
O K	52.53	64.39
Al K	0.19	0.14
P K	16.38	10.37
Fe K	19.78	6.94
Totals	100.00	

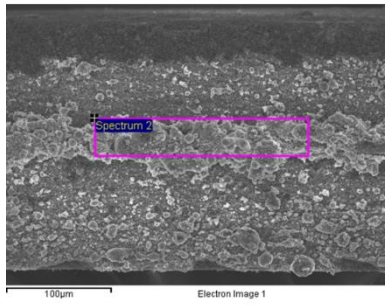

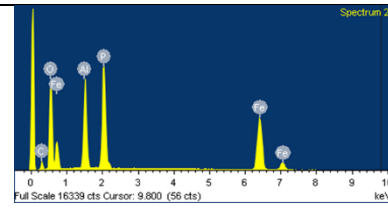

Element	Weight%	Atomic%
C K	12.72	22.08
O K	39.12	50.99
Al K	11.18	8.64
P K	14.95	10.07
Fe K	22.03	8.22
Totals	100.00	

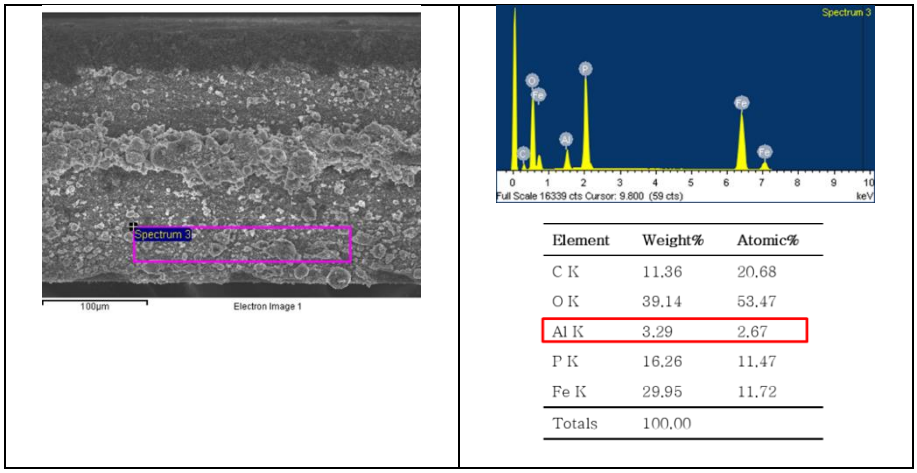

Element	Weight%	Atomic%
C K	11.36	20.68
O K	39.14	53.47
Al K	3.29	2.67
P K	16.26	11.47
Fe K	29.95	11.72
Totals	100.00	

Figure 6-24: Images and data of EDX analysis of Pulse laser results

Assuming that the thermal effect is relatively small compared to 30um at 150um point, it can be said that the element composition is changed by thermal effect at 30um point. At 30um point compared to 150um point, C increased more than 2 times, O was similar, P and Fe decreased. C, which shows the greatest change, appears to be the result of oxidation caused by heat affection, as in the CW case. In fact, at 30um point, the color of the surface is blackish and looks like a HAZ. The decrease in P and Fe appears to be lost due to the oxidation of each element by thermal effects. In cross section, the overall sizes of the particles are small compared to CW. The white colored small debris and fine spherical particles are spread all over the region except for a part of the top, through which we can deduce that there will be a change of components of the particles covered on the metal layer and the bottom active material layer. Unlike the topmost layer, the two layers below seem to be different with the detected components for this reason, as the surface looks like other materials covered with mixtures. The most noticeable of the three layers are O, Fe, and Al. Changes in O and Fe are almost similar to those in CW. Al was not detected in the upper active material layer and was detected in the lower active material layer because it can be deduced that the molten particles of Al descend downward by gravity. Fe, like Al, increases in the downward direction. The reason is that the molten solid has moved downward.

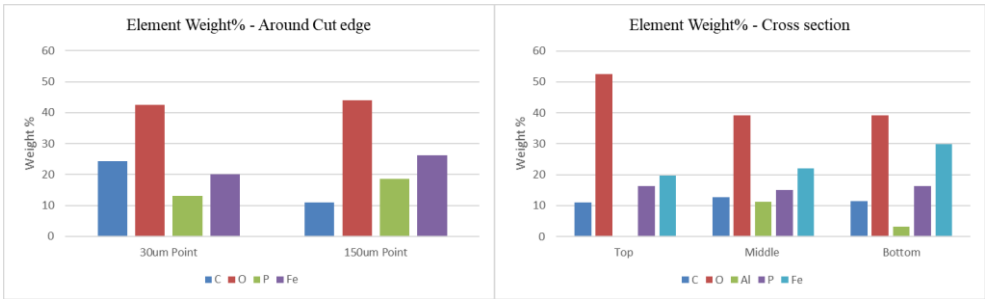

Graph 6-13: Summary of components detected in around cut edge (a), cross section (b)

6.4.3.7 Discussions

In the pulsed mode, there are other parameters besides the laser output. Pulse duration, PRR, pulse energy, and peak power. These variables are correlated so that changing one variable changes the other. For example, changing the PRR in the same pulse duration changes the pulse energy and peak power. Also, if pulse energy is the same, changing pulse duration will result in a change in peak power. Another variable is created by the PRR, which is the Overlap rate. Overlap means how much size of pulse beam is superimposed for each pulse and is an important parameter that affects the quality of the cut section. For this reason, it is not easy to control only one variable in a pulsed laser. And it is not easy to achieve meaningful results when only parameters to want to verify are variables and other parameters are controlled. For example, if controlling other variables and changing the pulse duration only, there would result in no-cut by changing the pulse duration. Because this experiment is intended to compare cutting quality, parameters that are not cut are meaningless. In other words, it was not easy to make either parameter as a fixed variable due to the correlation of the various parameters, and this experiment was conducted using all possible lasing range and used as fixed variables such as power and speed and as variables such as pulsed duration and PRR, and the results were summarized and analyzed. Earlier we looked at the effect of the pulsed parameters on this background. First, looking at the SEM picture of the cut edge in figure 6-25, as in CW, the active material layer at the upper part was ablated wider than the middle metal layer. That

is, the evidence that metal's ablation threshold is higher than the active material. About around of cut edge, the narrower the pulse duration, the more spread of particles around the cut line. It implies that there was a much more violent reaction

Controlled parameters : 200W, 800mm/sec, 0.25J/mm, 0.33mJ, 93.7% overlap		
30ns	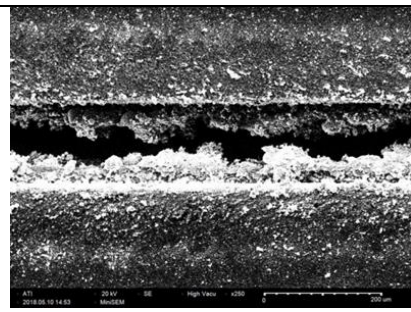	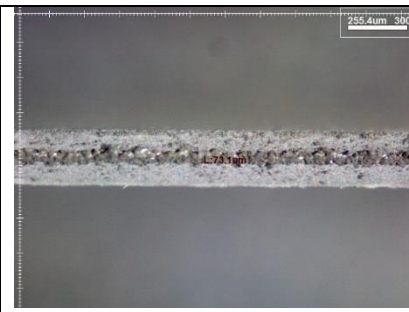
60ns	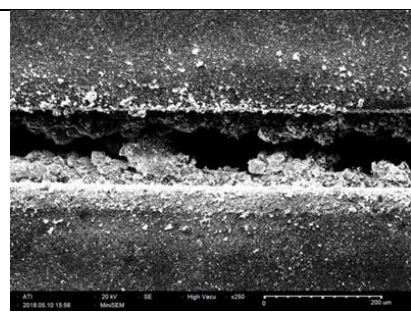	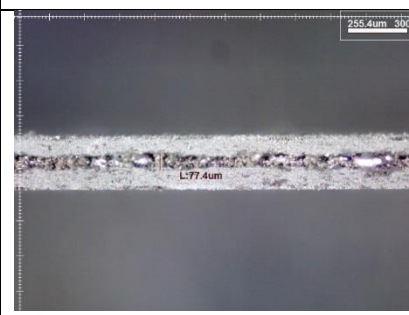
90ns	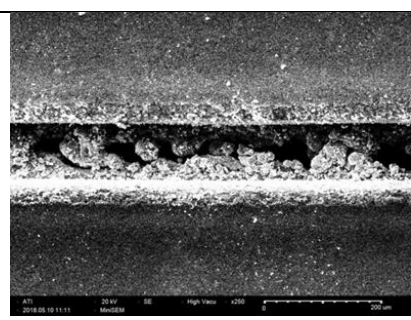	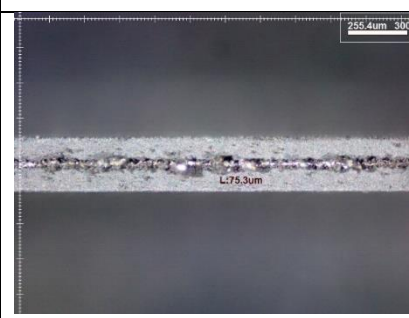

Figure 6-25: Cut edge and cross-section pictures of each pulse duration at 600kHz, 800mm/sec

at 30ns compared to 90ns. This can be inferred from the fact that peak power is high at 30ns, the material was subjected to a violent reaction by the high peak power or power intensity, and the resulting particles were scattered across a wide area. The shape of the metal layer below, the end looks round or smooth when it is 90ns compared to 30ns. At 30ns, the material was instantaneously reached to the boiling temperature by a short, high pulse, which caused pressure distribution by plasma

generated by the parts that were vaporized, and the molten fluid to be spread by this pressure. At relatively low power intensity at 90ns, the sample failed to reach a high temperature and then the melted material was not ejected much due to the insufficient vapor pressure.

Cross-section pictures show similar results. At 30ns, the high intensity of each pulse is applied deeply to the material at a time, and the molten of the upper active material is passed to the middle metal layer, so the color looks dark and the surface of the metal seems to be directly ablated by laser beam and the metal layer has undergone a violent response. On the other hand, at 60ns and 90ns, the metal layer appears to be shinny in places and the metal surface feels soft compared to 30ns. It seems that the heat transferred to the active material layer from laser beam has been transferred to the metal layer below and undergone re-solidification after melting process. In other words, due to low power intensity, the ablation depth was not reached to the metal layer, and the shallow thickness which was ablated by laser beam seems to have experienced thermal reaction.

In summary, it is evident that different laser-material interaction occurred between 30ns and 90ns. At 30ns the samples would have been subjected to a violent response due to the high-power intensity, and at 90ns the lower power intensity would have given a relatively benign response. It is assumed that the material removal mechanism at 30ns is ‘vaporization’ and ‘boiling’ at 90ns. In other words, theoretically, the different ablation mechanism took place at each pulse duration.

6.4.3.6 Comparision between CW and Pulsed

Additional experiments were conducted to investigate the effects of different mode between CW and pulsed mode. To do so, the power and the scanning speed were controlled for the same heat input. CW 200W and same cutting speed with pulsed tests were applied and then the cut quality was compared. PRR was selected where cut quality showed better qualities in each pulse duration. The purpose of this comparison is to compare the results of CW and pulsed modes at the same heat input.

Cut edge and cross-section pictures are arranged in Figure 6-26. The results of 300mm to 400mm/sec were excluded for proper photo size.

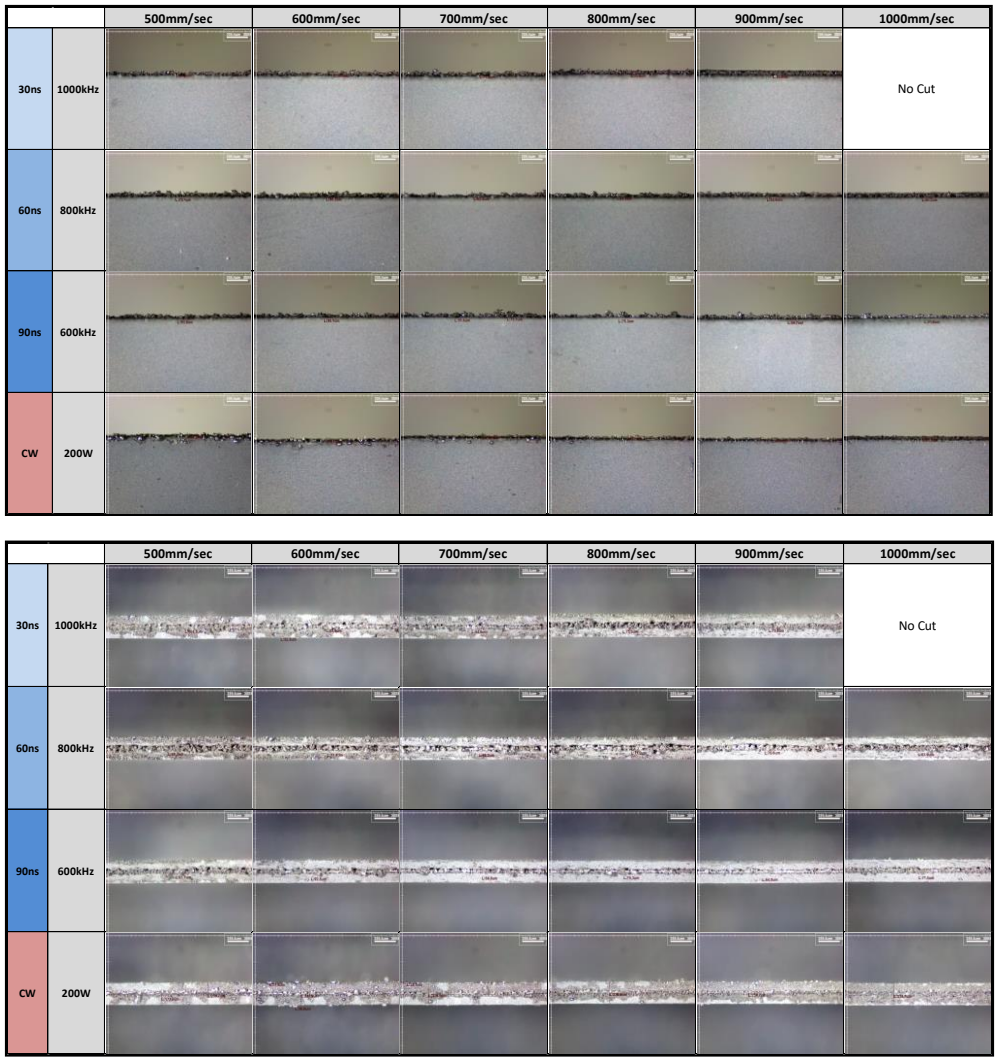

Figure 6-26: Cut edge and cross section pictures of CW vs Pulsed at same heat input

From cut edge pictures, the exposed metal is considerably wide and the metal edge looks rough and uneven for all pulse durations. It is important to note that the pulsed results overall has irregular metal protrusion. No metal particles or debris are visible around the HAZ. On the other hand, the exposed metal of CW is narrower than that of pulsed and the metal edge is more neaty. However, in areas of low cutting speeds, metal particles and debris are scattered around the HAZ, hardly seen in pulsed results.

Looking at the cross-section pictures, the 30s and 60ns of pulsed make it difficult to distinguish the three layers and the metal layer seem quite thick. The mixture of metal and active material is spread across the section and looks very rough. At 90ns, three layers may be identified above 700 mm/sec, but the metal in the middle is not uniform in width because it is lumped in parts. In CW the mixture of metal and active material covers the entire section in all areas, The solids of the mixture are covered like hard shells on the section wall, and these shells are cracked or peeled off in places so that the inner material is visible. It is difficult to distinguish three layers for all parameters of CW even though it was possible to distinguish three layers in pulsed results.

The SEM pictures of the cut edge viewed from top side are summarized with a much enlarged size. The cut edge not clearly seen in the microscope pictures, is clearly seen in the SEM pictures. Cross section pictures could not be taken because the sample could not be held vertically inside the SEM.

SEM pictures show cut quality more clearly. Comparing the results of pulsed and CW, there is a tendency on the laser mode. In pulsed, fine particles and debris are seen to be spread widely in the entire parameter area. On the other hand, in CW, large size metal particles are sticking around the cut edge, and particle size decreases as speed increases.

Comparing the quality of metal edges, Pulsed shows that it is rugged and coarse in all parameters and decreases as the speed increases. In CW, on the other hand, it looks less rugged than pulsed. It looks that there is a difference in the ablation mechanism between Pulsed and CW.

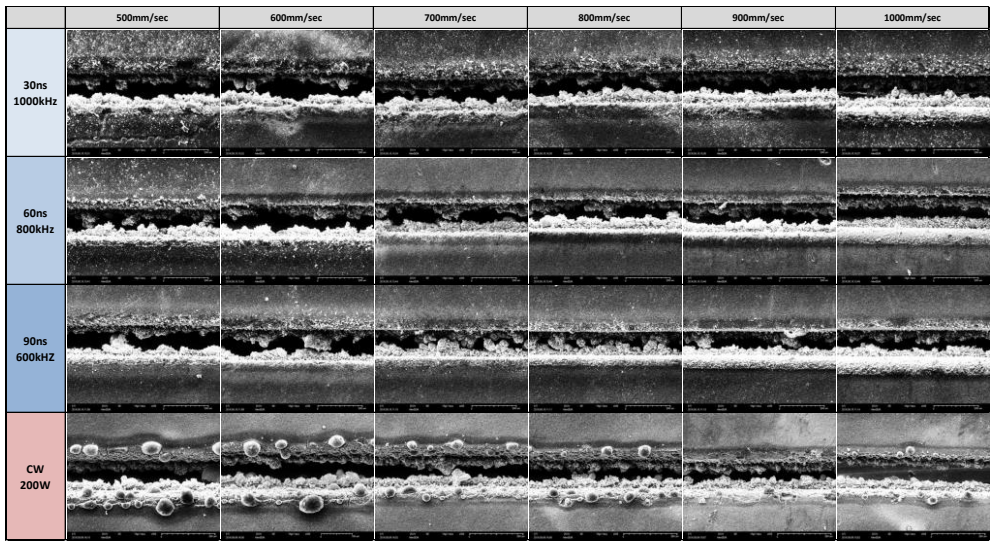

Figure 6-27: SEM pictures of Pulsed and CW with same heat input

In summary, at the same heat input, the pulsed result is that fine particles are spread around the cut edge, and the shape of the metal edge is not uniform and rough. The CW results show that large metal particles stick around the cut edge and the metal edge is more uniform and smooth than pulsed. From a laser-material interaction point of view, it is evident that the mechanism of material removal of CW and pulsed laser are completely different. In CW, the liquid expulsion is the predominant process, and in pulsed, the vaporization is the main process.

6.5 Summary

The positive electrode of a lithium-ion battery coated with $LiFePO_4$ on both sides of the Aluminum foil was tested and analyzed using two lasers. All possible parameters of each laser were tested, the results of each laser's parameters were compared, and the parameters showing good cut quality were found. For all the parameters tested, the cut edge and cross-section pictures were taken using SEM and Microscope, and all four defined factors for the cut quality evaluation were measured. The thickness of the thin samples made it difficult to measure the exact dimensions but tried to obtain the most accurate values. For all the parameters tested, SEM pictures and Microscope were qualitatively assessed in order to see how the cut

quality changed according to the parameter changes, and the measured values of the cut quality assessment factors were graphed and quantitatively evaluated. The cut samples were analyzed using EDX equipment to find out the changes in components after cutting around cut edge and cross section by selecting one of the samples tested with each laser. And tried to analyze the cause of phenomena theoretically from the perspective of laser-material interaction by selecting some of the results of each laser.

1) CW results

First, summarizing the qualitative assessment through SEM and microscope pictures of CW test results, the cut quality was improved with cutting speed increase overall for both cut edge and cross-section. About the cut edge viewed from the top, at low-speed areas, metal particles and debris, which look quite large, are scattered around cut edge, and the end of the metal also looks quite rough. However, at the fast-speed areas, both metal particles and debris are not seen, and the end of metal look smooth. At the speed of 2000mm/sec or above, particles and debris and cracks around cut edge are not seen in the microscope pictures.

About the cut quality of cross-section, the aspect of the change becomes more clearly. At low-speed areas, solidified materials are spread dirty on the cross-section surface and it is difficult to identify the width of metal in the center, while in fast-speed areas, the three layers of raw material are clearly visible. At the speed of 3000mm/sec or above, the cross section shows a clean section without solidified mixture.

The results of the quantitative assessment based on the defined assessment factors of the cut quality.

-Kerf width tends to be narrower as speed increases overall. In fast cutting speed areas, the higher the power, the narrower the kerf width is. When power is 1 kW and between 3000mm/sec and 5000mm/sec, the kerf width is the narrowest, and the value is approximately 70um.

-HAZ width also tends to decrease as speed increases. At the same speed, the lower the power, the narrower it tends to be. When power is 600W, it was narrowest at

3000~ 4000mm/sec and the HAZ width value is approximately 20um.

- The exposed metal width also tends to decrease as speed increases. When power was 600W to 1000W in 3500~4000mm/sec speed, 40um of width was observed and the best width was about 30um at Power 600W and 4000mm/sec.

-The extended metal width is about 40um in areas with power between 600W and 1,000W and speed between 4000mm and 5000mm/sec. Given the original aluminum thickness of 15-20um, this means that the metal was melted and spread widely during the cutting process.

The effect of heat input and power intensity on cut quality is also investigated. if the heat input is less than 0.2J/mm, Particle and debris are not visible around cut edge in all power intensities. And when power intensities are $1.44x10^8$ W/cm^2 and above, the metal of cut edge is also smooth, and solidified melts are not covered in the cross section and look neat. In the same heat input, it can be seen that the higher the power intensity, the better the cut quality. when the heat input was approximately 0.2J/mm, the power intensity about $2x10^8$ W/cm^2 showed the best cut quality in CW experiment.

The principal causes of the results of the CW experiment assumed that the relatively low peak power and the resulting power intensity caused incomplete evaporation and that boiling became the main mechanism of the material removal, leaving the larger size of droplets around the cut line.

2) Pulsed results

Summarizing the qualitative assessment through SEM and microscope pictures of pulsed laser test results, there is no linear trend according to the parameters. Especially noticeable is the metal edges that are uneven and protrude in many places. And the exposed metal color is darker than the CW results. overall the cut section is covered with material of re-solidified molten, the width of the metal is excessively expanded, and its shape is very rough. It shows better quality at 60ns and 90ns than 30ns, and at 600kHz and 800kHz of 90ns, there are fewer parts around cut edges,

and the width of HAZs is narrow.

-Pulse energy effects on cut quality: In the same pulse energy, it looks that the longer the pulse duration, the better the quality of cut edge and cross section. Cut quality was better with the pulse energy 0.33mJ.

-Heat input effects on cut quality: At the same pulse energy, cut quality showed better in the parameters of heat input of 0.2 to 0.25 [J/mm], and an overlap rate of 92% to 94%, and power intensity of $1.06x10^9 W/cm^2$.

-Overlap rate effects on cut quality: Clear metal lines can be seen in parameters near 93.7%. and the other parameter at that point are the pulse energy of 0.33mJ as that found in the previous case.

-Kerf width: Overall, as the scanning speed increases, the kerf width tends to decrease in the three pulse durations. The narrowest range we are interested in is about 100um similar in all durations. But at 90ns and 600 to 800 kHz, less than 100um was measured.

-HAZ width: When the width is narrowest, the measured value was about 10~20um at 60ns, 800~1000kHz.

-Exposed metal width: For all three pulse durations, the minimum value is about 50um and all three are similar.

-Extended metal width: The parameter showing the best result is at 90ns, 600kHz, 900mm/sec and the width is approximately 65um.

Approaching theoretically to the results of pulsed laser, it is evident that different laser-material interactions occurred at 30ns and 90ns. At 30ns the samples would have been subjected to a violent response due to the high power intensity, and at 90ns the lower power intensity would have given a relatively benign response. It is assumed that the material removal mechanism at 30ns is ‘vaporization’ and ‘boiling’ at 90ns. In other words, theoretically, the different ablation mechanism took place at each pulse duration.

3) Comparison of the best results of CW vs Pulsed

One of the best cut-quality of each laser experiment was selected. Then, experimental variables and dependent variables are summarized in Table 6-5.

CW	Parameters	Pulsed
1000W	Power	200W
5000mm/sec	Scanning Speed	900mm/sec
-	Pulse parameters	90ns, 600kHz, Pulse Energy 0.33mJ,
$2.41x10^8W/cm^2$	Power Intensity	$1.06x10^9W/cm^2$
0.2J/mm	Heat Input	0.22J/mm
-	Overlap rate	92.9%
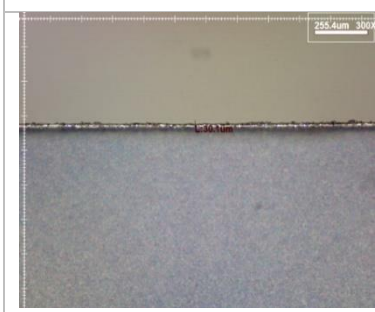	Cut edge	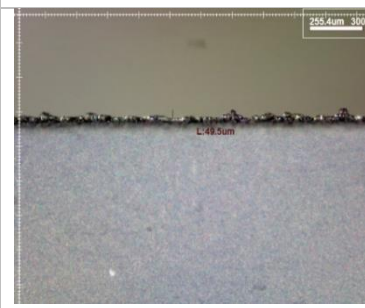
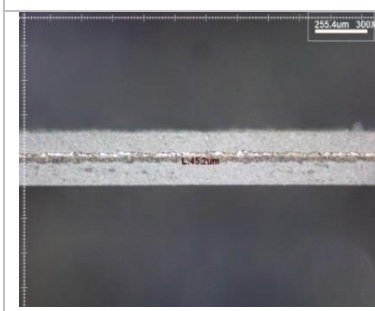	Cross section	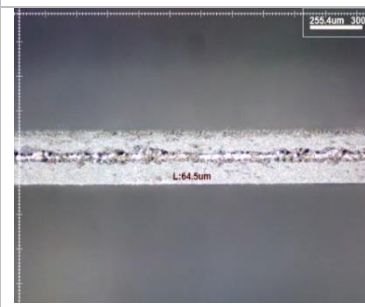

Table 6-5: Comparison of the best results of CW & Pulsed

Chapter 7

Conclusion and Future work

7.1 Conclusion

International agreements to limit the use of fossil fuels and global interest in eco-friendly energy have accelerated the development of new renewable energy sources. Since the development of the first lithium-ion battery in the 1990s, it has continued to develop and has become an indispensable factor in our daily lives. Furthermore, the advent of the era of electric vehicles is increasing the demand for lithium-ion batteries. Increasing productivity is essential to meeting this explosive demand.

Battery manufacturers are constantly trying to reduce prices and stabilize performance by developing mass-production and technology through standardization of products. In order to do so, it is necessary to enhance efficiency in each manufacturing process and improve productivity by reducing the process time by introducing the latest technologies. One such effort is laser cutting of electrodes. Although it has been producing using mechanical punching equipment until now, it needs the increasing unit price and interrupt the process by regular maintenance to minimize the change in the cut quality due to tool wear. To overcome these various shortcomings, it was suggested cutting using laser. Although initial investment costs are high for a process using laser comparing to the mechanical notching, there are advantages that once applied there are no regular or additional administrative costs. However, there are issues that need to be overcome before laser cutting can be applied to the production process. The first is to assess whether the cut quality of the laser cutting electrode is suitable for making batteries. It is possible to apply laser cutting process by achieving at least a similar level of cut quality compared to the existing process. Second, in terms of production speed, the speed

must be at least comparable to or greater than the existing mechanical notching process. Solving these two preconditions is the task of the electrode cutting process, which I believe will be a stepping stone to the growth of the secondary battery market.

The most important performance of the secondary batteries will be their safety. The safety of batteries should be a top priority, as smartphones, laptops, mobile devices, electronics, PHEVs and EVs are often close to the human body in everyday life. Poor batteries can cause electrical malfunctions and eventually cause explosions. In order to prevent accidents from these hazards, it is necessary to thoroughly remove any factors that may impair the safety of the battery from the manufacture of batteries and all processes in the manufacture will have to adhere to this principle. The primary cause of battery malfunction can be abnormal reactions that occur inside the battery cell. The positive and negative in the cell should be electrically entirely isolated, but electrical short circuits for some reason could lead to the explosion of the battery. One of the reasons for this is the metal particles of the positive and negative electrodes that produced during the electrode cutting process, which moves inside the battery and is most likely to cause a short circuit between the two electrodes, so free of metal particles of the electrode cutting is the most important factor to be investigated. The possibility of metal particles that may produce over time after being manufactured from batteries should also be avoided. To do so, cut quality should be high and processes that meet these criteria should be applied.

The purpose of this study was to find suitable laser sources for the electrode cutting process using laser that had been studied for a long time, and to compare and prove the results after testing with two types of laser. Choosing the right laser for the process is the first issue to be resolved.

In general, when it comes to laser cutting, the cutting of pulsed lasers with higher peak power and shorter pulse duration often produces better results than CW with lower peak power and high input heat. However, comparing the results of the experiments of CW and pulsed laser used in this study, the results of CW showed better than pulsed. Of course, the results of pulsed showed better than CW in case of

the same laser output applied. However, the results tested on all possible parameters of the two types of laser, with a focus on cut quality, showed different results from the general prejudices we had.

1) Perspective of Electrode Material

It is needed to think about the causes that the results of this study have shown. First, it is necessary to note the materials used in the experiment. Cathode electrode material of a lithium-ion battery is not a material that can be easily accessed and is not easy to obtain. The characteristic of this material is that $LiFePO_4$ powder sinter, which acts as an active material, is coated on both sides of Aluminum with a thickness of around 100um in one side. It is important to note that it is sintered, not bulk, of a common single material. The powder itself has a large surface area, which makes it much easier for chemical and physical reactions to occur than for bulk materials. The evidence is that although the thickness is much thicker than the Aluminum foil, the wide area is ablated. In other words, the ablation threshold of active material $LiFePO_4$ is low.

And we need to find out properties of the thermal and physical properties of the center positioned metal, the melting point of aluminum is 660.32°C and boiling point is 2519°C. Compared to the other metal, Fe, melting point 1538°C and boiling point 2862°C, melting point of aluminum is very low respectively. Also, one of the features of aluminum is its fourth highest electrical conductivity and thermal conductivity among metals. Heat spreads more quickly compared to other materials. The molten aluminum is also known to have a lower viscosity than other metals. When molten, it is highly flowable, resulting in much more violent reactions to external shocks, resulting in spatters and particles around. The optical characteristic of aluminum shows its very low absorption rate to the used laser wavelength (1064nm). The initial absorption on the aluminum surface in a cold state is very low approximately 5%. However, the aluminum surface used in the experiment is hidden from the active material at the top and is not directly exposed to the laser beam. Even if the initial

absorption rate of the material to laser beam is low, the absorption rate also increases once part of the laser beam is absorbed by the material and the temperature increases. This optical property is shown in all metallic materials, but perhaps part of the heat absorbed from the upper material has been conducted downward, causing states of aluminum to change.

It seems that it is difficult to find good cut quality in laser cutting due to the properties of active material as a powder sintered and the properties of aluminum and its relatively thin foil type.

2) Perspective of Laser–Material Interaction

If the laser beam of the high power intensity focused on the small beam size is incidented on a material, the temperature of the material surface reaches the melting point within a few tens of ns, melting the material surface locally. The additional laser energy reaches the boiling point and vaporize the material. The vapor generated by the vaporization reacts with the laser beam to form a plasma and produce a recoil pressure in turn. This recoil pressure causes the molten or vapor to expel around. This is why the material is cut by laser ablation. When laser is incident to the surface of the upper active material, thermodynamic reactions are easily made to reach melting or boiling point, resulting in melting and evaporation of the material. However, laser only reached material on beam size, but the surrounding heat would be conducted by rapid increase in temperature, and this conducted heat would have caused the surrounding area to experience the same process and resulting in material removal. The reason why the kerf width of the active material at the top is much wider than the laser beam size. The beam size was 23um in fact at CW experiments, but the kerf width is over 100um.

The remaining heat of the total conducted heat from upper material excluding heat used for ablating the thickness of the upper active material layer is also conducted to the aluminum layer. For the high heat conductivity aluminum will reach the melting or boiling point depending on the amount of heat that is conducted from the top. If

it does not reach the boiling point compared to aluminum's low melting temperature, it causes an injection of the molten material due to the recoil pressure generated by plasma. If the laser power is low and slow, through this mechanism large and spherical metal particles forms and spreads around the cut line. If more than the boiling point is reached, the aluminum is vaporized to form a vapor plume, which absorbs or scattering the laser beam and subsequently generates plasma. In this case, the temperature of the vapor is high, causing a strong recoil pressure, and the material is removed through vaporization. This is the reason why the molten particles around the cut edge is rarely visible in areas where laser power is high or fast, and only fine debris are observed.

After aluminum is removed and some of the remaining heat is transferred to the lower active material layer. For the high thermal conductivity of aluminum, the heat reaches the lower layer in a short period of time. For the relatively high ablation threshold of aluminum, small portion of the total transferred heat from the upper layer would be sufficient to ablated the lower active material layer due to relatively low ablation threshold of active material, which the upper active material would experience the process That is, if the energy is sufficient to ablate aluminum, then the energy needed for the lower active material is not necessary. There has not been a case where only the aluminum layer has been cut and the lower active material layer has not been cut.

3) Perspective of Laser operating modes

Two operating modes, Continuous wave and Pulsed laser were used for this study. All the configurable parameters of each laser were used. Both lasers have single mode beam characteristic and similar beam spot size through processing optics. Each laser itself has a completely different parameter. CW had a max. power of 1kW and the power intensities produced by beam size are 4.75×10^8 to 2.38×10^9 [W/cm^2]. Pulsed has a max. power of 200W, pulse durations of 30, 60, 90[ns], and PRR 133 to 1000[kHz]. The and the corresponding pulse energies are between 1.5 and 0.2[mJ].

Peak power shows between 2.2 ~16.6[kW]. The power intensity obtained through the beam size was between 6.41×10^8 and 4.81×10^9 [W/cm^2].

The parameters of the two lasers are completely different and showed different results. The principal causes of the results of the CW experiment assumed that the relatively low peak power and the resulting power intensity caused incomplete evaporation and that boiling became the main mechanism of the material removal, leaving the larger size of droplets around the cut line. However, interesting results are that there are no metal particles at high cutting speed, and the shape of aluminum edges looks soft and even there are few protruding parts.

About the results of pulsed laser, it is evident that different laser-material interactions occurred at 30ns and 90ns. At 30ns the samples would have been subjected to a violent response due to the high-power intensity, and at 90ns the lower power intensity would have given a relatively benign response. It is assumed that the material removal mechanism at 30ns is 'vaporization' and 'boiling' at 90ns. In other words, theoretically, the different ablation mechanism took place at each pulse duration.

Results according to different ablation mechanisms were found in the previous chapter. Contrary to author's expectations, it was found that the results of CW are superior to the results of pulsed, given the lasers used in this study. If the goal of this study is to find which ablation mechanics are appropriate for cut quality, then it seems that the ablation mechanism occurred in the CW experiment was more appropriate for cathode electrode of $LiFePO_4$ battery.

4) Perspective of Cut Quality

The clear criteria for cut quality required for the laser cutting of electrodes to be applied to the mass production process are not known. The possible criteria should be as small as possible as the elements defined for the assessment of cut quality and there should be no particles, debris and cracks. Then the solution would be to minimize the inevitable phenomena that occur in the laser cutting process and find

acceptable conditions. Metal particles are the most important quality element in the laser cutting process. The very first parameter to be investigated is that the metal particles should not be produced. And the following would be the width or shape of metal in cross-section. The exposed metal should also be minimized as metal particles may come off from the metal layer if the exposed part of metal is extensively large or the end of metal is rough. There should be no separation of the metal particles, so that there would not be any conditions that can cause an electrical short circuit by penetrating the separation film and contacting other electrodes.

Reviewing the experimental results of this study, the microscopic pictures of the samples showing good cutting quality of the CW test results show that the metal edge is round, smooth and not rough. However, in the pictures of the pulsed tests showing good cutting quality, the end of the metal is rough and protruding somewhere, which seems to be detached by the external stimulus. Considering the importance of the cutting quality of the metal part and comparing the results of the two lasers, it was evident that the result of CW is better than that of pulsed if electrode material is limited to $LiFePO_4$.

It is not clear whether the best results found in this experiment can be used in the actual battery process. However, various lasers have been developed for a long time, and researches have been conducted using various lasers, but even the appropriate laser type have yet to be selected. Experiments have been intensified using various pulsed laser, which have different parameters from pulse energy or pulse discharge. Studies using CW laser were initially attempted briefly, but since then most of the studies have been conducted with pulsed laser.

The purpose of this study was to check if the laser selection and research direction were correct in the laser cutting of electrode through a comparative experiment using the CW, which has been overlooked and the pulsed with which many studies have been done so far.

7.2 Suggestion for future work

Since the first attempt to cut electrodes using lasers, laser source has developed rapidly, creating a wide variety of excellent lasers. At the first time, only limited lasers could be used, but now high-power lasers with various parameters such as several kW Single mode lasers, and kW pulsed laser are available. Further researches are required to investigate of higher power pulsed than the pulsed laser used in this study with the parameters of increased power and speed.

Also, laser source development has been taking place in other wavelengths of laser. Recently a green laser(532nm) with 200W power appeared, as the green laser that was difficult to review due to low power even a few years ago. Good results are expected as absorption rate of electrode material to 532nm wavelength is relatively higher than IR laser wavelength. A comparative test using two wavelengths of laser is expected to provide a new breakthrough for laser electrode cutting.

Bibliography

[1] Wikipedia ‘Laser’, https://en.wikipedia.org/wiki/Laser

[2] http://www.physics-and-radioelectronics.com/physics/ laser /laserintroduction.html

[3] Elijah Kannatey-Asibu, Jr.(2009). Principles of Laser Materials Processing, © 2009 John Wiley & Sons, Inc.]

[4] Reza Negarestani, Laser cutting of carbon fiber-reinforced polymer composite materials, university of Manchester VOL. 8NOS. 11–12 319

[5] RANJAN, SEN. et al. HIGH POWER FIBER LASERS: FUNDAMENTALS TO APPLICATIONS

[6] C. J. Koester and E. Snitzer, (1964) Appl. Opt., 3 (10), 1182

[7] H. M. Pask, et al. (1995). IEEE J. Sel. Topics Quantum Electron, 1(1), 2 (1995)

[8] V. Fomin, et al. (2014) Laser Optics, International Conference

[9] M. N. Zervas and C. A. Codemard, (2014) IEEE J. Sel. Topics Quantum Electron, 20, 219.

[10] J. Limpert, et al. (1995) IEEE J. Sel. Topics Quantum Electron, 13,537

[11] Fiber lasers: The state of the art, https://www.laserfocusworld.com/articles/print/volume-48/issue-04/features/the-state-of-the-art.html

[12] IPG Photonics Inc. https://www.ipgphotonics.com/en/whyIpg#[history]

[13] Fiber Lasers, (2011) Seminar, Department of physics, University of Ljubljana, February 2011

[14] Fiber Laser, Fujikura, http://www.fiberlaser.fujikura.jp/eng/products/about-fiber-laser.html

[15]FOSCO,https://www.fiberoptics4sale.com/blogs/archive-posts/95046406-what-is-fiber-bragg-grating

[16]Fiber Bragg Grating, Wikipedia, https://en.wikipedia.org/wiki/Fiber_Bragg_grating

[17] Laser safety training manual, Toronto University, https://ehs.utoronto.ca/laser-

safety-program/ laser-safety-training-manual-b/

[18] Abubaker Hassan Hamad, Effects of Different Laser Pulse Regimes (Nanosecond, Picosecond and Femto-second) on the Ablation of Materials for Production of Nanoparticles in Liquid Solution, (2016)

[19] Understanding the Paraxial Gaussian Beam Formula, https://www.comsol. com /blogs/understanding-the-paraxial-gaussian-beam-formula/

[20] Gaussian Beam Optics, (2009) CVI Melles Griot

[21]RP Photonics Encyclopedia, https://www.rp-photonics.com/mode_locked_fiber_lasers.html

[22] Michalis N Zervas, (2014) High power ytterbium-doped fiber lasers– Fundamentals and applications, Article in international Journal of Modern Physics

[23] O'Neill W. et al., (2004) High power high brightness industrial fiber laser technology. In Proceedings of the 23rd International Congress on Applications of lasers and electro optics (ICALEO); San Francisco, USA; 2004. p. 1-7.

[22] J. D. Kafka *et al.*, (1989), Mode-locked erbium-doped fiber laser with soliton pulse shaping, Opt. Lett. 14 (22), 1269 (1989)

[23] I. N. Duling III, (1991), All-fiber ring soliton laser mode locked with a nonlinear mirror, Opt. Lett. 16 (8), 539 (1991)

[24] Hun, Lee et al, (2014) A review of recent development in membrane separator for rechargeable lithium-ion batteries. Energy Environ. Sci., 2014,7, 3857

[25] Borong Wu, Yonghuan Ren and Ning Li, LiFePO4 Cathode Material

[26] The Four Components of a Li-ion Battery, Samsung SDI, http://www.samsungsdi.com/column/ technology/detail/55272.html?listType=gallery

[27] Jagadish Babu Sirigineedi, (2016) Tennessee Technological University, ENHANCED ELECTROCHEM-ICAL PROPERTIES OF ALUMINUM DOPED LITHIUM IRON PHOSPHATE (LiFePO4) CATHODE MATERIAL FOR LI-ION BATTERY USING SOLID STATE SYNTHESIS (Master thesis). Retrieved from ProQuest Dissertation and These database (ProQuest Number: 10154742)

[28]Battery university, https://batteryuniversity.com/learn/article /types_of_lithium_ion

[29] The Boston Consulting Group Inc., (2010). Batteries for Electric Cars: Challenges, Opportunities, and the Outlook to 2020, The Boston Consulting Group Inc., Boston, Tech. Rep., 2010.

[30] Battery University, Summary table of Lithium based batteries, https://batteryuniversity.com/learn/article/bu_216_summary_table_of_lithium_based_batteries

[31] Michael Robert Kronthaler, (2012) Laser cutting in the production of Lithium ion cells. Article in Physics Procedia · December 2012

[32] G. Reinhart et al. (2011) Research and Demonstration Center for the Production of Large-Area Lithium-Ion Cells. Future Trends in Production Engineering, Proceedings of the First Conference of the German Academic Society for Production Engineering (WGP), Berlin, Germany, 8th-9th June 2011

[33] Green Lion, (2015) ADVANCED MANUFACTURING PROCESSES FOR LOW COST GREENER LI-ION BATTERIES, Electrode Laser cutting

[34] R. Patwa, H.J. Herfurth, H. Pantsar, S. Heinemann, J. Mazumder, D. Lee, (2010) Proceedings of the ICALEO, Anaheim, CA.

[35] M. Luetke, V. Franke, A. Techel, T. Himmer, U. Klotzbach, A. Wetzig, E. Beyer, (2011) A Compar-ative Study on Cutting Electrodes for Batteries with Lasers, Physics Procedia 12 (2011) 286–291

[36] D. Lee, R. Patwa, H. Herfurth, J. Mazumder, (2011) Computational and experimental studies of laser cutting of the current collectors for lithium-ion batteries. Journal of Power source 210(2012) 327-338

[37] A. Lutey, A. Fortunato, A. Ascari, S, Carmignato, C. Leone, (2015) Laser cutting of lithium iron phosphate battery electrodes: Characterization of process efficiency and quality, Optics & Laser Technology 65(2015) 164-174

[38] A. Lutey, A. Fortunato, S. Carmignato, A. Ascari, (2016) Quality and Productivity Considerations for Laser Cutting of LiFePO4 and LiNiMnCoO2

Battery Electrodes, Procedia CIRP 42(2016) 433-438

[39] Ali Gökhan Demir, Barbara Previtali, (2015) Microcutting of multi-layer foils with IR and green ns-pulsed fibre lasers for Li-Ion batteries, Procedia CIRP 33, 526 – 531

[40] N. M. Bulgakova, A. V. Bulgakov. (2001) Pulsed laser ablation of solids: Transition from normal vaporization to phase explosion, Appl. Phys. A 73, 199-208

[41] M. M. Martynyuk, (1983) Russ. J. Phys. Chem., 57, 494

[42] Q. Lu, S. S. Mao, X. Mao, R. E. Russo, (2002) A thermal model of phase explosion for high power laser ablation Proceedings of SPIE vol. 4760

[43] A. Miotello, R. Kelly, (1995) Appl. Phys. Lett., 67, 3535

[44] J. H. Yoo, S, H, Jeong, R. Greif, R. E. Russo, (2000) Journal of Applied Physics 88, 1638; doi: 10.1063/1.373865

[45] Maturose, Suchatawat. (2011). MATHEMATICAL MODELLING OF MULTIPLE PULSED LASER PERCUSSION DRILLING, School of Mechanical, Aerospace and Civil Engineering, The University of Manchester

[46] X.Chen and H.Wang, (2001) A Calculation Model for the Evaporation Recoil Pressure in Laser Material Processing, Journal of Physics D: Applied Physics, vol. 34, pp. 2637-2642.

[47] J.H. Yoo, S.H. Jenong, X.L Mao, R. Greif, R.E Russo, (2001) Evidence for phase-explosion and generation of large particles during high power nanosecond laser ablation of silicon

[48] Q. Lu, Samuel S. Mao, X. Mao, R.E. Russo, (2002) A thermal model of phase explosion for high power laser ablation, Proceeding of SPIE Vol.4760

[49] Vladimir Semak and Akira Matsunawa (1997) J. Phys. D: Appl. Phys. 30 2541

[50] M.Kronthaler, R.Wiedenmann, (2012) Laser cutting in the production of Lithium ion cells, Article in Physics Procedia · December 2012

[51] D. Lee, S. Ahn, (2017) Investigation of laser cutting width of LiCoO2 coated Aluminum for Lihium-Ion Batteries, Appl. Sci. 2017, 7, 914

[52] X-ray spectroscopy, https://en.wikipedia.org/wiki/Energy-dispersive_

X-ray_spectroscopy

[53] Jyotsna Dutta Majumdar, Indranil Manna Editors, (2013) Laser-Assisted Fabrication of Materials, Springer, DOI 10.1007/978-3-642-28359-8

[54] Narendra B. Dahotre, Sandip P. Harimkar, (2008) Laser Fabrication and Machining of Materials, Springer, e-ISBN 978-0-387-72344-0

[55] Salvatore Siano, (2004) Principles of Laser Cleaning in Conservation, e-version ISBN-10: 973 88109 30

[56] D. LEE, (2012) Modeling of high speed remote laser cutting of electrodes for lithium ion batteries, (Doctoral thesis, University of Michigan, USA)

[57] Warwick, Health & Safety Services, https://warwick.ac.uk/services /healthsafetywellbeing/guidance/lasers/laserproperties/

[58] A. E. Hussein, P. K. Diwakar, S. S. Harilal, and A. Hassanein (2013) The role of laser wavelength on plasma generation and expansion of ablation plumes in air, Journal of applied physics 113, 143305

[59] Vladimir Semak and Akira Matsunawa, (1997) The role of recoil pressure in energy balance during laser materials processing, D: Appl. Phys. 30 (1997) 2541-2552

국문 초록

화석연료 사용의 제한에 대한 국제적인 협의와 환경 친화적인 에너지에 대한 세계적인 관심은 재생 가능한 에너지원의 개발을 가속시켰다. Li-Ion Battery는 1990년대 초 처음 개발된 이래로, 계속해서 발전해왔으며 이제는 우리의 일상 생활에서 없어서는 안 될 요소가 되었다. 이러한 시대적인 흐름과 폭발적으로 증가하는 수요에 대응하기 위해서는 생산성 향상은 필수적이다. 그러기 위해서는 배터리 생산 기업들은 최신 기술을 도입하여 각 공정의 효율성을 높이고 공정 시간을 단축하여 생산성을 높여야 할 것이다. 그러한 노력 중 하나가 Li-Ion Battery의 전극 절단에 Laser를 적용하려는 것이다. 본 연구의 목적은 오랫동안 연구해 오고 있는 레이저를 이용한 전극 절단 공정에 적합한 Laser 소스를 찾기 위해, 두 가지 유형의 Laser를 이용하여 실험한 후 결과를 비교 분석하고 물리적인 현상의 원인을 고찰해 보려고 하였다.

실험에 사용된 전극 재료는 Aluminum Foil의 양면에 활성물질로 $LiFePO_4$이 코팅된 Li-Ion Battery의 양극 전극 물질이다. 이 전극 물질을 전혀 다른 발진 특성을 보이는 Single Mode CW Laser와 High power Pulsed Laser를 이용하여 실험하고 결과를 분석하였다. 각 레이저의 설정 가능한 모든 파라미터를 이용하였고, 우수한 절단 품질을 보이는 파라미터를 정성적 및 정량적 분석을 이용하여 찾으려고 하였다. 실험한 모든 샘플에 대해 SEM과 현미경을 사용해 Cut edge 및 Cross-section 사진을 촬영했으며, 절단 품질 평가를 위해 정의한 네

가지 요소를 모두 측정하고 비교하였다. 실험에 이용된 모든 파라미터에 대해서, 특정 파라미터의 변경이 절단 품질에 어떠한 영향을 미치는지 확인하였다. 또한 절단 품질 평가 요소에 대해 측정값을 그래프화 하여 파라미터 변화에 따른 추세도 확인하였다. 절단된 시료는 EDX 장비를 Cut edge 및 Cross-section 주변의 성분 분석을 하여 절단 후 재료의 성분 조성에 어떠한 변화가 생겼는지 확인하였다. 그리고 각 레이저의 결과 중 일부를 선택하여 이론적으로 레이저와 재료 상호작용의 관점에서 현상의 원인을 분석하려고 했다.

우선, 각 Laser의 실험 결과를 파라미터 변화가 Cut quality에 어떠한 영향을 미치는지 조사하였고, 다음으로 두 Laser의 실험 결과를 서로 비교하였다. 그리고 각 레이저를 이용한 실험 결과에 대해 이론적으로 접근하고 분석해 보았다.

CW 레이저 실험 결과를 요약해 보면, Heat Input이 0.2J/mm 미만일 경우 cut edge 주변에 particles 및 debris and cracks 모든 출력에서 보이지 않았다. 그리고 Power Intensity가 $1.44x10^8$ W/cm^2 이상일 때 금속의 끝부분이 전반적으로 균일하고 부드러움을 보였고, Cross-section에서도 세개의 층의 구분이 명확하게 구분되고 재 응고된 용융체도 들러붙어 있지 않았다. 같은 Heat Input일 때, Power Intensity가 높을수록 품질이 더 우수하다는 것을 확인할 수 있었다. Heat Input 대략 0.2J/mm이고, Power Intensity가 $2x10^8$ W/cm^2 일 때, CW 실험 결과 중 최고의 절단 품질을 보였다. CW 실험 결과의 주요 원인은 상대적으로 낮은 Peak Power와 결과적인 낮은 Power Intensity로 불완전한 Vaporization이 발생했으며, Boiling이 재료 제거의 주요 메커니즘이 되어 더 큰 사이즈의 Metal Particles 들이 컷 라인 주위에 남은 것이라고 유추할 수 있다.

Pulsed 레이저 실험 결과 중 특히 눈에 띄는 것은 절단된 금속의 단면의 형상이 고르지 않고 불규칙하게 돌출되었다는 점이다. 그리고 Exposed metal의 색깔이 전반적으로 CW 결과보다 어둡다. Cross-section은 재 응고된 용융체로 덮여 있어 지저분해 보인다. Metal인 Aluminum의 폭은 과도하게 확장되었고, 균일하지 않으며 매우 거칠어 보인다. 전반적으로 Cut edge와 Cross-section 모두 30ns보다는 60ns와 90ns에서 cut quality가 우수하며, 90ns의 600kHz와 800kHz에서는 절단 가장자리 주변에 Particles 나 debris가 적었고 HAZ의 폭이 좁았다. 최고의 절단 품질은 90ns, 600kHz, 800~1000mm/sec에서 관찰되었으며, 그 때의 다른 물리적 값은 Pulse Energy 0.33mJ, Power Intensity $1.06x10^{9}W/cm^{2}$ 그리고 Overlap rate는 93.7%였다. 30ns에서 샘플은 높은 Power Intensity로 인해 과격한 반응을 겪었고, 90ns에서는 상대적으로 낮은 Power Intensity로 온화한한 반응을 있었던 것으로 생각할 수 있다. 30ns의 재료 제거 매커니즘이 Vaporization이라면, 90ns에서는 Boiling 재료 제거의 주 매커니즘인 것으로 유추할 수 있다.

본 연구 결과를 바탕으로 실험에 사용된 레이저로만 한정한다면, CW의 결과가 Pulsed의 결과보다 우수한 것을 확인할 수 있었다. 본 연구의 목적은 전극 절단 품질에 더 효과적인 절단 매커니즘을 조사하고, 적합한 Laser 타입을 모색하는 것이었다. 본 연구에서 찾은 가장 양호한 cut quality가 실제 배터리 제조에 적합한지는 알 수 없다. 그러나 Laser를 이용한 전극 절단 공정에서 가장 먼저 해결해야 할 문제는 적합한 Laser의 선정일 것이다.